

THESIS ON CHEMISTRY AND CHEMICAL ENGINEERING G43

# **Leaching of the Water-Soluble Calcium Components of Oil Shale Waste Ash**

KADRIANN TAMM

**TUT**  
PRESS

TALLINN UNIVERSITY OF TECHNOLOGY  
Faculty of Chemical and Materials Technology  
Laboratory of Inorganic Materials

**This dissertation was accepted for the defence of the degree of Doctor of Philosophy in Chemical and Materials Technology on March 17, 2016**

**Supervisor:** Senior research Scientist, Mai Uibu, Laboratory Inorganic Materials, Tallinn University of Technology

**Co-Supervisor:** Professor Emeritus, Juha Kallas, Laboratory Inorganic Materials, Tallinn University of Technology

Senior research Scientist, Rein Kuusik, Laboratory Inorganic Materials, Tallinn University of Technology

**Opponents:** Prof. Mika Järvinen, Department of Mechanical Engineering, Aalto University, Finland

Dr. Taavo Tenno, Institute of Chemistry, Tartu University, Estonia

**Defence of the thesis:** May 25, at 10.30 2016, Lecture hall: U06A-229  
Tallinn University of Technology, Ehitajate tee 5, Tallinn

**Declaration:**

Hereby I declare that this doctoral thesis, my original investigation and achievement, submitted for the doctoral degree at Tallinn University of Technology has not been submitted for any academic degree.

*Kadriann Tamm*



European Union  
Structural Assistance



Investing in your future

This work has been partially supported by graduate school “Functional materials and processes” receiving funding from the European Social Fund under project 1.2.0401.09-0079 in Estonia.

Copyright: Kadriann Tamm, 2016

ISSN 1406-4766

ISBN 978-9949-23-920-7 (publication)

ISBN 978-9949-23-921-4 (PDF)

KEEMIA JA KEEMIASTEHNIKA G43

# **Kaltsiumiühendite leostumine põlevkivituha vesisüsteemides**

KADRIANN TAMM



## TABLE OF CONTENTS

LIST OF PUBLICATIONS .....	7
Closely related publications .....	8
THE AUTHOR'S CONTRIBUTIONS TO THE PUBLICATIONS.....	9
INTRODUCTION.....	10
1. LITERATURE REVIEW .....	12
1.1 Environmental impacts of fossil fuel processing.....	12
1.2 Estonian oil shale based energy sector .....	13
1.2.1 Pulverized firing technology.....	13
1.2.2 Circulating fluidized bed technology .....	14
1.2.3 Solid heat carrier technology .....	15
1.2.4 Atmospheric emissions.....	15
1.2.5 Waste ashes from oil shale processing.....	16
1.2.6 Hydraulic transportation and open-air deposition of ash.....	17
1.2.7 Prospects for oil shale ash utilization.....	18
1.3 Main water-soluble Ca and S compounds – oil shale mineral residues. 20	
1.3.1 Calcium and Sulfur in solid fossil fuels.....	20
1.3.2 Calcium and Sulfur in mineral waste.....	21
1.4 Summary of the literature review and objectives of the thesis .....	23
2. MATERIALS AND METHODS .....	25
2.1 Experimental methods and procedures.....	25
2.1.1 Applied methods.....	25
2.1.2 Characterization of materials .....	26
2.1.3 Experimental procedure – Apparatuses .....	27
2.2 Modeling .....	31
3. RESULTS AND DISCUSSION.....	32
3.1 Leachability of pure systems .....	32
3.1.1 $\text{Ca}(\text{OH})_2\text{-H}_2\text{O}$ system .....	32
3.1.2 $\text{CaSO}_4\cdot 2\text{H}_2\text{O-H}_2\text{O}$ system .....	33
3.1.3 $\text{CaS-H}_2\text{O}$ system.....	34
3.2 Leaching of oil shale ash systems.....	38
3.2.1 The equilibrium of oil shale ash-water systems.....	38
3.2.2 Model and real ash dissolution kinetics in the oil shale ash-H <sub>2</sub> O system .....	41
3.2.3 Implementing the dissolution of oil shale ash within Aspen plus..	45
4. CONCLUSION .....	54
REFERENCES.....	56
ACKNOWLEDGMENTS.....	64
ABSTRACT .....	65
KOKKUVÕTE .....	67
APPENDIX A: ORIGINAL PUBLICATIONS .....	69

PAPER I.....	69
PAPER II.....	81
PAPER III.....	91
APPENDIX B. CURRICULUM VITAE.....	113
ELULOOKIRJELDUS .....	114
<i>CURRICULUM VITAE</i> .....	117

## LIST OF PUBLICATIONS

The thesis is based on three original articles in peer-reviewed international research journals (hereafter referred to as *Paper I – Paper III*).

- I.** Uibu, M., *Tamm, K.*, Velts-Jänes, O., Kallaste, P., Kuusik, R., Kallas, J. Utilization of oil shale combustion wastes for PCC production: Quantifying the kinetics of  $\text{Ca}(\text{OH})_2$  and  $\text{CaSO}_4 \cdot 2\text{H}_2\text{O}$  dissolution in aqueous systems. - *Fuel Processing Technology* 2015, 140, 156-164.
- II.** *Tamm, K.*, Uibu, M., Kallas, J., Kallaste, P., Velts-Jänes, O., Kuusik, R. Thermodynamic and kinetic study of CaS in aqueous systems. - *Fuel Processing Technology* 2016, 142, 242-249.
- III.** *Tamm, K.*, Kallaste, P., Uibu, M., Kallas, J., Velts-Jänes, O., Kuusik, R. Leaching Thermodynamics and Kinetics of Oil Shale Waste Key Components. - *Oil Shale* 2016, 33, 1, 80-99.

Copies of these publications are included in APPEDIX A.

## Closely related publications

Tamm, K., Kuusik, R., Uibu, M., Kallas, J. Transformations of sulfur compounds in oil shale ash suspension. - *Waste Management and the Environment VI: 6th International Conference on Waste Management and the Environment*, Popov, V., Itoh, H., Brebbia, C.A. (eds.). Wessex Institute of Technology Press, (WIT Transactions on Ecology and the Environment; 163), New Forest, UK, 2012, 25-35.

Tamm, K., Kuusik, R., Uibu, M., Kallas, J. Transformations of sulfides during aqueous carbonation of oil shale ash. - *Energy Procedia* 2013, 37, 5905–5912.

Tamm, K., Kuusik, R., Uibu, M., Kallas, J. Behaviour of sulfur compounds during aqueous leaching of oil shale ash. - *Proceedings of the 4th International Conference on Accelerated Carbonation for Environmental and Materials Engineering ACEME 2013*, Leuven, Belgium, Nasser, R., Santos, R., Cizer, Ö., Van Gerven, T. (eds.) Leuven, 2013, 541–544.

Tamm, K., Uibu, M., Kallaste, P., Kuusik, R., Kallas, J. Equilibrium calculations in aqueous carbonation of oil shale waste – sulfur compounds. - *Journal of Petroleum & Environmental Biotechnology: 2nd World Congress on Petrochemistry and Chemical Engineering*, Las Vegas, 2014, 40.

Tamm, K., Kallaste, P., Uibu, M., Kallas, J., Kuusik, R. Leaching Thermodynamics of Oil Shale Waste Key Components. - *Proceedings of the 5th International Conference on Accelerated Carbonation for Environmental and Materials Engineering*, New York City, 2015.

## **THE AUTHOR'S CONTRIBUTIONS TO THE PUBLICATIONS**

- I.** The author carried out the experiments and was responsible for interpretation.
  
- II.** The author was responsible for planning and conducting the experiments, the interpretation of the results, the calculation work and writing the paper.
  
- III.** The author was responsible for planning and conducting the experiments, the interpretation of the results, the calculation work and writing the paper.

## INTRODUCTION

The global energy supply for human consumption more than doubled between the years 1971 and 2012, and fossil fuels still account for over 80% of this supply. Both environmentally safe disposal and/or reuse of solid wastes and atmospheric emissions ( $\text{CO}_2$ ,  $\text{SO}_2$ ,  $\text{NO}_x$ , etc) are among the most serious problems caused by the extensive use of fossil fuels, especially for heat and power production using low-grade solid fuels. Due to a lack of suitable applications, the majority of alkaline industrial residues are disposed in landfills, which, over a long period of time, could negatively impact both human health and the environment. One possible application for these fine-grained Ca(Mg)-rich waste materials could be as sorbents for  $\text{CO}_2$  sequestration.

The European Union (EU) is constantly introducing stricter conditions and new initiatives to both reduce greenhouse gas (GHG) emissions and mitigate the effects of other harmful pollutants. These initiatives cover environmental technology, waste recovery, and recycling and also affect the oil shale sector in Estonia. For example, by 2020, GHG emissions must be reduced by 20-30% and annual  $\text{SO}_2$  emissions by 25 thousand tons. In recent years, various carbonation routes have been evaluated to obtain a precipitated calcium carbonate (PCC)-type material from oil shale ash and its leaching waters. To achieve this goal one must fully understand ash leaching process chemistry.

An effective method of evaluating if a new technology can feasibly upgrade oil shale ash is to create a thermodynamically consistent kinetic model that defines the reaction kinetics and operating parameters. This model should account for both the leaching of water-soluble oil shale ash components and the crystallization of solid products in the multi-phase ash leachates.

The goal of this doctoral work was to develop leaching model for various oil shale ash systems. The first aim was to resolve gaps in our knowledge regarding the dissolution mechanisms of oil shale water soluble key components. Following this, simulate the oil shale ash dissolution process under various conditions to both predict the dynamics of  $\text{Ca}(\text{OH})_2$ ,  $\text{CaSO}_4 \cdot \text{H}_2\text{O}$  and CaS leaching at ash dumping sites and optimize the operating conditions to avoid  $\text{H}_2\text{S}$  emissions during the industrial handling of oil shale residues.

## LIST OF ABBREVIATIONS AND SYMBOLS

$\text{CaO}_{\text{free}}$	free lime
BET	Brunauer-Emmett-Teller particle surface area determination method
CFB	circulating fluidized bed
$d_{\text{mean}}$	mean diameter
DOC	dissolved organic carbon
EC	electrical conductivity
$k_i$	rate constant
$K_i$	equilibrium constant
OS	oil shale
OSA	oil shale ash
PCC	precipitated calcium carbonate
PF	pulverized firing
Q	duty
SHC	solid heat carrier
SSA	specific surface area
$t$	time
XRD	X-ray diffraction
XRF	X-ray photoelectron spectroscopy
[ ]	concentration mol/L

# 1. LITERATURE REVIEW

## 1.1 Environmental impacts of fossil fuel processing

The global energy supply for human consumption more than doubled between the years 1971 and 2012, and fossil fuels still account for over 80% of this supply [1]. Both environmentally safe disposal and/or reuse of solid wastes and atmospheric emissions ( $\text{CO}_2$ ,  $\text{SO}_2$ ,  $\text{NO}_x$ , etc) are among the most serious problems caused by the extensive use of fossil fuels for heat and power production, especially for heat and power production using low-grade solid fuels.

Global  $\text{CO}_2$  emissions from the combustion of fossil fuels is  $\sim 28$  GT per year with  $\sim 43\%$  originating from coal (aggregate of coal, peat and oil shale) and  $\sim 35\%$  from oil [1]. The concentration of  $\text{CO}_2$  in the atmosphere has increased from 280 ppm at the beginning of the industrial revolution to 400 ppm by the year 2013 [2]. However,  $\text{CO}_2$  emissions from fossil fuel combustion in the EU declined by 1.4% in 2013 compared with the previous year and by 0.4% in 2012 compared with 2011 [3]. Every year about half of the  $\text{CO}_2$  emitted from fossil fuel combustion stays in the atmosphere while the other half is taken up by the oceans or various land sinks. As more and more  $\text{CO}_2$  is absorbed by the world's oceans, the water is becoming more acidic [4].

The combustion of fossil fuels at power plants is the largest source of sulfur oxides emissions. Global  $\text{SO}_2$  emissions from stationary fuel combustion have been declined from 23.45 Mt in 1970 to 4.09 Mt by 2014, largely due to changes in national laws and regulations [5]. The majority of sulfur emissions pass over the oceans where they deposit as acid and mix with the upper water layers. A smaller portion of the sulfur emissions fall on continental soils and freshwater bodies downwind of the power plants [6].

Fossil fuel power plants that operate at high temperatures release nitrogen oxides, which also cause environmental problems; nitrogen oxides react with hydrocarbons in sunlight and produce toxic constituents [7].

The amount and composition of solid residues generated by the thermal treatment of fossil fuels depends on the combustion technology, raw material mineral matter, and other non-combustible substances in the fuel. The total amount of solid residues generated from industrial combustion (boiler slag, ashes from different types of boilers, and desulfurization products) in all the European member states is estimated to be about 100 Mt in 2010 [8].

The wastes from fossil fuel processing differ in their general composition and leaching characteristics. However, the solid wastes from other large-scale industrial processes (such as solid waste incineration, or cement, steel, and paper production) have similar characteristics (Table 1) and can be treated and/or utilized using similar methods.

Table 1. Characterization of fossil fuel residues and industrial waste materials

		Estonia oil shale ash [9, 10]	Spain coal ash [11, 12, 13]	South Africa coal ash [14, 15]	UK Cement waste [13, 16]	Finland steel slag [13, 17, 18]	China coal ash [19, 20]	Paper sludge ash [16, 21, 22]
Chemical composition, %	CaO	29-51	0.9-9.0	5.3-10.3	34-66	42-47	2.2-7.8	45-69
	MgO	5-12	1.0-2.7	0.9-2.7	1.1-1.5	1.4-1.8	0.7-0.9	2-5
	SO <sub>3</sub>	1.5-9.0	0.1-0.7	0.3-1.3	4.6-22.3	0.1 <sup>as S</sup>	1.9-2.9	0.5-6.4
	CO <sub>2</sub>	0.7-15	16	>9	5	10	1.1-4.2	10
Potential uptake of CO <sub>2</sub>		up to 209 kg CO <sub>2</sub> per t ash	up to 26 kg CO <sub>2</sub> per t ash	up to 62 kg CO <sub>2</sub> per t ash	10-26%	up to 23%	-	up to 218 kg CO <sub>2</sub> per t ash
Physical characteristic	SSA, m <sup>2</sup> ·g <sup>-1</sup>	0.4-8.0	0.6	0.3-0.8	~2·10 <sup>-3</sup>	-	4.2-8.5	0.2
	d <sub>mean</sub> , μm	25-197	0.1-100	0.5-200	13- 63	<250	30-80	1-100

Due to lack of suitable applications, the majority of alkaline industrial residues are disposed of in landfills, which, in the long term, could negatively impact both the environment and human health. On the other hand, these fine-grained Ca(Mg)-rich waste materials could be utilized as sorbents for CO<sub>2</sub> sequestration [10, 13, 16, 22-24].

## 1.2 Estonian oil shale based energy sector

About 60% of Estonia's fuel balance is covered by the combustion of local low-grade oil shale (OS). The majority of the OS (21 Mt annual output in 2014) is used in thermal power generation plants using both pulverized firing (PF) and circulating fluidized bed (CFB) technology. Roughly 20% of Estonian OS is utilized for shale oil and shale gas retorting using solid heat carrier technology (SHC), and the remaining OS is used in the cement industry [25].

### 1.2.1 Pulverized firing technology

PF technology is widely used for the combustion of solid fuels and has also been used to process oil OS. In Estonia, OS fueled PF boilers have been employed for heat and power production since the 1960s [26]. This PF technology employs pulverized OS (median size 35–60 μm and caloric value 8.16 MJ/kg [9]) that is fed to a combustion chamber using hot air as the transport medium. In addition, secondary hot air is fed to the furnace to ensure intensive fuel combustion.

During combustion, the fuel mineral matter undergoes various conversion processes and ash is formed [27]. The residence time of the fuel in the combustion furnace is short; high-temperature combustion (1350–1450°C) ensures that most carbonate mineral phases decompose and clay minerals melt, which controls the formation of secondary Ca-silicate and Ca-Al-silicate phases [27, 28]. From a conservation viewpoint, the biggest problems with the use of PF technology are the atmospheric emissions of SO<sub>2</sub>, which can be as high as ~2200 mg/Nm<sup>3</sup> in the combustion gas [29], CO<sub>2</sub>, as well as the production of highly alkaline ash, which may contain up to 26% free lime (CaO<sub>free</sub>). All of these occur regardless of the ash separation system used [9]. One way to reduce SO<sub>2</sub> emissions is to improve the capture effect of SO<sub>2</sub> in the PF boilers, without reducing the efficiency of the energy blocks. Outdated PF combustion technology requires constant renovation and upgrading to fulfill the stringent requirements in the EU [30]. Therefore, to simultaneously improve the efficiency and decrease hazardous emissions, some PF blocks have been decommissioned and replaced with CFB technology in the past decade. CFB technology has a smaller environmental impact while combusting low-grade fuel [26].

### **1.2.2 Circulating fluidized bed technology**

CFB technology has rapidly developed since 2005 and has an important role in the Estonian energy industry. CFB boilers are operated in a rapid turbulent gaseous suspension of OS particles that have a median size of between 1–2 mm and range from fine dust up to 10 mm [27]. Finely ground solid fuel with a heating value of 8.0–11.0 MJ/kg [9] is burned in an air stream directed into the combustion chamber from below creating a so-called fluidized bed [28, 31]. The combustion temperatures (750–850°C) are substantially lower compared with PF boilers. Higher temperatures are not required because the fuel is fed into the combustion bed at a temperature equal to or slightly higher than the fuel ignition temperature that supports continuous combustion [27, 31]. After exiting the furnace, the coarse ash particles are separated from the flue gas in a separator and directed from the sedimentation chamber either directly or through a heat exchanger back into the furnace. As a result, a permanent circulating circuit of ash particles is formed. The high content of carbonate minerals makes OS advantageous for SO<sub>2</sub> binding (sulfur dioxide in flue gas is almost zero) in CFB boilers without the need for additional lime to control sulfur emissions. The ash contains enough free lime to bind SO<sub>2</sub>, thereby forming a solid anhydrite phase (up to 29.9 wt%) in the ash [9, 28, 27, 31]. The concentration of NO<sub>x</sub> in the flue gas for upgraded OS remains well below the regulated level of 200 mg/Nm<sup>3</sup> [32]. Under these combustion conditions, dolomite is completely decomposed yet calcite and clay mineral phases are only partially decomposed. As a consequence, the ash generated in a CFB contains a higher fraction of residual phases comparing with the ash generated using PF technology [27].

### 1.2.3 Solid heat carrier technology

The total amount of black ash residue that has been produced at Estonian shale oil retorting plants remains relatively small. The shale oil producers in Estonia are shifting their focus and oil production could potentially rise to over a million tons per year if new oil production retorts are installed. Both gaseous heat carrier and solid heat carrier (SHC) retorts are used to produce shale oil using Enefit (Eesti Energia Oil Industry) and Petroter technology (VKG OIL Ltd.). In the SHC process, the OS is heated in the absence of oxygen by continuously mixing combusted retorting residue at  $\sim 800^{\circ}\text{C}$  [33, 34]. During the last stage of the process, the retorting residue is combusted in an aero furnace at temperatures up to  $950^{\circ}\text{C}$ . The resulting solid residue consists of mainly calcite, quartz, K-feldspar, dolomite, Ca-silicates and oldhamite, with only trace amounts of  $\text{CaO}_{\text{free}}$  [35]. The composition of this residue is similar to the ash produced in CFB furnaces within the thermal power plants, but contains up to a few percent of unburnt organic matter due to the residence time of the combustion stage [34, 36]. About 87% of the initial sulfur remains in the solid residue. The Enefit Technology process is a modification of the Galoter process being developed by Enefit Outotec Technology [37]. Compared to the traditional Galoter technology, the Enefit process allows for complete combustion of carbonaceous residue and improves the energy efficiency by maximizing the utilization of waste heat, and utilizes less water for quenching. According to its promoters, the Enefit process has a lower retorting time compared to the classical Galoter process, and therefore, has greater throughput. All of the organic matter is fully utilized, and high performance in oil extraction is further aided by additional revenue streams in the Estonian Enefit280 oil plant [37].

In the Estonian registry of waste, the solid residues described above are registered as hazardous waste, due to the high alkalinity ( $\text{pH} < 11.5$  [38]) of their leachates, untreated or unused, poses a potential long-term environmental risk.

### 1.2.4 Atmospheric emissions

The above mentioned power plants in Estonia, excepting Enefit280, are considered to be the major source of air pollution in the region. The main contaminants are  $\text{SO}_x$ ,  $\text{NO}_x$ , particulate matter, and  $\text{CO}_2$ .

To follow EU requirements, Estonia is obligated to limit the annual  $\text{SO}_2$  emissions to 25 000 tons. However, because PF combustion technology leads to relatively high  $\text{SO}_2$  emissions [34], the flue gas desulfurization systems within PF power units are permitted to follow a specific emission of  $400 \text{ mg}/\text{Nm}^3$  of  $\text{SO}_2$  [29]. CFBs almost completely eliminate sulfur oxide emissions which are typically below  $15 \text{ mg}/\text{Nm}^3$  [32]. This technology allows the sulfur compounds to bind with the solid mineral waste [39]. At the end of 2013, one boiler at an Estonian power plant was equipped with a  $\text{NO}_x$  capture system. This has reduced its  $\text{NO}_x$  emissions by about two times from 14 to 8 Mt  $\text{NO}_x$  per year. The

installation of nitrogen emission reducing systems in seven power plant boilers near Narva came online in 2014 to extend their lives beyond 2016 when stricter environmental requirements will begin to be enforced in the EU [37]. It has been shown that between 1–2% of the ash produced is emitted into the atmosphere because the filters do not capture all ash particles that form during OS combustion. Renovation of the power units and installing electrostatic precipitators has led to a reduction of fly ash particles [40], still the amount of emissions is remarkable with 8.5 Mt emitted in 2014 [37]. Dust emissions are not solely a localized problem because fine particles can be transported far from their source [40]. Due to the extensive use of OS for energy production, Estonia is one of the highest per-capita CO<sub>2</sub> emitters among EU Member States [37] and is ranked 19<sup>th</sup> overall worldwide [41]. The combustion of OS is characterized by elevated specific carbon emissions due to the high content of mineral carbonates (limestone and dolomite) in the OS. Many types of OS are rich in carbonate mineral phases [42, 43], which means that, in addition to CO<sub>2</sub> emissions from burning organic matter, significant quantities of this gas are also released due to the partial or complete thermal dissociation of carbonate phases. In the new Enefit280 plant, the content of incomplete combustion products in the flue gas is very low and all air emission indicators are significantly lower than those of the older technology. OS gas combustion generates considerably less CO<sub>2</sub> than direct combustion of OS [37]. Also, the implementation of oxy-fuel technology can act to decrease CO<sub>2</sub> emissions [44]. However, both proposed and upcoming regulatory changes have reduced power plant emissions and changed the mineral residue content.

### **1.2.5 Waste ashes from oil shale processing**

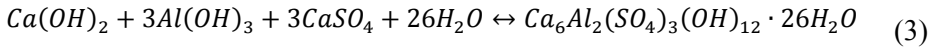
Oil shale processing generates vast amounts of different types of solid waste. The composition of these wastes depends on both the raw OS composition and processing conditions [28]. Between 45–48% of the OS dry matter remains as solid waste, which is nearly an order of magnitude more than is produced from a typical coal fuel [45]. The mineral forms found in the waste either exist in the original OS, perhaps with changed structure, or are formed during processing. The oil shale ashes (OSA) from thermal power plants contain mainly CaO<sub>free</sub>, Ca-sulfate, secondary Ca(Mg)-silicate minerals, and an amorphous Al-Si glass phase [9, 27, 46]. The combustion conditions – in both PF and CFB furnaces ensure that all of the organic matter contained in the OS (up to 65% by mass and mainly kerogen [47]) is combusted [28]. Eesti Energia, the major power utility company in Estonia, deposited 7.9 Mt of OSA and emitted 12.8 Mt of CO<sub>2</sub> in 2014 [37]. The largest OS retorting company in Estonia, VKG OIL Ltd. processed 2.9 Mt of OS in 2014 while producing 433 000 t of shale oil [48]. In 2013, VKG processed 2.8 Mt of OS, generated ~1.48 Mt of ash, and ~970 000 t of semicoke [49]. Thus, the extensive use of OS is among the most serious environmental problems that Estonia currently faces.

Thus, efforts have to be made to minimize the environmental impact of OS processing wastes by increasing the share of utilization and reducing the environmental impact of the waste deposits.

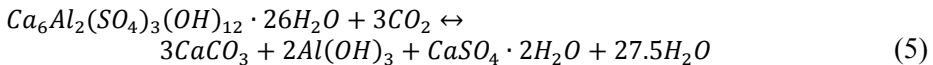
## 1.2.6 Hydraulic transportation and open-air deposition of ash

Long-term operating experience shows that hydraulic transport and open-air deposition of mineral waste formed by OS combustion have proven to be the most economically viable handling methods. Approximately 95% of the mineral waste is transported to ash fields and remains there for indefinite periods. Today, almost 300 Mt of mineral waste that take up ~500 ha of space is added to the Estonian ash deposits every year [37, 41].

OSA handling consists of different processes: transportation of ash (mixing of the ash collected from the boilers in water slurry with water- ash ratio of 1:15–1:20), depositing the ash slurry in fields through a pipe system, and recirculating the transportation waters that settle, thereby forming a closed recirculation system. The volume of water that circulates in the system is influenced by both precipitation/evaporation, and chemical binding by the ash. This method of solid waste transfer is subject to several environmental risks such as possible leakages or infiltration that could lead to the contamination of surface and groundwater [27, 50]. In this recirculating system, the water contacts with the ash multiple times and both the composition and fluid dynamic properties of the suspension continuously change. OSA is characterized by high concentrations of lime and anhydrite (Table 1) that are hydrated upon contact with the recirculation water:



CaO conversion (fast) into portlandite (Eq. (1)) and CaSO<sub>4</sub> to gypsum (Eq. (2)) and ettringite (Eq. (3)), are the most important reactions that occur in the OSA hydration processes which continues to occur in the open plateaus where they are deposited [50, 51]. The alkalinity of the leachates depends on both the composition of the ash and diagenetic evolution of the sediments. Under atmospheric conditions, portlandite and ettringite are metastable (controlled by pH) Eqs. (4) and (5).



Ettringite is a stable mineral phase in both alkali and sulfate-rich environments, however, under acidic conditions it dissolves incongruently into gypsum, aragonite/calcite, Al-hydroxide, and/or Ca-aluminate type phases [50, 51]. The transformation of the secondary Ca-silicate phases can be regarded as minor, although belite can react with atmospheric CO<sub>2</sub> to form both calcite (CaCO<sub>3</sub>) and quartz (SiO<sub>2</sub>):



OS retorting residues are characterized by a high sulfide content (mainly as CaS) [34, 35, 52]. CaS is chemically unstable under atmospheric conditions and also disintegrates at the ash dump site during leaching. Upon hydration, CaS decomposes and releases sulfides into the environment and generates toxic H<sub>2</sub>S under certain conditions [53]. In suspensions where HS<sup>-</sup> (main sulfide form in the present model systems pH>11) predominates, sulfites, thiosulfates, and sulfates are observed together with other sulfide oxidation-reduction products [54, 55].

The pH of the ash–water system seems to be controlled by the ratio between the plentiful Ca and the concentration of S in the residue. Based on the Ca/S ratio (high Ca/S molar ratio 8–10 characterized Estonian OS [28]) and pH, mineral waste can become strongly alkaline waste, if CaO dissolution dominates, or mildly alkaline, if CaSO<sub>4</sub> dissolution dominates [56]. Dissolution of CaS generates hydroxide ions, while additional CaS produces a higher value for the system pH [57]. The typically high alkalinity (pH 12–13) of OSA sediment waters is maintained by the content of the main Ca-hydrate phases [51]. However, the pH of the ash-water system is not static and changes over time. It has been estimated that complete neutralization of OSA fields under natural conditions may take hundreds of years [44].

## 1.2.7 Prospects for oil shale ash utilization

To date, only a small percentage of OS mineral waste has been utilized, either in the building materials industry, in agriculture as a liming agent, or during road construction [27, 37]. The EU is constantly introducing stricter conditions for greenhouse gas (GHG) emissions and other harmful pollutants and regularly introduces new initiatives to promote the adoption of environmental technology and improved waste recovery and recycling techniques, the economics of which affect the OS sector in Estonia. For example, one goal is to reduce GHG emissions by between 20–30% and annual SO<sub>2</sub> emissions to 25 thousand tons by 2020, which is 2.5 times lower than the current limits [37]. Because Estonia is located in the northern, shallow part of the Baltic sedimentary basin that possesses a limited amount of potable water, its CO<sub>2</sub> geological storage capacity has been estimated as zero [58, 59]. The countries without geological storage sites could adopt *exsitu* mineral carbonation for CO<sub>2</sub> fixation. Natural Ca- and

Mg-rich minerals (serpentinite, olivine, wollastonite, talc) [60] as well as several alkali wastes, such as steel slag and ashes from power plants [11-18, 21, 22, 61] have been studied as possible CO<sub>2</sub> sorbents (Table 1). It has been demonstrated that an OS ash–water suspension is able to bind up to 290 kg of CO<sub>2</sub> per ton of ash [62]. Moreover, upgrading industrial wastes into commercial products (e.g., precipitated calcium carbonate or magnesium carbonate) [10, 61-67] via the carbonation route is one of the most promising directions for achieving a cost-effective CO<sub>2</sub> sequestration process. In recent years, various carbonation routes have been studied in various reactor configurations to produce PCC-type materials using both OSA and its leaching waters that are saturated with calcium and accompanied ions, including sulfur [46, 68-70].

Table 2. pH–range, TDS and chemical composition(mg/kg) in waste ash leaching waters

	OSA PF	OSA SHC	OSA CFB	Coal ash FGD	Coal ash	Cement kiln dust	Steel - making slag	Paper sludge ash
Reference	[71,72,73]	[34,35,74]	[71,73,75]	[76,77]	[78,79]	[16,80]	[18,81,82]	[16,80]
Components		Values						
pH	12.2-12.7	12.5-12.9	12.2-13.0	7.4-8.1	11.7-12.9	12.9-13.2	12-13	11.6-13.1
TDS	5400-7150	30700	6200-6960	-	4820-6830	-	1970-2480	4410
Ca <sup>2+</sup>	7920-8780	4000-7750	9290	5640-8070	1670-10900	high	8210-9945	high
Na <sup>+</sup>	4-12	-	17-18	30-40	36-172	-	>3000	-
K <sup>+</sup>	72-572	-	76-578	1130	115-284	-	450-760	-
SO <sub>4</sub> <sup>2-</sup>	4500-9910	495-800	5160-11980	14590-15850	5000-14000	9100-34500	1450-3220	up to 6900
Cl <sup>-</sup>	250-380	1170	720-1070	8410	600	1000-9800	80-200	<9
S <sup>2-</sup>	5	750	25	-	-	-	high	-
CO <sub>3</sub> <sup>2-</sup>	60-180	180	180-360	-	-	-	6-54	-
PO <sub>4</sub> <sup>2-</sup>	60-120	-	-	<120	-	-	<0.1	-
Mg <sup>2+</sup>	<0.1	0-72	<0.2	340-410	25-172	-	~1	-
Phenols	-	7	-	-	-	-	-	-
DOC	270	59-320	100	-	-	-	-	-

It has been forecasted that the use of OS to produce electricity will decrease in the next few years and the production of oil will increase. The proportional change in the types of waste generated will also influence long-term waste management decisions. Waste minimization strategies [83] drive the development of new recycling technologies. These new technologies must pay attention to the various components in the ash that may leach in an aqueous medium and cause problems (high pH, release of sulfur compounds, etc.) at both disposal sites and during processing. In addition to the calcium leaching dynamics, one must also consider the interactions between different substances ( $\text{Ca}^{2+}$ ,  $\text{SO}_4^{2-}$ ,  $\text{K}^+$ ,  $\text{Na}^+$ ) that may leach from the waste ash and alkaline residues (Table 2).

The dynamics and equilibrium of leaching  $\text{Ca}^{2+}$  and accompanying ions from OSAs has been studied and it is known that the major ions in OSA leachates are  $\text{Ca}^{2+}$  and  $\text{SO}_4^{2-}$ . It is further known that sulfur is the major soluble element in alkaline wastes, together with Ca (Table 2). After calcium,  $\text{K}^+$  is the second most abundant cation present in OSA leachates, however,  $\text{Na}^+$ ,  $\text{Al}^{3+}$ , and  $\text{Mg}^{2+}$  have been also identified [71, 73]. In addition,  $\text{Cl}^-$ ,  $\text{S}^{2-}$ ,  $\text{SO}_3^{2-}$ ,  $\text{S}_2\text{O}_3^{2-}$ , and  $\text{PO}_4^{3-}$  have been detected in small concentrations [72, 84]. The leachability of heavy metals is typically below the detection limit [71, 73]. The mean electrical conductivity (EC) is also within the range of published data for alkaline mineral waste leachates [71]. The phase composition, occurrence, and quantity of Ca-containing components in mineral waste all play a significant role in the leaching behavior of OSA samples.

The latter is important when determining whether the environmental safety standards are being met or when exploring possible effects that could influence the utilization by-products. Investigations into the dissolution of OSAs have shown that  $\text{Ca}(\text{OH})_2$ ,  $\text{CaSO}_4 \cdot 2\text{H}_2\text{O}$  and  $\text{CaS}$  are the main water-soluble Ca and S species in aqueous systems and these influence the chemical composition of ash leachates [85].

## **1.3 Main water-soluble Ca and S compounds – oil shale mineral residues**

### **1.3.1 Calcium and Sulfur in solid fossil fuels**

Calcium is an important component within fossil fuels. While Ca is not regarded as an element of concern, it does play a primary role during the transformations that occur in fossil fuel residues [9, 10, 56]. Sulfur (S) may be present in various fossil fuels at different concentrations and in various forms (elemental, molecular form attached to hydrocarbons, and as sulfide) [6]. S occurs in relatively high concentrations in fossil fuels, e.g. Estonian OS is characterized by a content of sulfur 1.4–1.8 %, in coal <1–14 %, petroleum 0.05–14 % [6, 28]. S is the major soluble element in fossil fuel mineral wastes, along with calcium [6, 56].

### 1.3.2 Calcium and Sulfur in mineral waste

The leaching behavior of Ca and S is associated with the phase composition of the OS mineral residues.

The mineral part of OS waste Ca is present in multiple forms, primarily as lime (10–25 wt%, depending on the combustion technology), anhydrite, and calcite and within the glassy matrix as silicates [9, 34, 36]. The amount of calcium (relation to that of sulfur) dictates the OS ash-water system pH, and most trace elements indicate a pH-dependent solubility. The presence of calcium is essential for the precipitation of ettringite and other secondary Ca-hydrated phases that involve and maintain environmentally important elements (e.g. As, Cr, Se). Therefore, it can be stated that Ca controls the leachate composition for the most part [50, 51, 56].

The distribution of sulfur between gaseous and solid OS phases depends on the combustion technology [28]. Sulfur (<2% in Estonian OS) remains in the OS power plant ashes mainly as sulfates (1.1–4.8 wt%), but also as sulfides (0.006–0.28 wt%) [9, 84], and in the solid waste of shale oil production mainly as sulfides (1.2–3.0 wt%) with a small amount of sulfates (0.36–1.0 wt%) [55, 85, 86]. The absolute level of leachability varies depending upon the chemical environment (i.e. system pH and oxidants) [34, 52, 55, 71, 73]. The sulfate leaching limit of 1000 mg/kg waste is generally exceeded with industrial alkaline residues (Table 2).

OSA disposal plays an important role in terms of the fate of water-soluble Ca compounds such as lime and anhydrite, and, from an environmental point of view, is also important for the behavior of aqueous calcium sulfide. Thus, the key components are: CaO (model component with Ca(OH)<sub>2</sub>), CaSO<sub>4</sub> (model component CaSO<sub>4</sub> 2H<sub>2</sub>O), and CaS.

#### 1.3.2.1 Lime

The most active compound in oil shale mineral waste is free lime (CaO<sub>free</sub>), which, when it comes into contact with water, provides a strong alkaline effect (pH>12) and a leachate saturated with calcium ions. The conversion of calcium oxide to calcium hydroxide (Eq. (1)) is followed by Ca(OH)<sub>2</sub> dissolution (ions form on the surface of particles and finally diffuse into the bulk solution) [87, 88], and finally by a carbonization reaction under mild conditions or when treated with flue gases (Eq. (7)) [88].



The mechanism for Ca(OH)<sub>2</sub> dissociation can be presented as a single step reaction system (Eq. (8)) [87] or as two coupled reactions (Eqs. (9)–(10)) [89].



It has been shown that the solubility of  $Ca(OH)_2$  decreases with increasing temperature, albeit with faster kinetics (the dissolution time decreases) [87, 89]. The increment of alkali concentration sharply decreases the solubility (common ion effect of  $OH^-$ ), beyond this scope, it will increase gradually with the declining pH value. The solubility of  $Ca(OH)_2$  is about 1.55–1.84 g/L as the pH value is located at 12.1–14.0 (at 25°C) [89, 90].

### 1.3.2.2 Calcium sulfate

Calcium sulfate ( $CaSO_4$ ) can be crystalized into various crystal types: gypsum ( $CaSO_4 \cdot 2H_2O$ ), hemihydrate ( $CaSO_4 \cdot 0.5H_2O$ ), soluble anhydrite (hexagonal symmetry) and insoluble anhydrite (orthorhombic).  $CaSO_4$  solubility varies by crystal type, temperature, and co-components. The slightly soluble gypsum, has attracted more attention and has been extensively studied [91]. Beyond system pH values of 3.5–11.0 the dissolution of  $CaSO_4 \cdot 2H_2O$  increases slightly:



The properties of the solution, such as density and viscosity, do not significantly change with a reduction in the pH of the solution; however, the solution properties are appreciably altered in the basic medium. The solubility of gypsum in pure water increases slightly and then decreases with an increase in temperature (in the range of 25–98°C) [92]. The solubility of  $CaSO_4 \cdot 2H_2O$  has been reported in the range of 2.1–2.6 g/L (at 25°C) [89, 93].

### 1.3.2.3 Calcium sulfide

CaS is the most hazardous sulfur based ash component for the environment [39, 94]. Determining the leaching behavior of CaS under inert conditions allows one to quantify the dissolution environment in the deeper layers within ash piles. The dissolution of calcium sulfide is defined in Eq. (12) [57, 94].



CaS dissolution occurs together with a notable change in the system pH due to the formation of both  $HS^-$  and  $H_2S$  as  $S^{2-}$  dissociation products (Eq. (13) and (14)) [57].



Several processes have been proposed for sulfide oxidation in aqueous systems. Both the reaction mechanism and the nature of the products strongly depend on the system pH [94–97]. Mölder et al. proposed the following chain of oxidation reactions for deeply alkaline systems [94], where  $HS^-$  is the main reacting sulfide species and the most stable reduced sulfide oxidation forms are thiosulfate, given in Eq. (15), and sulfate, given by Eq. (16):



Currently, the literature information about CaS leaching is ambiguous, including different reported values ( $<1.38 \cdot 10^{-2}$  to  $2.94 \cdot 10^{-3}$  mol/L) for the solubility of CaS (*Table 1 in Paper II*).

## 1.4 Summary of the literature review and objectives of the thesis

Globally, a huge amount of alkaline industrial waste is generated every year. The residues have a number of similar characteristics such as high levels of calcium and sulfur content, electrical conductivity, pH of aqueous systems, and persistent minerals.

The safe disposal of mineral waste and excessive atmospheric emissions are among the most serious problems caused by the extensive use of oil shale for both power and shale oil production. Currently, only up to 5% of oil shale mineral wastes are utilized.

When OSA (as a mineral waste), comes in contact with water (during hydro-transportation and open-air deposition of ash), several ions leach out (mainly calcium and sulfur) make the pH of the aqueous system highly alkaline (pH 12–13).

In light of the constantly tightening waste management regulations, it is important to find new environmentally safe handling applications for both current and future ash flows as well as for the large inventory of deposited oil shale wastes. In all of these applications, OSA leaching is one of the key processes.

So far, Ca extraction from OSA has been described by mass transfer models to estimate its potential as an alternative calcium source for both  $CO_2$  absorption

and to produce PCC-type fillers. However, the mechanism of OSA dissolution is more complex and one must be also taken into consideration the interactions between the different species in aqueous OSA systems. Mathematical models which define the operating parameters and simulate the leaching of water-soluble OSA components would allow one to determine the usability of different OSA types as Ca-source in PCC-production.

To provide a better understanding of the behavior of OSA suspensions and leachates especially by wet deposition, it is necessary to develop the methodology, which incorporates dissolution mechanisms of water-soluble Ca compounds such as lime and anhydrite, as well as environmental point of view is also important for the behavior calcium sulfide aqueous medium. In this regard, several values of both CaS solubility and equilibrium constants of dissolution reactions are illustrated in the scientific literature. To reconcile these differences, both solubility and dissolution mechanism of CaS under inert and air conditions have to be investigated.

Thus, the aims of this doctoral work were: (i) to investigate the dissolution mechanisms of the main water-soluble Ca-compounds ( $\text{Ca}(\text{OH})_2$ ,  $\text{CaSO}_4 \cdot 2\text{H}_2\text{O}$ , CaS) of OSAs, (ii) to propose models that account for both thermodynamic equilibrium and reaction kinetics and can be verified using measurable parameters, (iii) to investigate the consistency of the theoretical models with experimental data for various model ash systems and find the optimal model parameters, (iv) to simulate various OSA leaching processes using these models.

The aim was to develop the methodology, which can be used for the calculations of the ash streams pollution as well as for designing the leaching reactor. With the results of these studies, it is possible to design various industrial processes such as leaching, before aqueous carbonation processes, and explore more complex and safe waste handling technologies.

## 2. MATERIALS AND METHODS

### 2.1 Experimental methods and procedures

An outline of the chemical systems studied in this work are presented in Table 3. The dissolution mechanism of the main water-soluble Ca-compounds (as pure systems  $\text{Ca}(\text{OH})_2$ ,  $\text{CaSO}_4 \cdot 2\text{H}_2\text{O}$  and  $\text{CaS}$ ) of three types of oil shale (OS) mineral waste (from pulverized firing – PF, circulating fluidized bed combustion – CFB and solid heat carrier – SHC). For comparison, the binary ( $\text{Ca}(\text{OH})_2$ – $\text{CaSO}_4 \cdot 2\text{H}_2\text{O}$ – $\text{H}_2\text{O}$ ) and ternary ( $\text{Ca}(\text{OH})_2$ – $\text{CaSO}_4 \cdot 2\text{H}_2\text{O}$ – $\text{CaS}$ – $\text{H}_2\text{O}$ ) model systems were prepared to match the composition of OS processing ashes, was investigated. The selected solid/water ratios ranged from 1/5 to 1/250.

Table 3. Outline of the chemical systems under investigation

Investigated systems				Paper	
		Leaching thermodynamics	Leaching kinetics		
Pure systems	$\text{Ca}(\text{OH})_2 + \text{H}_2\text{O}$		x	x	I
	$\text{CaSO}_4 + \text{H}_2\text{O}$		x	x	
	$\text{CaS} + \text{H}_2\text{O}$	inert	x	x	II
		in air	x	x	
Binary system	$\text{Ca}(\text{OH})_2 + \text{CaSO}_4 + \text{H}_2\text{O}$		x	x;-	I; III
Ternary system	$\text{Ca}(\text{OH})_2 + \text{CaSO}_4 + \text{CaS} + \text{H}_2\text{O}$		x	x	III
Ash systems	CFBA+ $\text{H}_2\text{O}$		x	x	
	PFA+ $\text{H}_2\text{O}$		x	x	
	SHCA + $\text{H}_2\text{O}$		x	x	

The apparatus used to study these systems are presented in more detail below.

#### 2.1.1 Applied methods

The chemical analysis methods used to characterize the solid liquid, and gaseous phases are briefly described in Table 4.

Table 4. Applied methods

Properties	Characterization methods
<b>Solid phase</b>	
Chemical composition	free lime ( $\text{CaO}_{\text{free}}$ ) <sup>1</sup> (ethylene glycol method), different forms of sulfur (sulfate and sulfide), total carbon (TC) and inorganic carbon (TIC) <sup>1</sup> (Electra CS - 580 Carbon/Sulfur Determinator)
Specific surface area <sup>2</sup>	BET Kelvin 1042 sorptometer
Phase composition <sup>3</sup>	X-ray fluorescence spectroscopy (XRF, Rigakus Primus II) quantitative X-ray diffraction (XRD, Bruker D8 Advanced) methods
<b>Liquid phase</b>	
Chemical analysis	$\text{Ca}^{2+}$ (ISO – 6058:1984) [98], total sulfide (sum of dissolved $\text{H}_2\text{S}$ , $\text{HS}^-$ and $\text{S}^{2-}$ ) and $\text{SO}_4^{2-}$ (Lovibond Spectro Direct spectrometer, method: DPD/Catalyst, Bariumsulfate – Turbidity), total reduced sulfur (total sulfide and other sulfide intermediate oxidative forms) iodometrically [99], alkalinity (ISO – 9963-1: 1994(E)) [99], dissolved oxygen (oxygen-meter Marvet Junior MJ2000 (Elke Sensor, Estonia)), pH (MT SevenGo pH and Knick Portamess 913 pH; pH-meter sensor: Hamilton Polylyte Plus VP360), conductivity (Mettler Toledo SevenGO Duo Pro with LabX software).
<b>Gas phase</b>	
$\text{O}_2$ , $\text{N}_2$ , $\text{H}_2\text{S}$ content	flue gas analyzer (Testo 350-S/XI)

<sup>1</sup> Performed by H. Ehala and R. Viires at the Laboratory of Inorganic Materials, TUT

<sup>2</sup> Performed by Dr. M. Uibu at the Laboratory of Inorganic Materials, TUT

<sup>3</sup> Performed by Prof. K Kirsimäe at the Institute of Geology, UT

## 2.1.2 Characterization of materials

PF ash and CFB ash residues from electricity production, together with SHC ash from shale oil production residue, were used as Ca-rich raw materials. The CFB ash used was a mixture of ashes taken from a common ash silo, whereby the ash was collected from different equipment before depositing on the ash fields. The PF ashes originated from a cyclone separator, from the electricity production boilers. CFB and PF ashes were collected from the Eesti Power Plant of Narva Power Plants in 2011. The SHC ash was the final residue from the shale oil production process at the Viru Keemia Group Ltd. retorting plant. The main characteristics of the three ashes are provided in *Paper III: Table 1*.

The model chemical systems were composed using  $\text{Ca}(\text{OH})_2$  (BDH, purity 95%) as a  $\text{Ca}^{2+}$ -ion source,  $\text{CaSO}_4 \cdot 2\text{H}_2\text{O}$  (Iach:ner, purity 99%) as a  $\text{SO}_4^{2-}$  ion source, and CaS (Alfa Aeser, purity 99.9%) as a  $\text{S}^{2-}$  ion source. The mean size of the OSAs particles studied lie in the same range as the model systems constructed from pure components *Paper I: Table 1*. The model systems were

prepared to match the composition of the OSAs so that we may compare the results from each.

## 2.1.3 Experimental procedure – Apparatuses

### 2.1.3.1 Experimental set-ups for thermodynamic studies

To achieve an equilibrium state, each ash–water suspension was prepared in a 50 mL centrifuge tube, hermetically sealed, and kept for 3 h in an overhead shaker (GFL 3025) at 45 rpm at room temperature (25°C). The pH and electrical conductivity (EC) of these suspensions were measured immediately after the 3 h period, and then vacuum filtered using Munktell 100 g·m<sup>-2</sup> (1-2µm) filter paper.

### 2.1.3.2 Experimental set-ups for kinetic studies

Batch kinetic dissolution experiments were carried out in a 1 L Lara Controlled Lab Reactor (LCLR) (Figure 1) operated with software provided by the manufacturer (Radleys).

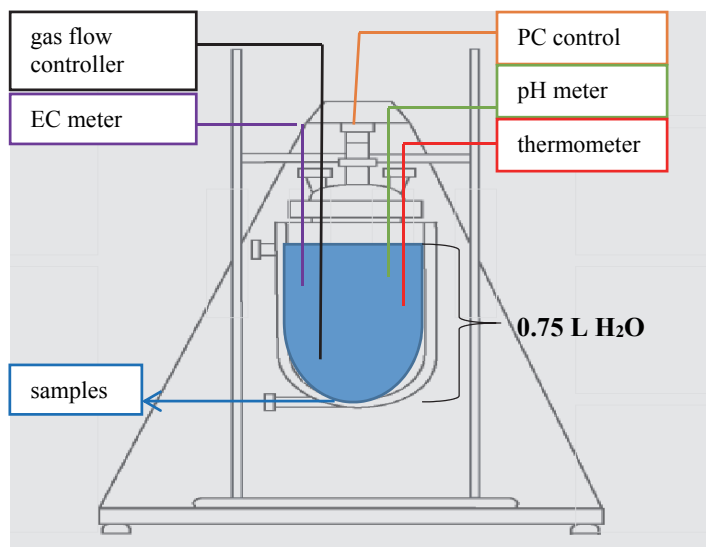
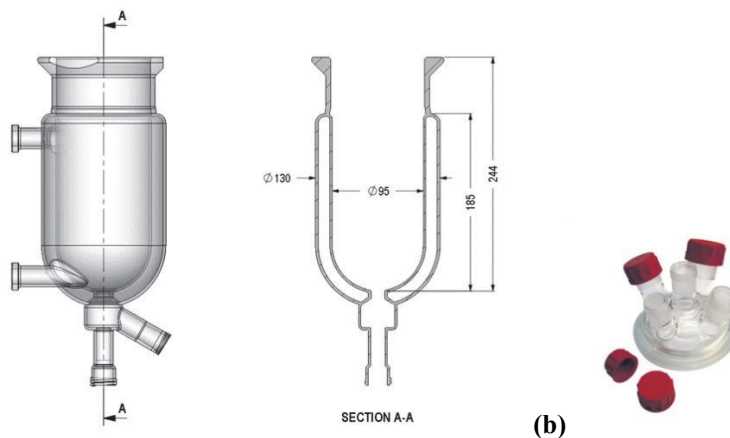


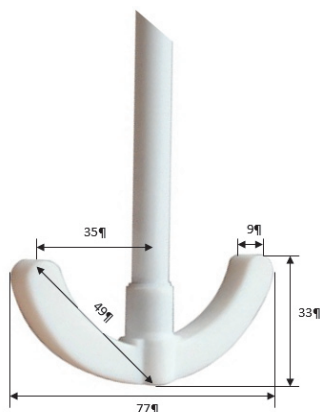
Figure 1. A single reaction batch reactor system.

During the experiment, the composition of the gaseous phase, system pH, and temperature were recorded every 10 sec. Initially, 0.750 L of deionized water with a conductivity of 0.05 µS/cm was poured into the reactor. The vessel was single jacketed with an internal height of 185 mm and diameter of 95 mm, an external diameter of 510 mm (Figure 2a [100]). The vessel was purified with an acid solution and distilled water (more than three times) prior to each experiment. The vessel lid (Figure 2b) and the unused ports were tightly sealed

during the experiment. The suspensions were continuously mixed with an anchor type stirrer, 80mm  $\varnothing$ , 455mm long x 10mm  $\varnothing$  shaft (Figure 3 [100]), and a thermostat (Huber Unistat 405). The entire system was kept at 25 $\pm$  0.1  $^{\circ}$ C during the course of the experiment.



**(a)** *Single Jacket 1L vessel size parameters in mm (a) and Lara reactor vessel Lid (b).*



*PTFE Anchor Stirrer paddle, size parameters in mm.*

In order to define the power characteristics of the mixer, the power consumption at various revolutions was measured both in pure water and the experimental suspensions. The net amount of power used for mixing was calculated from the difference between the consumed power at a given rotation speed and the power consumed at an idle state (3 W). The latter was considered to be the minimal power required to overcome the friction of the bearings in the absence of a fluid.

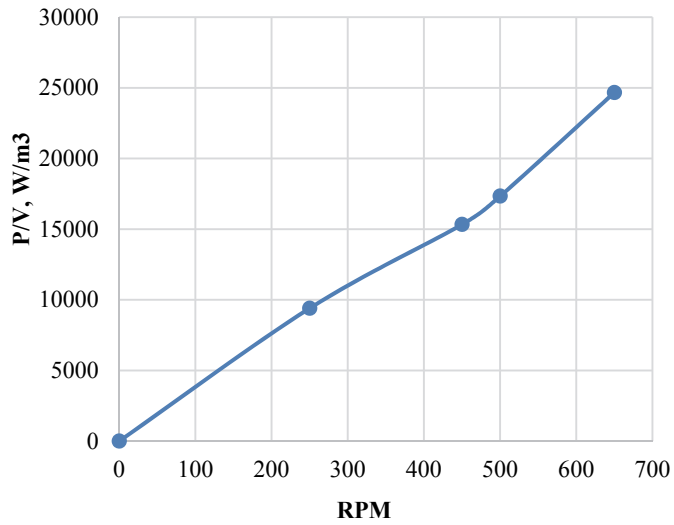


Figure 4. *The consumed power of the suspension mixing at different mixing speeds.*

From Figure 4 we deduce that 250 rpm is not a limit of speed ratio. This opens up an opportunity to describe the leaching process at higher speeds in both pure water and in ash suspensions (S/L 1/250 to 1/10), torque difference between pure water and the suspensions were negligible.



Figure 5. *Mixing at 250 rpm (up) and at 650 rpm (down).*

Due to the formation of an extensive whirlpool, a rotational speed of 650 rpm (Figure 5, down) was found to be too much for our systems, the recommended stirrer speed from manual of Lara equipment's (250 rpm) was used to further work. Considering the vessel geometry, stirrer, and other experimental parameters, the P/V dependencies (according to 250 rpm specific power is  $9400 \text{ W/m}^3$ ) can be transferred to a larger reactor.

The control software followed the recipe (Figure 6a and Figure 6b), respectively the inert and air systems): (i) The stirrer was turned on (250 rpm), (ii) for the inert system  $\text{N}_2$  was bubbled through the water for 20 minutes, (iii) the stirring was paused to allow one to add quickly a specific amount of solid phase using a funnel, finally (iv) mixing continued at the same speed in a closed system.

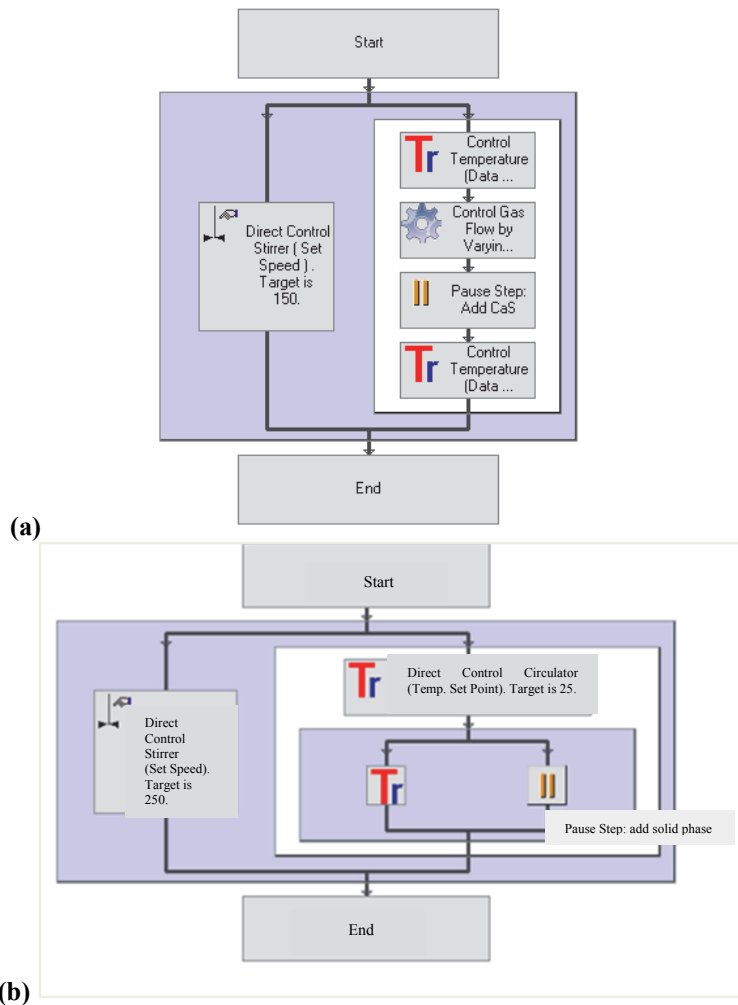


Figure 6. The recipe of the experiment as it proceeds in inert (a) and in air (b) system.

The software automatically stepped through each of the steps in the recipe, until it reached the end. The process temperature was monitored with a control circulator (Control Temperature of Process), and the target value was sent directly to the device. The Fixed Setpoint enables users to enter a single target value. In our experiments we set this to 25°C for 10 minutes and, after a pause, 25°C for either 130 or 230 minutes. The Pause step suspend the reaction at a given point and then waited for a user to return to carry out the instruction on the message “add solid phase” and un-paused the recipe. The Analysis section allows one to review, analyze, and export experiment data. After each experiment, the contents of the reactor were filtered. Air systems were filtered using a vacuum filter while inert systems were hermetically obtained with a syringe to avoid further oxidation and filtrated using a syringe filters with a Luer tip, FB0674-1,  $\varnothing$  13 mm, pore size 0.45 $\mu$ m. The chemical composition of the filtrate was then analyzed (see Section 2.1.1; Table 4).

## 2.2 Modeling

The equilibrium calculations were performed using thermodynamic programs based on the Gibbs free energy minimization technique. The HSC Chemistry<sup>®</sup> 7.1 program [102] was used to determine both the composition of each phase and predict the equilibrium composition of the each system under investigation.

Kinetic calculations and dissolution process simulations were performed using the MODEST 6.1 software package [103] which is designed for various model building tasks such as simulation, parameter estimation, sensitivity analysis, and optimization. The software consists of a FORTRAN 95/90 library of objective functions, solvers, and optimizers linked to model problem-dependent routines. Each system of differential equations was solved by the means of linear multi-step methods implemented in ODESSA (a systematized collection of the ordinary differential equations solver), which is based on LSODE (Livermore Solver for Ordinary Differential Equations) software [104].

In addition, both equilibrium calculations and process modeling were carried out using ASPEN Plus V8.6 (APV86) software, which is a process modeling tool for conceptual design, optimization, and performance monitoring widely used in the chemical, mining, and solid fuel power generation industries [105].

### 3. RESULTS AND DISCUSSION

#### 3.1 Leachability of pure systems

To determine the feasibility of the technologies for upgrading OS mineral waste, it is useful to create mathematical models that provide the operating parameters of the process and simulate the leaching of water-soluble OSA components, the binding of CO<sub>2</sub> and SO<sub>2</sub> from flue gases, and the crystallization of solid products in the multi-phase ash leachate – flue gas system. In order to better understand the behaviour and impact of the key components on the OSA leaching process the dissolution mechanisms aspects of main water-soluble Ca-species in OS ash-water systems (Ca(OH)<sub>2</sub>, CaSO<sub>4</sub>·2H<sub>2</sub>O and CaS) are discussed in detail in *Paper I* and *Paper II*.

##### 3.1.1 Ca(OH)<sub>2</sub>-H<sub>2</sub>O system

The modeling algorithms that account for both thermodynamic equilibrium and reaction kinetics were proposed after investigating the dissolution of portlandite in pure deionized water at room temperature (25°C) (*Paper I*).

###### 3.1.1.1 Ca(OH)<sub>2</sub> dissolution equilibrium in aqueous systems

Two approaches were applied to describe the Ca(OH)<sub>2</sub>-H<sub>2</sub>O system, *Paper I: Eqs. (1), (2)* (as a more complex approach), and *Eq. (4)* (as single step reaction system). The Aspen Plus RGibbs reactor model was employed to predict the equilibrium composition of the Ca(OH)<sub>2</sub>-H<sub>2</sub>O (*Paper I: Figure 1a*). For each of the systems defined (*Paper I: Eqs. (1), (2)* and *Eq. (4)*) the equilibrium constants was computed (*Paper I: Figures 1b*) together with the equilibrium compositions and material balance. This was also performed for dilute solutions and reported as apparent equilibrium.

###### 3.1.1.2 Ca(OH)<sub>2</sub> dissolution kinetics in the Ca(OH)<sub>2</sub>-H<sub>2</sub>O system

Kinetic models of the Ca(OH)<sub>2</sub>-H<sub>2</sub>O system were constructed using experimental data. pH profiles were measured at different concentrations of Ca(OH)<sub>2</sub>(s) which are presented in *Paper I, Figure 3*. Two dissolution models were constructed to describe the Ca(OH)<sub>2</sub>-H<sub>2</sub>O system using respective kinetics parameters. The more complex of the two approaches was expressed as a two-step first order reaction system (*Paper I: Eqs. (16) and (17)*), and the other was simplified to a one-step first order reaction system (*Paper I: Eq. (22)*). Using those dissolution models, the dynamic concentration profiles of the characteristic species that participate in the lime dissolution process was modeled using differential equations (*Paper I: Eqs. (18)-(21) and Eqs. (23)-(25)*). The reaction rate constants were determined using a parameter estimation procedure that

minimized the difference between simulations of the system using the proposed model equations and experimental data that was obtained in batch experiments at various concentrations of  $\text{Ca}(\text{OH})_2$ . This optimization approach provided values for the reaction rate constants for both the two-step ( $0.0345 \text{ s}^{-1}$  and  $0.0544 \text{ L}\cdot(\text{mol}\cdot\text{s})^{-1}$ ) and one-step ( $0.0282 \text{ s}^{-1}$ ) dissolution models (*Paper I: Eq. (16)-(17) and (22)*, respectively.). We found that the one-step  $\text{Ca}(\text{OH})_2$  dissolution model is more accurate for dilute solutions (*Paper I: Figure 5a, b, c versus d*) and the two-step model is more appropriate under more saturated conditions (*Paper I: Figure 5d vs 4d*) when the share of  $\text{CaOH}^+$  (*Paper: Figure 1a*) becomes significant enough to influence the  $\text{Ca}(\text{OH})_2$  dissolution kinetics. The two-step model elaborates the dissolution mechanism in more detail; however, the simplified one-step model provides a sufficient fit with the experimental results and is easier to handle in practice.

### 3.1.2 $\text{CaSO}_4\cdot 2\text{H}_2\text{O}-\text{H}_2\text{O}$ system

After studying the dissolution mechanisms, we measured the kinetics of the  $\text{CaSO}_4\cdot 2\text{H}_2\text{O}$  dissolution process in a batch reactor (Section 2.1 3.2).

#### 3.1.2.1 $\text{CaSO}_4\cdot 2\text{H}_2\text{O}$ dissolution equilibrium in aqueous systems

The thermodynamic equilibrium constant for the gypsum dissociation reaction (Eq. (11)) is provided in *Paper I: Eq. (7)*. The thermodynamic equilibrium for the  $\text{CaSO}_4\cdot 2\text{H}_2\text{O}-\text{H}_2\text{O}$  binary systems were modeled using the Pitzer model embedded within the Aspen Plus platform. The Pitzer model interaction parameters for both the  $\text{Ca}(\text{OH})_2-\text{H}_2\text{O}$  and  $\text{CaSO}_4\cdot 2\text{H}_2\text{O}-\text{H}_2\text{O}$  systems are presented in *Paper I: Table 2*. In that the equilibrium composition and equilibrium constant for gypsum solutions was also determined (*Paper I: Figures 2a and 2b, respectively*).

#### 3.1.2.2 $\text{CaSO}_4\cdot 2\text{H}_2\text{O}$ dissolution kinetics in the $\text{CaSO}_4\cdot 2\text{H}_2\text{O}-\text{H}_2\text{O}$ system

The next goal was to create a kinetic model of the gypsum–water system using experimental data. First, we determined the dissolution kinetics of gypsum in a batch reactor by measuring the EC profiles at different  $\text{CaSO}_4\cdot 2\text{H}_2\text{O}(\text{s})$  concentrations (*Paper I: Figure 6*). The molar concentration of  $\text{Ca}^{2+}$  at each time point was calculated using EC measurements. The correlation between the measured concentrations of EC and  $\text{Ca}^{2+}$  ( $R^2=0.99$ ) is presented in *Paper I: Figure 7*. The dissolution of gypsum in water can be expressed as *Eq. (26) in Paper I*. The reaction rate constant was evaluated ( $R^2>95\%$ ) from the differential equations (*Paper I: Eqs. (27)–(29)*) using several experimental data sets for comparison. An average value of the reaction rate constant for gypsum dissolution was found to be  $0.051 \text{ s}^{-1}$ .

We also confirmed the accuracy of the proposed dissolution models ( $R^2 > 90\%$ ) by comparing the simulation results with experimental data (*Paper I: Figure 8*) that was not used during the optimization process.

### 3.1.3 CaS–H<sub>2</sub>O system

In *Paper II*, the thermodynamics and kinetics of the CaS–H<sub>2</sub>O system at 25°C under both inert and atmospheric conditions was studied. This work allowed us to suggest a mechanism of CaS dissolution based on both thermodynamic calculations (HSC Chemistry<sup>®</sup>7.1) (*Paper II: Section 4.1.1.*) and experimental data (*Paper II: Section 4.1.2.*).

#### 3.1.3.1 CaS dissolution equilibrium in aqueous systems

The leaching behavior of CaS under inert conditions imitates the dissolution environment in the deeper layers within ash piles. The dissolution of CaS is defined in Eq. (12), and the thermodynamic equilibrium constant ( $K_I$ ) is defined in *Paper II: Eq. (6)*. Because the solution used in this paper contains an equal amount of calcium and sulfide ions ( $K_{sp} = [Ca^{2+}] \cdot [S_{sulfide}] = [Ca^{2+}] \cdot [Ca^{2+}]$ ), the value of  $K_I$  can be expressed as the square of the Ca ion concentration.

CaS dissolution occurs together with a notable change in the system pH due to the formation of both HS<sup>-</sup> and H<sub>2</sub>S as S<sup>2-</sup> dissociation products Eqs. (13) and (14). The dissociation of S<sup>2-</sup> can be characterized by the basicity constants  $K_2$  and  $K_3$  (Eq. (19) and (20) (in *Paper II* these constants are presented as  $K_{b2}$  and  $K_{b1}$ , respectively: *Eqs. (8) and (10)*).

The dissolution of CaS can also include hydrolysis, which excludes S<sup>2-</sup> formation (*Paper II: Eq. (15)*). The reaction equilibrium can be calculated as the ion-product  $K_s$  (*Paper II: Eq. (16)*). The quotient of  $K_s$  to the second basicity constant simplifies to *Eq. (6)* in *Paper II*:

$$K_s/K_2 = [Ca^{2+}] \times [S^{2-}] = K_1 \quad (17)$$

Although several processes have been proposed for sulfide oxidation in aqueous systems we adopted the simplified chain of oxidation reactions provided in *Eqs. (15) and (16)* in *Paper II*, which display first order kinetics and proceed simultaneously.

Thermodynamic calculations demonstrated that the distribution of the sulfide species strongly depends on the system conditions and is a strong function of pH. To illustrate this, we used HSC equilibrium calculations to determine the distribution between various forms of sulfide (S<sup>2-</sup>, HS<sup>-</sup>, H<sub>2</sub>S(a)) as a function of pH in an aqueous solution (Figure 7).

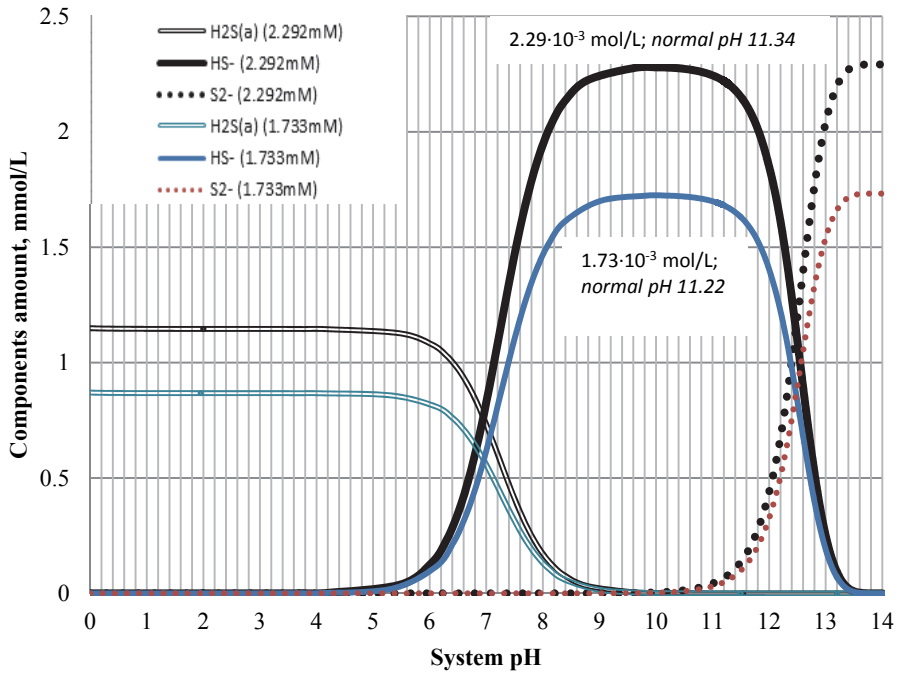


Figure 7. HSC calculations of CaS-H<sub>2</sub>O inert system showing changes in sulfide forms over a large pH range

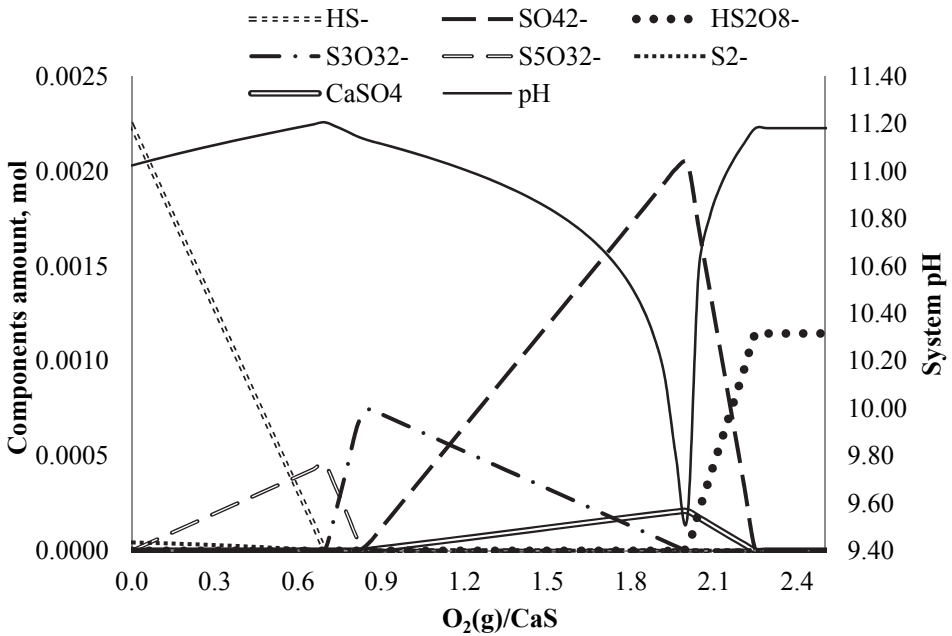


Figure 8. HSC calculation of CaS-H<sub>2</sub>O (2.292mM) in air system at 25°C showing changes in sulfur components and system pH over a large oxidative range

At higher pH values, the concentration of calcium at equilibrium is lower than the total sulfide concentration due to the formation of calcium hydroxide (2.2% of the  $\text{Ca}^{2+}$ ). The concentration of other species (e.g.  $\text{CaHS}^+$  and  $\text{Ca}(\text{HS})_2$ ) is very low over the pH range under study (Figure 7), so these were excluded from the present work. The basicity constants (in *Paper II*  $K_{b2}$  (0.0653 mol/L) and  $K_{b1}$  ( $1.11 \cdot 10^{-7}$  mol/L)) values were derived from the HSC calculations using the experimentally determined equilibrium concentration of  $2.29 \cdot 10^{-3}$  mol/L CaS.

To determine the thermodynamic equilibrium of the  $\text{CaS-H}_2\text{O}$  system, we used the standard atmospheric composition, however, over a larger range of oxidative environments at  $25^\circ\text{C}$ , the distribution of the main sulfur species and system pH changes (Figure 8). This indicates that the equilibrium state and system pH depends on the consumption of oxygen.

The oxidation of sulfides in an aqueous system is a complex process that may involve parallel reactions. The equilibrium calculation model simulated to produce Figure 8 can be used to help describe the reaction mechanism (Eqs. (13) and (14) together with *Eqs. (29)–(31)* from *Paper II*).

The solubility of CaS was experimentally determined under (Section 2.1.3.2) both an inert atmosphere ( $2.29 \cdot 10^{-3}$  mol/L) and under atmospheric conditions ( $2.74 \cdot 10^{-3}$  mol/L) after three hours of dissolution (Figure 9).

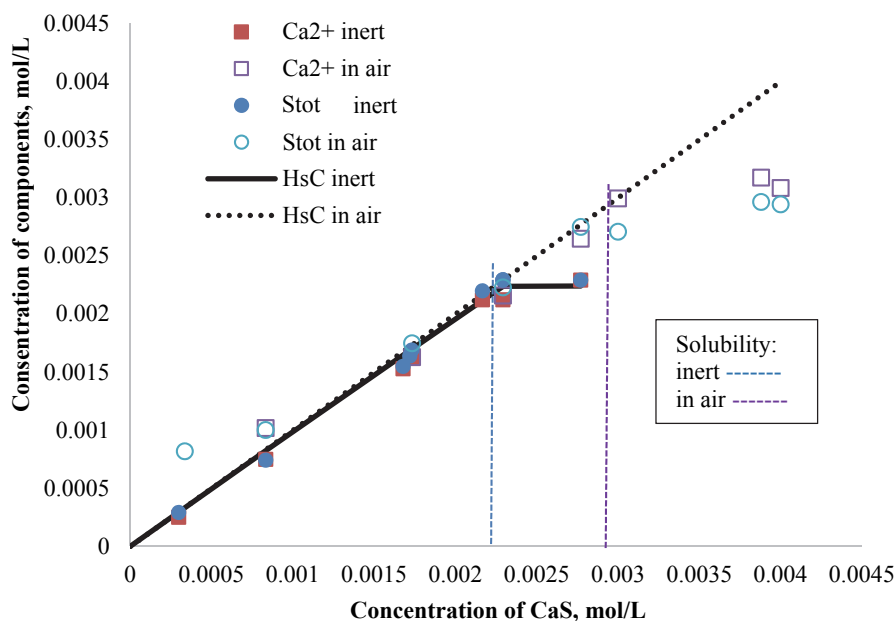


Figure 9. Measured and calculated concentrations for calcium - ions and sulfide - ions in  $\text{CaS-H}_2\text{O}$  inert and in air system, at  $25^\circ\text{C}$

The concentrations provided in Figure 9 after three hours of dissolution show that oxidized sulfur compounds in aqueous systems accelerate the dissociation of CaS due to the oxidation of HS<sup>-</sup> (Eqs. (15) and (16)).

Using Eqs. (36) and (37) from *Paper II*, HS<sup>-</sup> and S<sup>2-</sup> could be individually determined from pH and Ca<sup>2+</sup> measurements. Likewise, Eq. (8) from *Paper II* could be used to calculate the value of  $K_{b2}$  on the basis of OH<sup>-</sup> and sulfide species concentration measurements.

The approach we took to determine the equilibrium constants for the aqueous CaS system was to measure the concentrations of Ca<sup>2+</sup>, S<sub>sulfide</sub>, and OH<sup>-</sup> and apply Eqs. (8), (14), and (17) from *Paper II*. The results are illustrated in *Paper II: Table 2*.

The CaS solubility data display a clear linear dependence between the Ca<sup>2+</sup> concentration and conductivity (*Paper II: Figure 3*); this means that Ca<sup>2+</sup> concentration values could be calculated on the basis of EC measurements. Applying Eq. (32) from *Paper II* for inert conditions, these two parameters have a linear correlation with  $R^2 = 0.97$ . Likewise, Eq. (33) provides a linear correlation with  $R^2 = 0.93$  for atmospheric conditions.

### 3.1.3.2 CaS dissolution kinetics in the CaS–H<sub>2</sub>O system

The concentration profiles of the characteristic species that take part in the CaS dissolution process can be modeled as a function of time using an appropriate system of differential equations.

In *Paper II*, we defined both an inert system (Eqs. (38)–(43)) and an aqueous oxidative system (Eqs. (38)–(42) together with Eqs. (44)–(46)). The kinetic parameters for these two CaS–H<sub>2</sub>O systems were determined by minimizing the difference between simulated and experimentally determined solubility and reaction kinetic data. Average values for the forward reaction rate constants,  $k_1$ ,  $k_2$ , and  $k_3$  were found to be  $1.49 \cdot 10^{-3}$ , 2.77, and  $4.49 \text{ s}^{-1}$ , respectively. The backward reaction rate constants,  $k_{-1}$ ,  $k_{-2}$ , and  $k_{-3}$ , can be expressed in terms of the equilibrium constants as  $k_1/K_1$ ,  $k_2/K_{b2}$ , and  $k_3/K_{b1}$ , respectively. The average estimated values of the rate constants  $k_4$  and  $k_5$  were found to be  $2.01 \cdot 10^{-4} \text{ s}^{-1}$  and  $8.66 \cdot 10^{-5} \text{ s}^{-1}$ .

The simulated concentration profiles for our batch reactor are in good agreement with the experimental data for the inert system (*Paper II: Figure 7*) and provide a satisfactory representation of the CaS–H<sub>2</sub>O system under atmospheric conditions (*Paper II: Figure 9*).

## 3.2 Leaching of oil shale ash systems

The main Ca-compounds in the OS ash-water systems can be viewed as sorbents for both CO<sub>2</sub> mineralization and PCC production [10, 68-70]. To aid in the development of these technologies we studied the behavior of OSA suspensions and leachates, including the wet deposition of these residues. For this we conducted three hour comparative equilibrium batch experiments with three different types of OS ash-water systems (CFB, PF and SHC *Paper III: Table I*) and corresponding model water systems. Furthermore, we constructed a kinetic reaction model to describe OS ash-water systems which incorporate Ca(OH)<sub>2</sub>, CaSO<sub>4</sub>·2H<sub>2</sub>O (*Paper I*), and CaS (*Paper II*) dissolution mechanisms.

The differences in both the composition and physical properties of various OSAs originate mainly from the type of OS and combustion technology [27, 34]. To gain an appreciation of these differences, we compare these ashes with other kinds of industrial wastes in Table 1. PF ash is characterized by the highest free lime concentration of the three ashes. The high concentration of sulfates in CFB ash is present mainly in the form of anhydrite (CaSO<sub>4</sub>), which, in water systems, crystallizes into gypsum (CaSO<sub>4</sub>·2H<sub>2</sub>O). In both the CFB and PF ashes, the content of sulfides (mainly CaS) is relatively low. SHC ash is characterized by its high sulfide content. The SSA of both CFB and SHC ashes are over ten times higher than that of the PF ash (*Paper III: Table I*). Under ambient conditions over a series of chemical reactions, part of the sulfides from each of these ashes can be emitted into the atmosphere as gaseous H<sub>2</sub>S, generating atmospheric pollution. Sulfides, which remain in the aqueous phase, may also induce toxic effects depending on the pH value of the suspension [106].

The main leaching properties of the present OS mineral wastes were in good agreement with other alkaline industry residue leaching characteristics (Table 2). Both calcium and sulfur were dominant in all leachates. It has been shown that carbonation leads to (i) changes in the pH of ash-water suspensions, (ii) transformations of the sulfur compounds during the course of leaching (in both anaerobic and aerobic environments), and (iii) aqueous carbonation of OSA (and CaS as a model compound). All of these processes contribute to environmental issues related to ash leaching [106, 107].

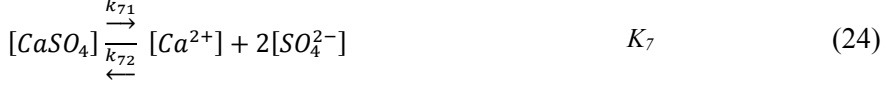
### 3.2.1 The equilibrium of oil shale ash-water systems

The ashes that remain after thermal treatment are complex matrix systems. In order to better understand the leaching of OSAs and how the various components interact, it is important to characterize the behavior of the most abundant components both individually and together. For this, we studied the ash leaching process of simplified binary and ternary systems that mimic complex PF, CFB, and SHC - water systems.

The thermodynamic calculations we performed show that (i) oxides are present in the equilibrium state in their hydrated forms, (ii) gypsum is formed

from the original anhydrate, and (iii) unstable compounds are bound to Ca-silicates (*Paper III: Figure 1*). All model systems used  $\text{Ca}(\text{OH})_2$ ,  $\text{CaSO}_4 \cdot 2\text{H}_2\text{O}$  and  $\text{CaS}$  as the main  $\text{Ca}^{2+}$ ,  $\text{SO}_4^{2-}$  and  $\text{S}^{2-}$  ion sources in the OS ash-water systems.

A simulation of the main system parameters (systems pH, EC, ion composition) coincide with the experimental results (Section 2.1.3) of the saturated OSA systems (*Paper III*). This confirms that the OSA leaching process is dominated by the dissociation of a few key components. We propose that all of these the OS ash-water systems and the ternary model system ( $\text{Ca}(\text{OH})_2$ – $\text{CaSO}_4 \cdot 2\text{H}_2\text{O}$ – $\text{CaS}$ – $\text{H}_2\text{O}$ ) can be described by a general reaction model with Eqs. (18)–(24) representing simplified dissociation and Eqs. (18)–(20) and (23)–(24) representing the equilibrium states:



where  $K_1 - K_3$  and  $K_6 - K_7$  are the equilibrium constants, expressed on a molar basis;  $k_{11} - k_{71}$  are the forward reaction rate constants, and  $k_{12} - k_{72}$  are the reverse reaction rate constants,  $\text{s}^{-1}$ .

The equilibrium constant  $K_2$  for Eq. (19), was calculated from the simulated equilibrium composition for the OS ash-water model systems (*Paper III: Figure 2*). The equilibrium constant  $K_3$  for Eq. (3) was calculated from the equilibrium concentration of pure  $\text{CaS}$  (*Paper II*). The equilibrium constants ( $K_1$ ,  $K_6$  and  $K_7$ ) were calculated from the experimental data using the thermodynamic model and are presented as average values in *Paper III: Table 2*. The oxidation reactions Eqs. (21) and (22) are expressed as unidirectional reactions because the reverse reactions do not occur during the initial combustion processes. However, oxidation in the aqueous suspensions takes place in the presence of sulfide ions which are considered “combustible matter”. Considering this, our three hour experiments do not reflect the endpoint of sulfide oxidation in the suspension.

The concentrations of the model components of the OS ash-water systems were varied by adjusting the ash/water ratios from 0.004 to 0.200.

After equilibrium was achieved, we measured the system pH, EC, and the concentration of the main ion species ( $\text{Ca}^{2+}$ ,  $\text{SO}_4^{2-}$ ,  $\text{S}_{\text{sulfide}}$ ,  $\text{OH}^-$ ) in the liquid phase. Other cations and anions (e.g.,  $\text{K}^+$ ,  $\text{Na}^+$ ,  $\text{Mg}^{2+}$ ,  $\text{Al}^{3+}$ ,  $\text{Cl}^-$ ,  $\text{PO}_4^{3-}$ , and  $\text{SO}_3^{2-}$ ) were not measured in the ash suspensions because their concentrations are very low [71, 72, 73, 84, 107]. The main leaching characteristics of OSAs were in good agreement with literature data [34, 71, 73]. The leaching equilibrium of the three types of ashes and the corresponding ternary model systems are presented in *Paper III: Figure 3*. The pH (12.31–12.66) of the saturated binary and ternary model systems coincided with the real process OS ash-water systems. Among the real process OS ash-water systems, the SHC systems have the lowest conductivity (10.35 mS/cm) while the PF ash-water systems have the highest conductivity (up to 12.25 mS/cm), which in this case is driven by the higher content of free lime. At saturation, both  $\text{Ca}^{2+}$ - and  $\text{SO}_4^{2-}$ -ions are present in similar concentrations in all model systems ( $\sim 0.033$ – $0.035$  and  $\sim 0.014$ – $0.015$  mol/L, respectively) and are slightly higher in the ternary model systems due to the dissolution (Eqs. (18)–(20)) of CaS and the oxidation of sulfide ions to intermediate forms (Eq. (21)) and sulfate (Eq. (22)). The concentration of  $\text{Ca}^{2+}$ - and  $\text{SO}_4^{2-}$ -ions ( $\sim 0.034$  and  $0.009$  mol/L, respectively) are lower in SHC ash-water systems compared with both CFB and PF ash-water systems ( $\sim 0.040$  and  $\sim 0.016$  mol/L, respectively). The latter value is related to the original composition of the SHC ash. Total sulfide concentrations in the leachates of CFB and PF ash-water systems remain at  $1.5 \cdot 10^{-5}$  mol/L and are up to 20 times higher in SHC ash-water systems, which remain steady at  $2.2 \cdot 10^{-4}$  mol/L. Though there was no remarkable difference in initial CaS content between the ashes compared, the leaching of CaS was favored in the SHC ash-water system.

The predicted dissociation results for the OS ash-water system (Eqs. (18)–(24)) were compared with experimental data (*Paper III: Figure 3*). The relatively small deviations between the measured and predicted data confirm the ability of our proposed model to accurately describe the dissolution process of OS ash-water systems.

The experimental results show a clear dependence between the  $\text{Ca}^{2+}$  ion concentration and EC of the solution for all of the OS ash-water systems, including the ternary ( $\text{Ca}(\text{OH})_2$ – $\text{CaSO}_4 \cdot 2\text{H}_2\text{O}$ –CaS) model systems ( $R^2 = 0.986$ ), and the CFB, PF, and SHC ash-water systems (*Paper III: Figure 4*).

Based on this optimal linear approximation, the concentration of  $\text{Ca}^{2+}$  ions can be determined for OS ash-water systems from conductivity measurements (*Paper III: Eq. (17)*) and compared with the predictions from the kinetic model. This approach may aid in optimizing an industrial PCC process using OS ash-water systems as a feedstock.

### 3.2.2 Model and real ash dissolution kinetics in the oil shale ash–H<sub>2</sub>O system

The main characteristics of the Ca dissolution process for OS ash-water systems was established using a reaction kinetics approach. In previous studies [73, 108, 109], the Ca dissolution process for OSA were investigated on the basis of mass transfer mechanisms.

Using the dissolution model defined by Eqs. (18)–(24), the dynamic concentration profiles of the characteristic species that participate in the OSA dissolution process can be modeled using the differential equations presented below:

$$\frac{d[CaS]}{dt} = -k_{11}[CaS] + \frac{k_{11}}{K_1}[CaS][Ca^{2+}][S^{2-}] \quad (25)$$

$$\begin{aligned} \frac{d[Ca^{2+}]}{dt} = & k_{11}[CaS] - \frac{k_{11}}{K_1}[CaS][Ca^{2+}][S^{2-}] + k_{61}[Ca(OH)_2] \\ & - \frac{k_{71}}{K_7}[CaSO_4][Ca^{2+}][SO_4^{2-}] - \frac{k_{61}}{K_6}[Ca(OH)_2][Ca^{2+}][OH^-]^2 \\ & + k_{71}[CaSO_4] \end{aligned} \quad (26)$$

$$\begin{aligned} \frac{d[OH^-]}{dt} = & k_{21}[S^{2-}] - \frac{k_{21}}{K_2}[OH^-][HS^-] + k_{31}[HS^-] - \frac{k_{31}}{K_3}[OH^-][H_2S] \\ & + 2k_{61}[Ca(OH)_2] - \frac{k_{61}}{K_6}[Ca(OH)_2][Ca^{2+}][OH^-]^2 \end{aligned} \quad (27)$$

$$\begin{aligned} \frac{d[HS^-]}{dt} = & -k_{41}[HS^-] - k_{51}[HS^-] + k_{21}[S^{2-}] - \frac{k_{21}}{K_2}[HS^-][OH^-] - k_{31}[HS^-] \\ & + \frac{k_{31}}{K_3}[OH^-][H_2S] \end{aligned} \quad (28)$$

$$\frac{d[S_2O_3^{2-}]}{dt} = 0.5k_{41}[HS^-] \quad (29)$$

$$\frac{d[SO_4^{2-}]}{dt} = k_{51}[HS^-] + k_{71}[CaSO_4] - \frac{k_{71}}{K_7}[CaSO_4][Ca^{2+}][SO_4^{2-}] \quad (30)$$

$$\frac{d[S^{2-}]}{dt} = k_{11}[CaS] - \frac{k_{11}}{K_1}[CaS][Ca^{2+}][S^{2-}] - k_{41}[S^{2-}] + \frac{k_{21}}{K_2}[HS^-][OH^-] \quad (31)$$

$$\frac{d[Ca(OH)_2]}{dt} = -k_{61}[Ca(OH)_2] + \frac{k_{61}}{K_6}[Ca(OH)_2][Ca^{2+}][OH^-]^2 \quad (32)$$

$$\frac{d[CaSO_4]}{dt} = -k_{71}[CaSO_4] + \frac{k_{71}}{K_7}[CaSO_4][Ca^{2+}][SO_4^{2-}] \quad (33)$$

The reaction rate constants  $k_{11}$ - $k_{51}$  that appear in Eqs. (25)–(33), were estimated based on the pure CaS model of OS ash-water dissolution. The rate constants  $k_{41}$  ( $2.01 \cdot 10^{-4} \text{ s}^{-1}$ ) and  $k_{51}$  ( $8.66 \cdot 10^{-5} \text{ s}^{-1}$ ) are one order of magnitude higher than the results reported by Mölder et al. [94] who investigated the rate of hydrolysis and oxidation (saturating the system with the air) of CaS in a hydraulic ash-disposal system. The reaction rate constants  $k_{61}$  and  $k_{71}$  were determined for various solid/liquid ratios ranging from 0.004 to 0.2 using a parameter estimation procedure (performed using the MODEST 6.1 software package (see Section 2.2)) that iteratively solves the proposed model equations and finds the minimal difference between these predictions and the experimental data obtained in the batch experiments. At this point we compared the reaction rate constants between each real process ash-water systems and their corresponding ternary model-water system. With this comparison, the most notable discrepancy appears in the under-saturated model systems. The saturated systems displayed better correlation between the real process ash-water systems and their corresponding ternary model-water systems than the two model systems had between themselves. This indicates that the real ash systems contain impurities that affect the diffusion of the key ions into the bulk solution. Yet, the reaction rate constants between different ashes and their corresponding ternary systems were consistent.

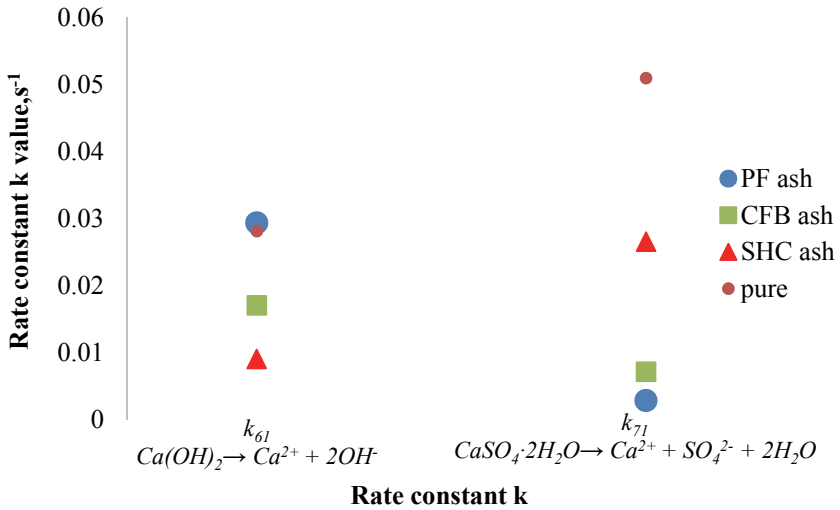
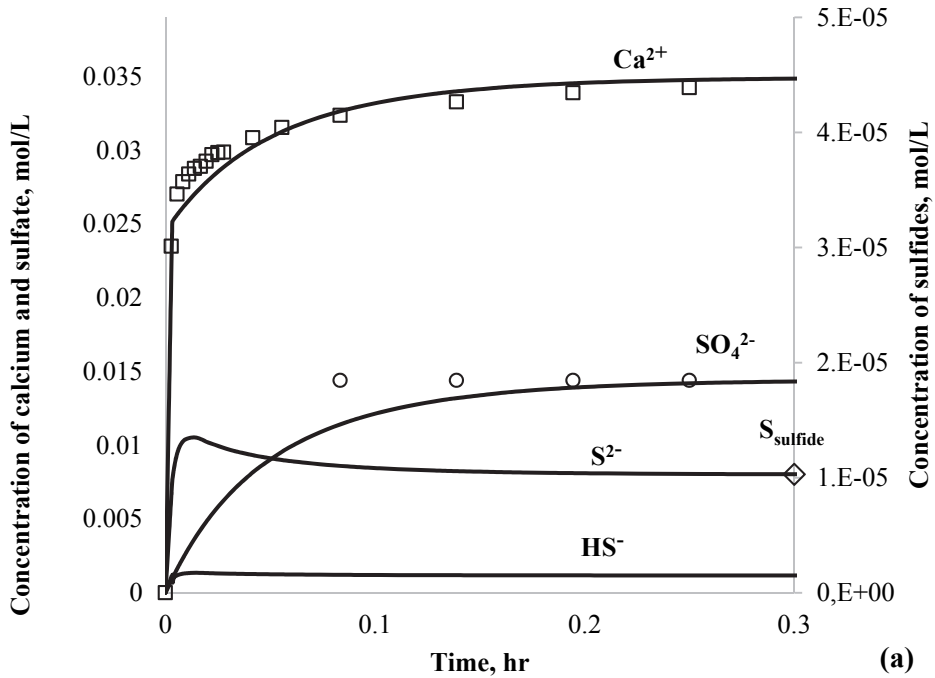


Figure 10. The reaction rate constants comparison for OSA and pure compounds systems.

The minimal difference between OSA and ternary systems was achieved for the rate constant  $k_{61}$  for the PF ash-water system and  $k_{71}$  for the SHC ash-water systems (*Paper II: Table 3*). Also, the value for the reaction rate constant for Eq. (6) for the pure  $\text{Ca}(\text{OH})_2$  one-step ( $0.0282 \text{ s}^{-1}$ ) dissolution model matches with both the PF ash system rate constant ( $0.0294 \text{ s}^{-1}$ ) and the value of the reaction

rate constant for pure gypsum dissolution defined by Eq. (7) ( $0.051 \text{ s}^{-1}$ ), but is closest to the SHC ash constant, which was found to be  $0.027 \text{ s}^{-1}$  (Figure 10).

Comparing the experimental and simulated data reveals that the pH of the system depends on the amount of solid phase added because a greater amount of OSA generates a faster increase in the system pH. We also found that the rate of formation of the equilibrium pH value is different between the selected ashes: the rate is slower for the actual SHC ash systems while the actual PF ash reaches equilibrium more rapidly (*Paper III: Figure 5*). This implies that PF ash contains more compounds that provide a fast basic reaction. This can also be seen by observing the reaction rate constants reported in *Table 3* within *Paper III*. Plots of experimental and simulated concentration profiles for various solid/liquid ratios for the PF ash-water systems are presented in Figure 11. The accuracy of our proposed dissolution model ( $R^2 > 90\%$ ) was confirmed by directly comparing the results of process simulations with experimental data.



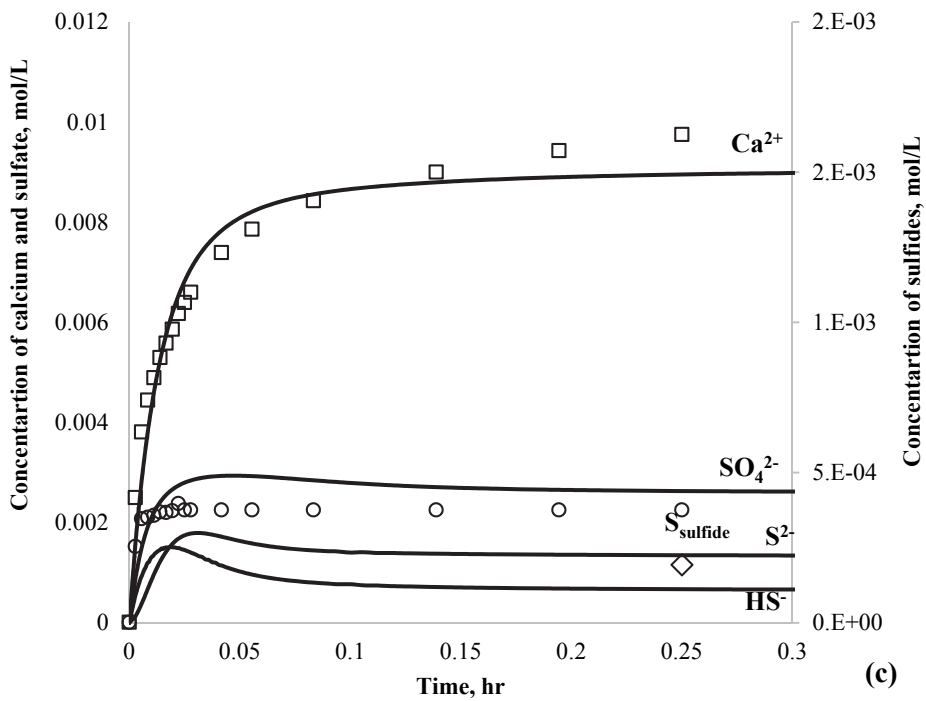
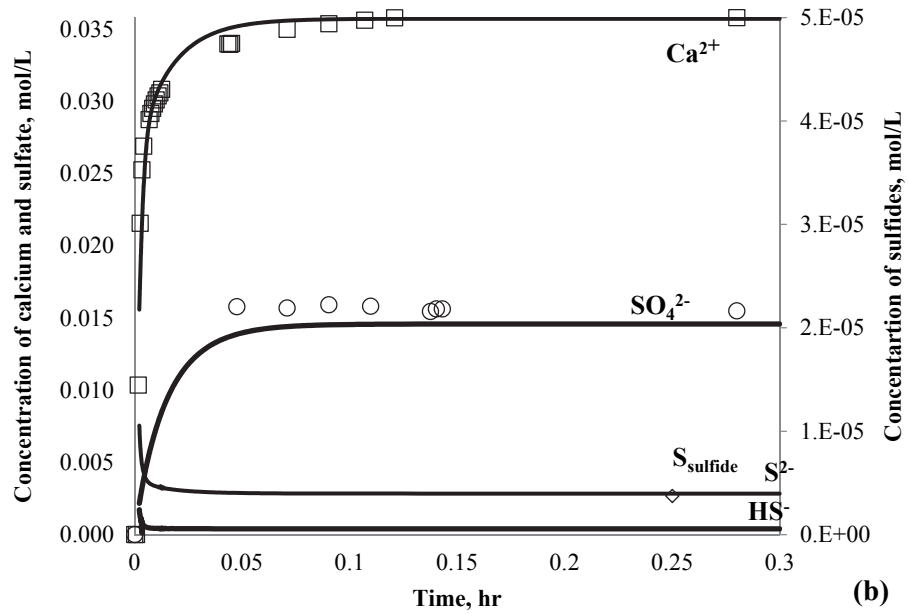


Figure 11. OSA ((a) PF - S/L: 1/10; (b) CFB - S/L: 1/20; (c) SHC - S/L: 1/50) leaching dynamics of key components: experimental ( $\square$ ) vs simulation (—MODEST 6.1)

The model we have constructed for the OS ash-water system incorporates mechanisms for  $\text{Ca}(\text{OH})_2$ ,  $\text{CaSO}_4 \cdot 2\text{H}_2\text{O}$ , and  $\text{CaS}$  dissolution. This model can be used to simulate all three main types of OSA (CFB, PF, and SHC), which differ in their chemical and physical structure (*Paper III: Table I*). The model we propose, together with the different sets of estimated parameters, is suitable for describing the leaching of various types of ash that originate from the OS shale industry.

### **3.2.3 Implementing the dissolution of oil shale ash within Aspen plus**

Dissolution models for the various OS ash- $\text{H}_2\text{O}$  systems were implemented within the Aspen Plus simulation platform by inserting the dissociation reactions and corresponding thermodynamic and kinetic constants for each system into the continuously stirred tank reactors (CSTR) reactor model (Figure 15) ( $t = 25^\circ\text{C}$ ,  $P = 1 \text{ bar}$ ,  $Q = 0 \text{ Gcal/hr}$ ).

#### **3.2.3.1 The oil shale ash leaching process by natural precipitation**

We simulated one scenario for an industrial ash plateau (formed by OS combustion for power and shale oil production) washing process in a natural environment over an indefinite period using the following assumptions. In Estonia approximately 5 Mt of OSA is transported to wet open-air deposits. In accordance with the combustion technologies, the distribution of the ash formation quantities per year [37] and the distribution of Ca species are presented in Figure 12.

Understanding the leaching of key components ( $\text{Ca}(\text{OH})_2$ ,  $\text{CaSO}_4 \cdot 2\text{H}_2\text{O}$ ,  $\text{CaS}$ ) from OS mineral waste is required to accurately predicting its impact on the quality of the leaching water, which may contaminate soil, groundwater, and surface water, and may even reach the Baltic Sea.

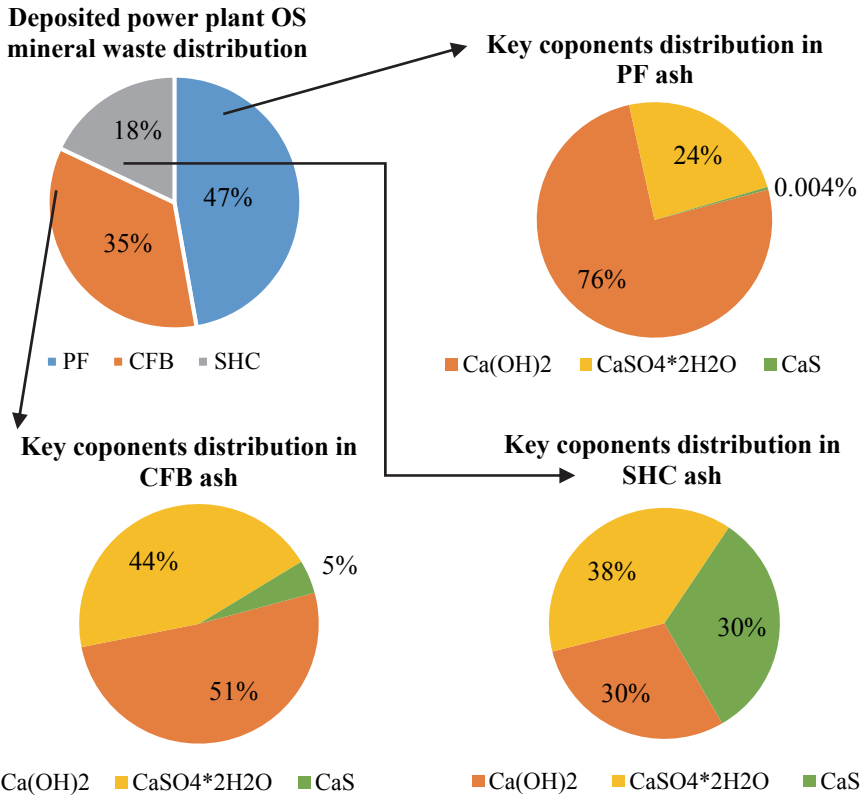


Figure 12. The distribution of the depositing ashes

We also carried out simulations of the washing of the key components from OSA deposits using CSTR reactors simulated with Aspen Plus (Figure 13) assuming OSA dissolution equilibrium. In the first stage, a total of  $5 \cdot 10^9$  kg of ash was formed by the PF, CFB, and SHC power plants (Figure 12). The characteristics of the ashes and the thermodynamic equilibrium constants were taken into account (*Paper III, Table I and Table II*) and we assumed that these ashes were transported at an ash/water ratio of 1:20 and uniformly distributed over an area of  $5 \cdot 10^9$  m<sup>2</sup>.

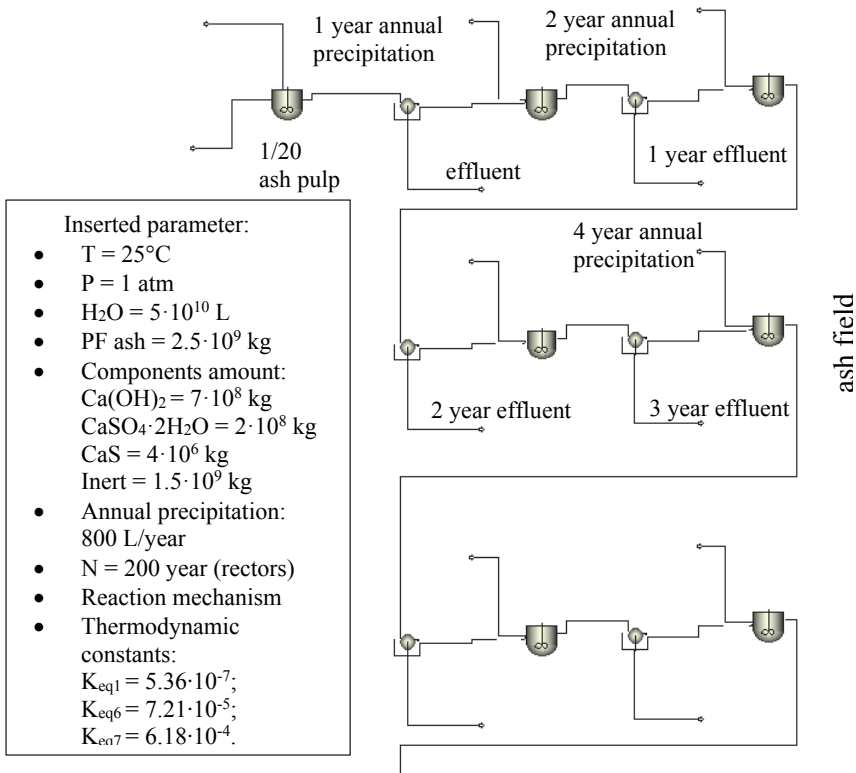
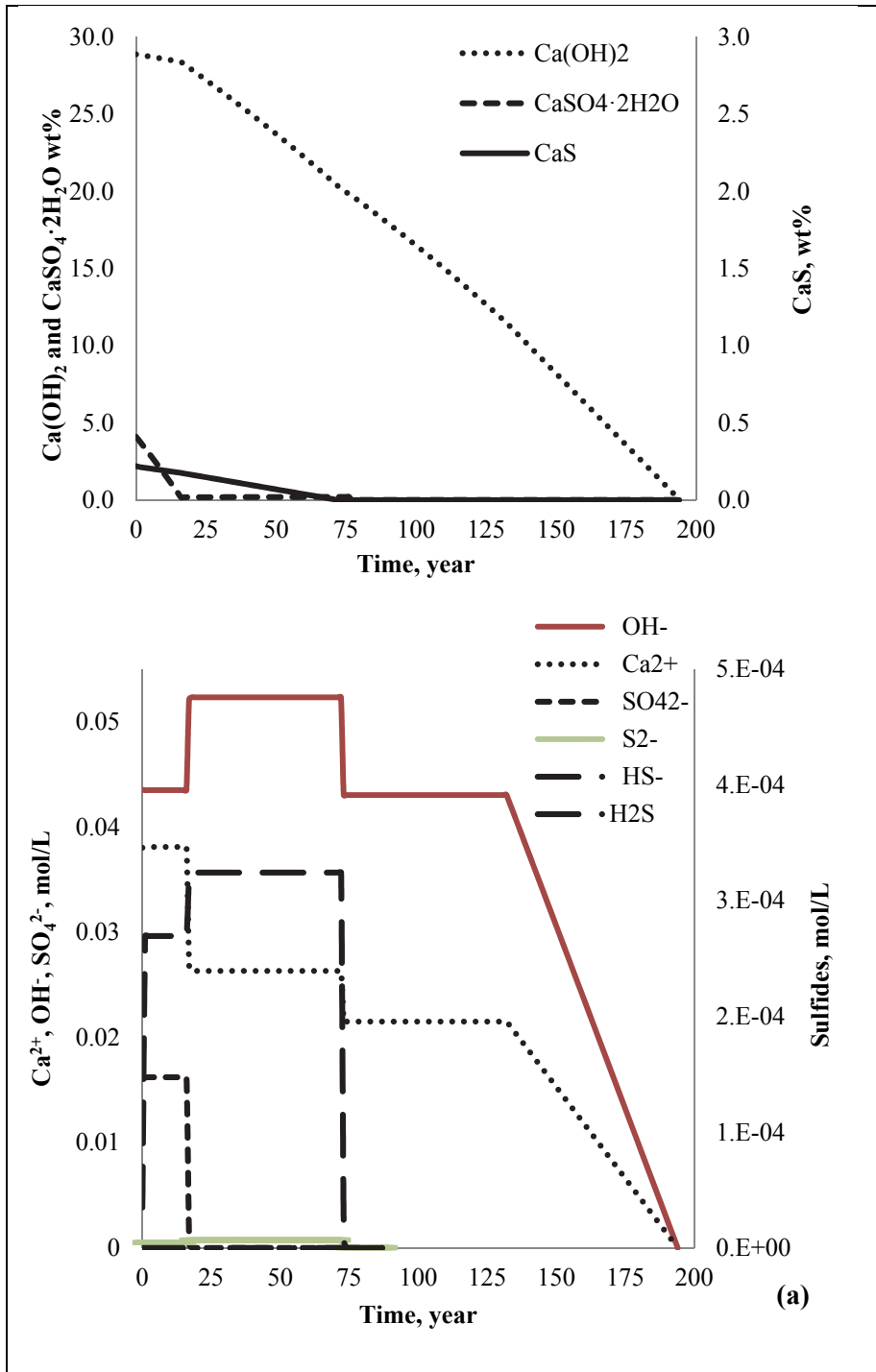
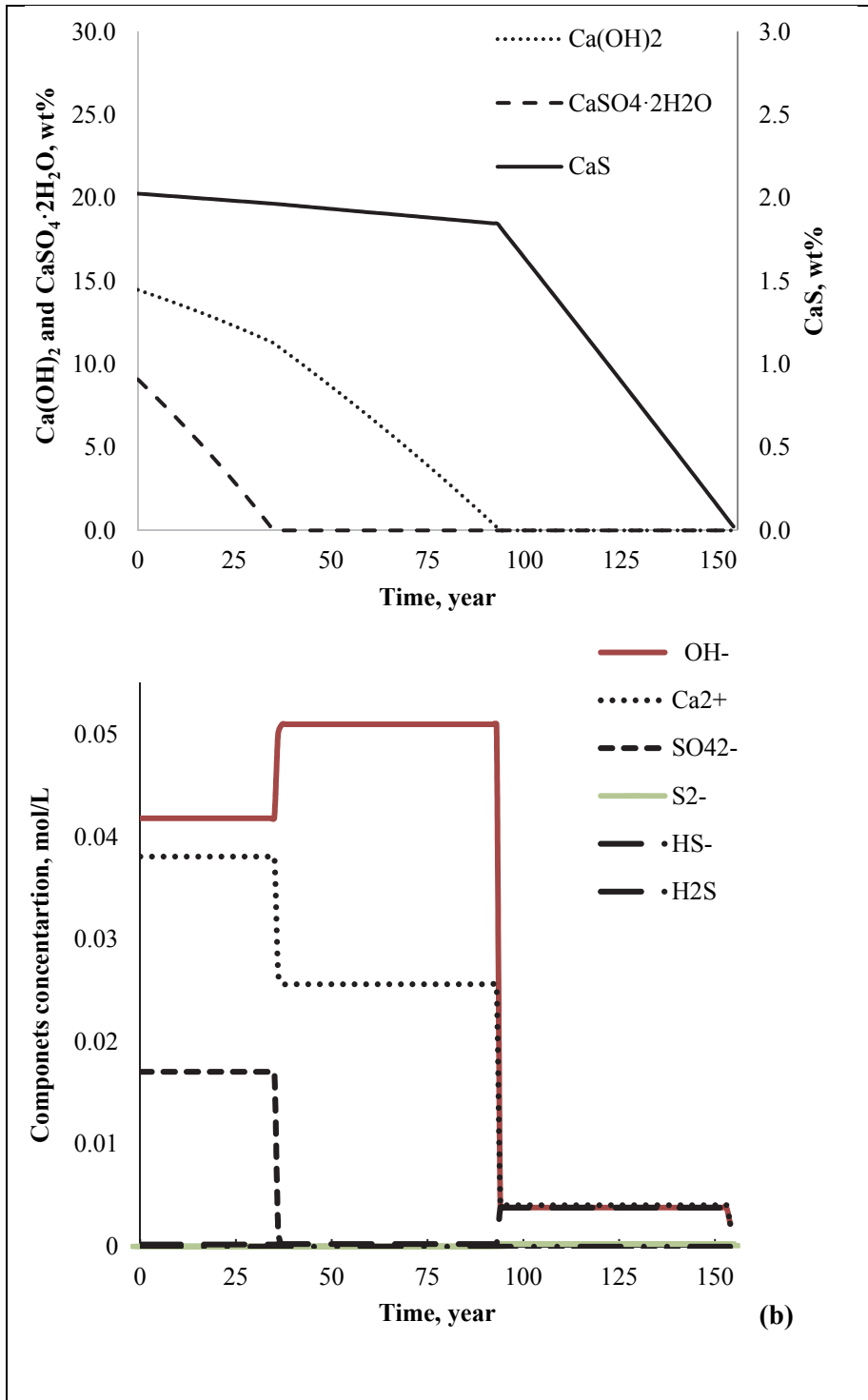


Figure 13. The Aspen Plus simulation model for precipitation of ash field

In the second stage, 0.2% effluent is removed to imitate draining. In the next natural precipitation stages the average annual amount of rainfall (in Estonia 550–800 mm [110]) is inserted. Up to 200 model reactors (simulating one year) were combined to estimate the changes in both the solid phases and in the leaching liquid during the entire washing process. However, current model does not take into account the chemical reaction between the atmospheric  $\text{CO}_2$  and alkaline suspension.

The key compounds that form during the continuous washing of the OSA plateau (made up of three different types of mineral waste) are presented in Figure 14. The equilibrium concentrations of the ions are in accordance with the components from dissociation Eqs. (1)–(3) and (6)–(7) (*Paper III: Eqs. (1)–(3), (6), (7)*). If only one component remained in the OSA, the pure substance equilibrium constant (*Paper I and Paper II: Table II*) was used to simulate the washing process. The equilibrium concentrations of the main ions are directly dependent on the quantity of their precursors. The concentration of  $\text{Ca}^{2+}$  ions is the highest during the stages where all of key components influence the process, after some precursors are washed out, the  $\text{Ca}^{2+}$  ions concentration decreases. The concentration of  $\text{OH}^-$  ions is the highest during the stages where lime and  $\text{CaS}$  influence the process; as a result, the alkalinity increases.





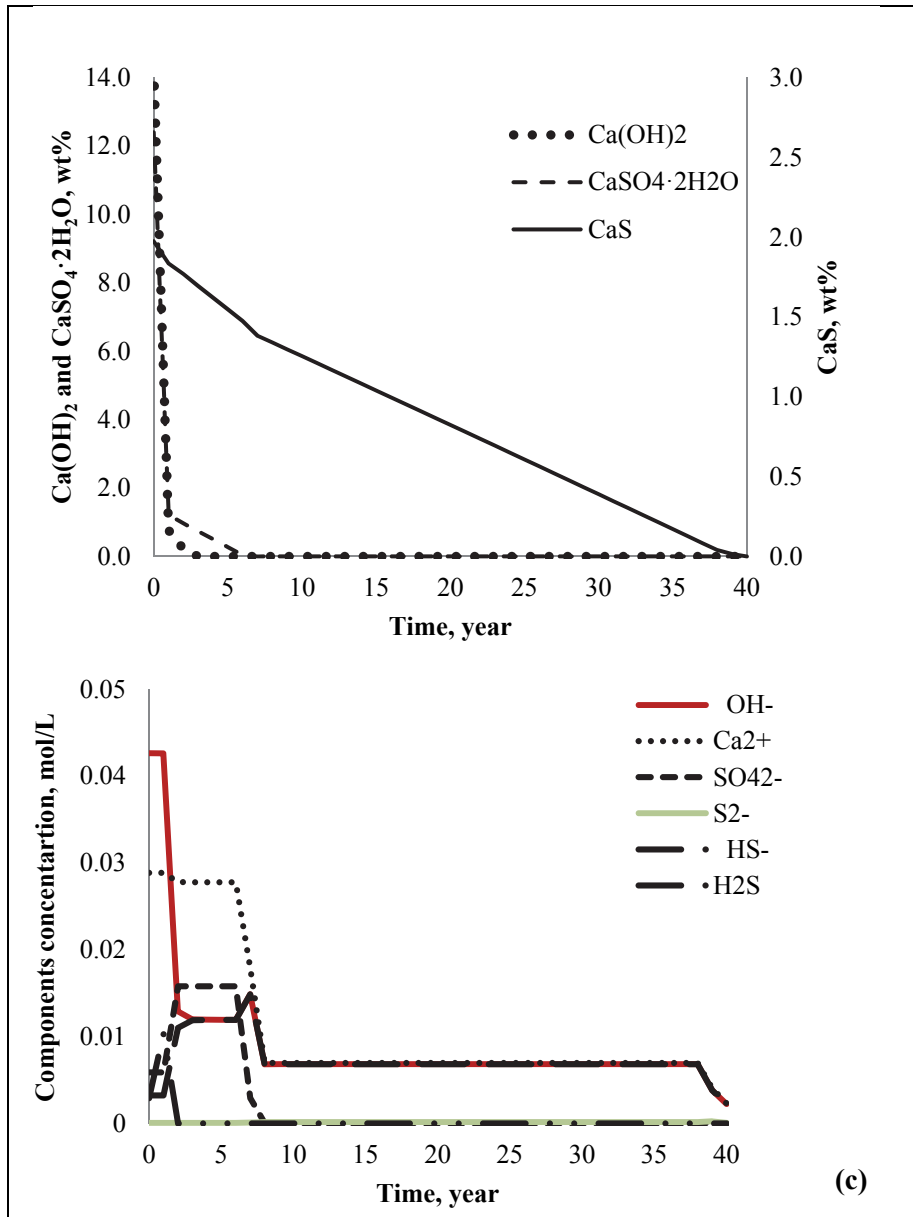


Figure 14. Simulation of the key components washing process for a 500 ha industrial OSA deposit (PF ash (a), CFB ash (b) and SHC ash (c)) by the average annual amount of precipitation

The mean annual amount of precipitation in Estonia is up to 800 mm per year and the density of the OSA sediments varies between 1800 and 2800 kg m<sup>-3</sup> (average 2500 kg m<sup>-3</sup>). Under these conditions, when the OSA is deposited annually over 500 ha, the leaching process of the main ions from three different types of mineral waste (Figure 12) would take approximately 200 years (Figure

14). This figure is in accordance with the neutralization of ash sediments with natural precipitation [50, 109].

The leaching behavior depends on the characteristics of the OSA (*Paper III: Table I*) and how the ash formation is distributed (Figure 12). For every OSA system, there are three main leaching regimes. In the case of PF ash, presented in Figure 14 (a), sulfates leach out for the first 20 years and the leachate is similar to the leachate from the ternary water systems. For the next 55 years, portlandite and CaS dissolution provide the most alkaline reactions and during the last 125 years,  $\text{Ca}^{2+}$  and  $\text{OH}^-$  ions dominate and the leachate is similar to the  $\text{Ca}(\text{OH})_2$  water system. In the case of CFB ash, presented in Figure 14 (b), sulfates leach out for the first 38 years and portlandite and CaS dissolution provide the alkalinity for the next 60 years. During the last 60 years,  $\text{Ca}^{2+}$ ,  $\text{HS}^-$ , and  $\text{OH}^-$  ions dominate and the leachate is similar to the hydrolysis of CaS hydrolyses presented in *Eq. (15)* within *Paper II*. In the case of SHC ash, presented in Figure 14 (c), the first five years portlandite leaches out and the leachate is similar to the leachate from ternary water systems. Over the next four years, sulfates leach out, however, CaS dissolution provides the alkalinity, which should not be surprising considering that *Eq. (36)* within *Paper II* presents  $\text{HS}^-$  as being equivalent to  $\text{OH}^-$ . During the last 30 years CaS dissolution occurs. Based on our simulation results presented in Figure 14, we can state that the highest concentrations of  $\text{Ca}^{2+}$  and  $\text{SO}_4^{2-}$  ions (0.038 mol/L and 0.017 mol/L) occurs after the annual OSA is deposited during the first 40 years. The highest leachable content of  $\text{OH}^-$  occurs during the period from year 15 up to year 90 (0.052 mol/L). The leachable content of sulfide occurs in year 8 (0.015 mol/L) and remains at  $\sim 0.006$  mmol/L for the next 150 years. We can further state that the amount of Ca, particularly in relation to that of S, dictates the OSA water system pH. Our simulation results demonstrate that under certain conditions, OS mineral waste can act as a source of contaminants over a long period of time.

### 3.2.3.2 The kinetics of real process oil shale leaching

The kinetic parameters presented in *Table 3* within *Paper III* for the OS ash– $\text{H}_2\text{O}$  system were also inserted into a CSTR reactor model ( $t = 25$  °C,  $P = 1$  bar,  $Q = 0$  Gcal/h) to estimate the residence time and reactor volume required for continuous extraction of  $\text{Ca}^{2+}$  from the OSA (see also the  $\text{Ca}(\text{OH})_2$ – $\text{H}_2\text{O}$  system in *Paper I: Figure 9*).

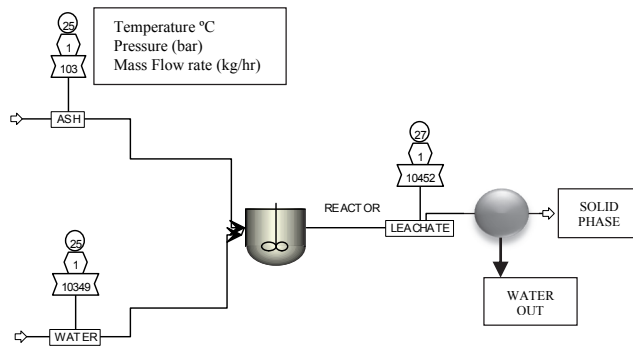
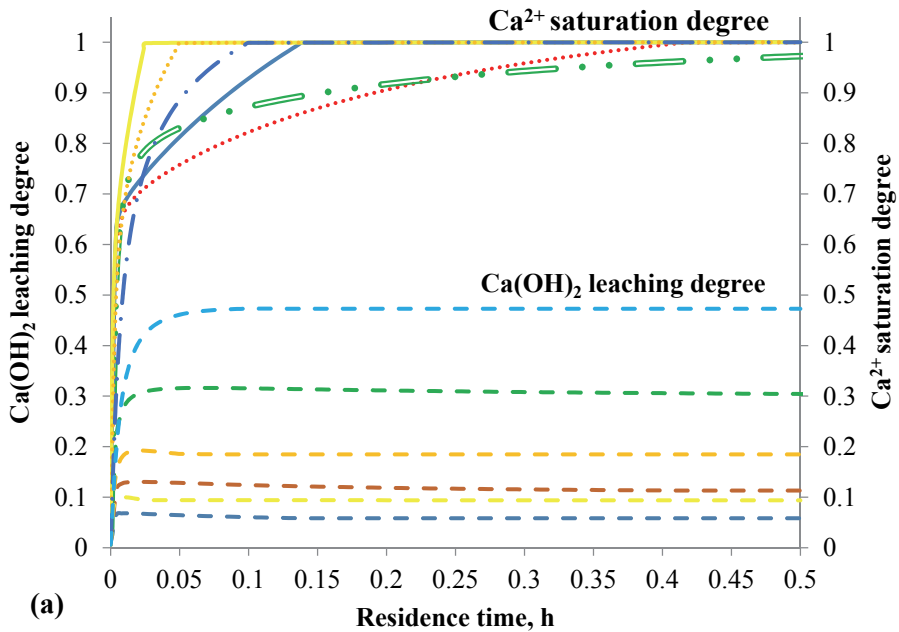


Figure 15. The continuously stirred tank reactors reactor model

Using the simplified dissolution model (*Paper III: Eq. (1)-(3), (6), (7)*) and responsive characterizations of OSAs (*Paper III: Table I*), we performed this calculation with respect to one Mt of OSA per year (114 t/h) and the results are presented in Figure 16.



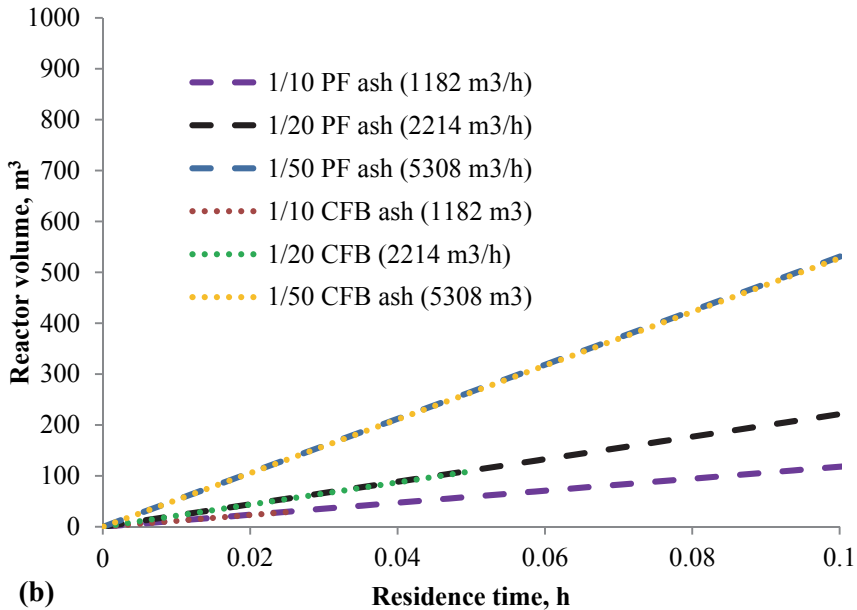


Figure 16. Continuous model of  $\text{Ca}^{2+}$  extraction from OSA (1 Mt OSA/year = 114 t/h): dependence of  $\text{Ca}(\text{OH})_2$  leaching degree (- -) and leachate  $\text{Ca}^{2+}$  saturation degree (—) on residence time (a) or reactor volume needed for respective residence time (b) at given solid to liquid ratios (for CFB ash 1/10 – red; CFB ash 1/20 – green and CFB ash 1/50 – yellow; PF ash 1/10 – purple; PF ash 1/20 – black and PF ash 1/50 – blue).

It can be seen from Figure 16 that the degree of  $\text{Ca}(\text{OH})_2$  that leaches out and the degree of  $\text{Ca}^{2+}$  saturation in the leachate are governed by the solid to liquid ratio (1/10, 1/20, 1/50, and 1/100) and depend on the residence time of the CSTR. Due to the low solubility of  $\text{Ca}(\text{OH})_2$ , either a very large reactor or repetitive extractions would be required to maximize both the  $\text{Ca}(\text{OH})_2$  leaching from ash and  $\text{Ca}^{2+}$  saturation in the solution. Comparing real process OSA with the pure  $\text{Ca}(\text{OH})_2$  system, the degree of  $\text{Ca}(\text{OH})_2$  leaching is lower from real process ashes. The differences we observe are caused by a combination of other water-soluble OSA components and the kinetic parameters. As an example, a reactor volume of  $\sim 150 \text{ m}^3$  is required to extract 50% of the calcium from the OS ash- $\text{H}_2\text{O}$  system using 1 Mt of OSA per year with a solid to liquid ratio of 1/20. Transferring the experimentally observed P/V ratio (Section 2.1.3.2) to this reactor, about two megawatts of energy is required to mix this suspension. For both the PF and CFB ash water system, the degree of  $\text{CaSO}_4 \cdot 2\text{H}_2\text{O}$  leaching (0.3 and 0.5, respectively) was higher than the degree of  $\text{Ca}(\text{OH})_2$  leaching at a residence time of 0.1 h. However, in the current Estonian power plants, more than 5 million  $\text{m}^3$  of alkaline water (pH 12–13) is circulating in a hydraulic system between the plant and the sedimentary pond [27] which has a high degree of  $\text{Ca}^{2+}$  saturation. Direct utilization of this water is expected to be more economically viable than processing ash directly.

## 4. CONCLUSION

In this work the leaching behavior of the main water-soluble Ca-compounds ( $\text{Ca(OH)}_2$ ,  $\text{CaSO}_4 \cdot 2\text{H}_2\text{O}$  and  $\text{CaS}$ ) in both real process and model oil shale ash-water systems, have elucidated. This work is useful in the context of operating and managing the risks of oil shale ash wet deposition as well as designing  $\text{CO}_2$  mineralization, as next processes after leaching, that produce precipitated calcium carbonate-type filler from oil shale ash.

The current study presents both the mechanisms and kinetics of oil shale mineral waste dissolution. In addition, the influence of the key components that occur during oil shale ash leaching individually, in binary ( $\text{Ca(OH)}_2$ – $\text{CaSO}_4 \cdot 2\text{H}_2\text{O}$ – $\text{H}_2\text{O}$ ) and ternary ( $\text{Ca(OH)}_2$ – $\text{CaSO}_4 \cdot 2\text{H}_2\text{O}$ – $\text{CaS}$ – $\text{H}_2\text{O}$ ) model systems, as well as in real process, pulverized firing – PF, circulating fluidized bed combustion – CFB, and solid heat carrier – SHC ashes, have been studied. Both the equilibrium and dynamics of the leaching of the main water-soluble Ca-compounds within oil shale ashes were combined into a mathematical model that is able to simulate the processes of leaching for different types of oil shale ashes. We suggest that this model provides a good basis for designing a complete alkaline mineral stabilization and/or utilization process.

Based on the work, we can make the following conclusions:

- The solubility and kinetics of the  $\text{Ca(OH)}_2$ ,  $\text{CaSO}_4 \cdot 2\text{H}_2\text{O}$  and  $\text{CaS}$  (both under inert as well as atmospheric conditions) water systems at  $25^\circ\text{C}$  have been evaluated.  $\text{CaS}$  solubility was experimentally determined under an inert atmosphere ( $2.29 \cdot 10^{-3}$  mol/L) and a higher solubility was evaluated under atmospheric conditions ( $2.74 \cdot 10^{-3}$  mol/L) (after 3 hours of dissolution). The equilibrium and kinetic constants for main water-soluble Ca-compounds (as pure components) have been estimated.
- The results of leaching equilibrium constants on the basis of batch experiments with the aqueous systems of three different types of oil shale ashes (CFB, PF and SHC) as well as corresponding model systems and an empirical equation to calculate the concentration of  $\text{Ca}^{2+}$ -ions from conductivity measurements have been obtained.
- The mathematical model for describing oil shale ash-water systems which incorporates  $\text{Ca(OH)}_2$ ,  $\text{CaSO}_4 \cdot 2\text{H}_2\text{O}$ , and  $\text{CaS}$  dissolution mechanisms have been developed.
- The leaching mechanisms of different real process ashes once with the leaching mechanisms of corresponding model systems (both binary and ternary) have been evaluated. This allows one to accurately describe the leaching behaviour of various ash-water systems using a single overall reaction model.
- By comparing leaching simulation results with experimental data, it have been demonstrated that the leaching behavior of the key Ca-compounds in oil shale ash can be described by the developed generalized model.

- The determined equilibrium and kinetics constants can be used to compose a complete oil shale ash-water leaching model and design a pilot-scale oil shale ash-water carbonation reactor. The latter could significantly reduce the environmental impact of using oil shale and other Ca-rich fossil fuels in the energy sector, irrespective of the thermal treatment technology used to create the ash.
- The proposed leaching model was used, in Aspen Plus platform, for elucidating the composition of contaminated water per year, required reactor volume and residence time. As an example, a reactor volume of  $\sim 150 \text{ m}^3$  is required to extract 50% of the calcium from the oil ash- $\text{H}_2\text{O}$  system using 1 Mt of oil shale ash per year with a solid to liquid ratio of 1/20. The ash field leaching simulation results demonstrated that oil shale mineral waste can act as a source contaminates over a long period of time (in case of PF ash approximately 200 years).
- The experimental methodology and a mathematical model, together with optimal kinetic parameters that can be used to calculations of ash fields leachate pollution and develop Ca compounds containing ash treatment technologies in the waste management sector for a variety of mineral residues.

## REFERENCES

1. International Energy Agency. CO<sub>2</sub> Emissions from Fuel Combustion 2014, IEA, Paris, 2014.
2. Redrawing the energy climate map - World Energy Outlook Special Report, IEA 2013: <http://www.worldenergyoutlook.org/weo2013/>, 07.01.2016.
3. Trends in global CO<sub>2</sub> emissions: 2014 Report/ Olivier, J. G. J., Janssens-Maenhout, G., Muntean, M, Peters, J. A . H. W. (eds.). PBL Netherlands Environmental Assessment Agency, Italy 2014. 10 p.
4. IPCC - The Carbon Cycle and Atmospheric Carbon Dioxide: [http://www.ipcc-data.org/observ/ddc\\_co2.html](http://www.ipcc-data.org/observ/ddc_co2.html), 07.01.2015.
5. US EPA 2015 National Emissions Inventory, Air Pollutant Emissions Trends Data, 1970–2014 Average Annual Emissions, All Criteria Pollutant: <http://www.epa.gov/ttn/chieftrends/index.html>, 07.01.2016.
6. Rappold, T. A., Lackner, K. S. Large scale disposal of waste sulfur: From sulfide fuels to sulfate sequestration. – *Energy* **2010**, 35(3), 1368-1380.
7. Environment and Health in Electricity Generation: <http://www.world-nuclear.org/info/Energy-and-Environment/Environment-and-Health-in-Electricity-Generation/>, 07.01.2015.
8. Caldas-Vieira, F., Feuerborn, H. J. CCP Management in Europe, *Proceedings of the EUROCOALASH 2012 Conference, Thessaloniki*, 2012.
9. Kuusik, R., Uibu, M., Kirsimäe, K. Characterization of oil shale ashes formed at industrial scale boilers. - *Oil Shale* **2005**, 22, 407-419.
10. Uibu, M., Uus, M., Kuusik, R. CO<sub>2</sub> mineral sequestration by oil shale wastes from Estonian power production. – *J. Environ. Manage.* **2009**, 90, 1253-1260.
11. Querol, X., Umaña, J. C, Alastuey, A., Ayora, C., Lopez-Soler, A., Plana, F. Extraction of soluble major and trace elements from fly ash in open and closed leaching systems. – *Fuel* **2001**, 80, 6, 801-813.
12. Montes-Hernandez, G., Perez-Lopez, R., Renard, F., Nieto, J.M., Charlet, L. Mineral sequestration of CO<sub>2</sub> by aqueous carbonation of coal combustion fly-ash. – *J. Hazard. Mater.* **2009**, 161, 1347-1354.
13. Sanna, A., Uibu, M., Caramanna, G., Kuusik, R., Marotot-Valer, M. M. A review of mineral carbonation technologies to sequester CO<sub>2</sub>. - *Chem. Soc. Rev.* **2014**, 43, 8049-8079.
14. Nyambura, M. G., Mugeru, G. W., Felicia, P. L., Gathura, N. P. Carbonation of brine impacted fractionated coal fly ash: Implications for CO<sub>2</sub> sequestration. – *J. Environ. Manage.* **2001**, 92, 655-664.

15. Sow, M., Hot, J., Tribout, C., Cyr, M. Characterization of Spreader Stoker Coal Fly Ashes (SSCFA) for their use in cement-based applications. – *Fuel* **2015**, 162, 224-233.
16. Gunning, P. J., Hills, C. D., Carey, P. J. Production of lightweight aggregate from industrial waste and carbon dioxide. – *Waste Manage.* **2009**, 29, 2722-2729.
17. Mattila, H. P., Grigaliunaite, I., Zevenhoven, R. Chemical kinetics modeling and process parameter sensitivity for precipitated calcium carbonate production from steelmaking slags. – *Chem. Eng. J.* **2012**, 192, 77-89.
18. Mattila, H.P., Zevenhoven, R. Design of a continuous process setup for precipitated calcium carbonate production from steel converter slag. *Chem. SuS. Chem.* **2014**, 7, 903-913.
19. Liu, G., Zhang, H., Gao, L., Zheng, L., Peng, Z. Petrological and mineralogical characterizations and chemical composition of coal ashes from power plants in Yanzhou mining district, China – *Fuel Process. Technol.* **2004**, 85, 1635-1646.
20. Deng, S., Shu, Y., Li, S., Tian, G., Huang, J., Zhang, F. Chemical forms of the fluorine, chlorine, oxygen and carbon in coal fly ash and their correlations with mercury retention. – *J. Hazard. Mater.* **2016**, 301, 400-406.
21. Wajima, T., Munakata, K. Material conversion from paper sludge ash in NaOH solution to synthesize adsorbent for removal of  $Pb^{2+}$ ,  $NH_4^+$  and  $PO_4^{3-}$  from aqueous solution.- *J. Environ. Sci.* **2011**, 23(5) 718–724.
22. Perez-Lopez, R., Montes-Hernandez, G., Nieto, J. M., Renard, F., Charlet, L. Carbonation of alkaline paper mill waste to reduce CO<sub>2</sub> greenhouse gas emissions into the atmosphere. – *App. Geochem.* **2008**, 23, 2292-2309.
23. Ukwattage, N. L., Ranjith, P. G., Yellishetty, M., Bui, H. H., Xu, T. A laboratory-scale study of the aqueous mineral carbonation of coal fly ash for CO<sub>2</sub> sequestration. – *J. Clean Prod.* **2015**, 103, 665-674.
24. Pan, S. Y., Chang, E. E., Chiang, P. C. CO<sub>2</sub> Capture by Accelerated Carbonation of Alkaline Wastes: A Review on Its Principles and Applications. - *Aerosol Air Qual. Res.* **2012**, 12, 770-791.
25. Statistical Yearbook of Estonia. Tallinn, 2015: [http://energiatalgud.ee/img\\_auth.php/e/e2/Eesti\\_Statistika\\_Eesti\\_statistika\\_aastaraamat\\_2015\\_2015.pdf](http://energiatalgud.ee/img_auth.php/e/e2/Eesti_Statistika_Eesti_statistika_aastaraamat_2015_2015.pdf), 20.10.2015.
26. Konist, A., Pihu, T., Neshumayev, D., Siirde, A. Oil shale pulverized firing: boiler efficiency, ash balance and flue gas composition. - *Oil Shale* **2013**, 30, 1, 6-18.
27. Kuusik, R., Uibu, M., Kirsimäe, K., Mõtsep, R., Meriste, T. Open-air deposition of Estonian oil shale ash: formation, state of art, problems

- and prospects for the abatement of environmental impact. - *Oil Shale* **2012**, 29(4), 376 - 403.
28. Ots A. Oil Shale Fuel Combustion, Tallinn University of Technology Press, Tallinn, 2006.
  29. Kleesmaa, J., Latõsov. E., Karolin, R. Primary method for reduction of SO<sub>2</sub> emission and its impact on CO<sub>2</sub> in pulverized oil shale-fired boilers at Narva Power Plant. – *Oil Shale* **2011**, 28, 2 321-336.
  30. Directive 2001/80/EC of the European Parliament and of the Council of 23 October 2001 on the limitation of emissions of certain pollutants into the air from large combustion plants.
  31. Ots. A., Poobus, A., Lausmaa, T. Technical and ecological aspects of shale oil and power cogeneration. – *Oil shale* **2011**, 28, 1S, 101-112.
  32. Plamus, K., Soosaar, S., Ots, A., Neshumayev, D. Firing Estonian Oil Shale of Higher Quality in CFB Boilers - Environmental and Economic Impact. - *Oil Shale* **2011**, 28, 1S, 113–126.
  33. Golubev, N. Solid oil shale heat carrier technology for oil shale retorting. - *Oil Shale* **2003**, 20(3S), 324-332.
  34. Reinik, J., Irha, N., Steinnes, E., Piirisalu, E., Aruoja, V., Schultz, E., Leppänen, M. Characterization of water extracts of oil shale retorting residues form gaseous and solid heat carrier processes. - *Fuel Process. Technol.* **2015**, 131, 443-451.
  35. Paaver, P. Geopolymerization of the Estonian oil shale solid heat carrier retorting waste ash: changes in mineral-chemical composition on uniaxial compressive strength development, B.Sc. Thesis. Univesity of Tartu: Tartu, Estonia, 2014.
  36. Talviste P., Sedman A., Mõtlep R., Kirsimäe, K. Self-cementing properties of oil shale solid heat carrier retorting residue. - *Waste Manage. Res.* **2013**, 31(6), 641-647.
  37. Eesti Energia Annual Report 2014: [https://www.energia.ee/-/doc/10187/pdf/concern/annual\\_report\\_2014\\_eng.pdf](https://www.energia.ee/-/doc/10187/pdf/concern/annual_report_2014_eng.pdf), 25.07.2015.
  38. List of Waste, Including Hazardous Waste. Regulation of the Government of the Republic of Estonia. Riigi Teataja RT I 2010, 46, 273 (in Estonian). <https://www.riigiteataja.ee/akt/13338680>, 29.12.2015
  39. Anthony E.J., Jia L., Iribarne, A.P., Welford, G., Wang, J., Trass, O., Calcium sulphide in FBC boilers and its fate using liquid water reactivation.- *Fuel* **2006**, 85(12-13), 1871-1879.
  40. Liblik, V., Kaasik, M., Pensa, M., Rätsep, A., Rull, E., Tordik, A., Reduction of Sulphr Dioxide Emissions and Transboundary Effects of Oil Shale Based Energy Production. - *Oil Shale* **2006**, 23,1 29-38.
  41. Carbon Dioxide Information Analysis Center: Fossil-Fuel CO<sub>2</sub> Emissions: <http://cdiac.ornl.gov/trends/emis/top2011.cap>, 12. 11. 2015.

42. Speight, J. G. Shale Oil Production Processes - Origin and Properties of Oil Shale. Gulf Professional Publishing, Laramie, Wyoming, USA, 2012, p. 1- 30.
43. Kattai, V. Ülevaade põlevkivitööstuse arengust. - *Keskonnatehnika* **2008**, 4, 26-30.
44. Yörük C. R., Meriste, T., Trikkel, A., Kuusik, R., Thermo-oxidation characteristics of oil shale and oil shale char under oxy-fuel combustion conditions. *J. Therm. Anal. Calorim.* **2015**, 121, 1, 509-516.
45. Bauert, H., Kattai, V. Kukersite Oil Shale, Geology and Mineral Resources of Estonia, A. Raukas, A. Teedumae (eds.). Estonian Academy Publishers, Tallinn, 1997, 313-327.
46. Bitjukova, L., Mõtlep, R., Kirsimäe, K. Composition of oil shale ashes from pulverized firing and circulating fluidized-bed boiler in Narva Thermal Power Plants, Estonia. - *Oil Shale* **2010**, 27(4), 339-353.
47. Kattai, V., Saadre, T., Savitski, L. Estonian oil shale: geology, resource, mining conditions. Tallinn: Geological Survey of Estonia, 2000, p 226.
48. VKG yearbook 2014. Viru Keemia Grupp: <http://www.vkg.ee/cms-data/upload/juhatus/vkg-aastaraamat-eng-2014.pdf>, 01.08.2015.
49. VKG yearbook 2013. Viru Keemia Grupp. <http://www.vkg.ee/cms-data/upload/juhatus/vkg-aastaraamat-eng-2013.pdf> 01.08. 2015.
50. Mõtlep, R., Sild, T., Puura, E., Kirsimäe, K. Composition, diagenetic transformation and alkalinity potential of oil shale ash sediments, - *J. Hazard. Mater.* 2010, 184, 567-573.
51. Liira, M., Kirsimäe, K., Kuusik, R., Mõtlep, R. Transformation of calcareous oil-shale circulating fluidized-bed combustion boiler ashes under wet conditions. - *Fuel* **2009**, 88, 712-718.
52. Mõtlep, R., Kirsimäe, K., Talviste, P., Puura, E., Jürgenson, J. Mineral composition of Estonian oil shale semi-coke sediments. - *Oil shale*, **2007**, 24 (3), 405-422.
53. Carcia-Calzada, M., Marbán, G., Fuertes, A. B, Decomposition of CaS Particles at Ambient Conditions. - *Chem. Eng. Sci.* **2000**, 55(9). 1661-1674.
54. O'Brien, D. J., Birkner, F. B. Kinetics of Oxygenation of Reduced Sulfur Species in Aqueous Solution. - *Environ. Sci. Technol.* **1977**, 11(12), 1114-1120.
55. Mölder, L., Elenurm, A., Tamvelius, H., Transformation of Sulphur Compounds in a Hydraulic Ash-Discharge Unit. - *Proc. Estonian Acad. Sci. Chem.* **1998**, 47(1), 3-10.
56. Izquierdo, M., Querol, X. Leaching behaviour of elements from coal combustion fly ash: an overview. - *Int. J. Coal Geol.* **2012**, 94, 54-66.

57. Zekker, I., Tenno, T., Selberg, A., Uiga, K. Dissolution Modeling and Experimental Measurement of CaS-H<sub>2</sub>O Binary System. - *Chinese J. Chem.* **2011**, 29 (11), 2327–2336.
58. Shogenova, A., Sliapura, S., Shogenov, K., Sliapiene, R., Pomeranceva, R., Vaher, R., Uibu, M., Kuusik, R. Possibilities for geological storage and mineral trapping of industrial CO<sub>2</sub> emissions in the Baltic region. - *Energy Procedia* **2009**, 1, 2753-2760.
59. Sliapura, S., Shogenova, A., Shogenov, K., Sliapiene, R., Zabele, A., Vaher, R. Industrial carbon dioxide emissions and potential geological sinks in the Baltic States. - *Oil Shale* **2008**, 25(4), 465-484.
60. Park, A. H., Jadhav, R. A., Fan, L. S. CO<sub>2</sub> mineral sequestration: chemical enhanced aqueous carbonation of serpentine. - *Can. J. Chem. Eng.* **2003**, 81, 885-890.
61. Van Gerven, T., Van Keer, E., Arickx, S., Jaspers, M., Wauters, G., Vandecasteele, C. Carbonation of MSWI-bottom ash to decrease heavy metal leaching, in view of recycling. - *Waste Manage.* **2005**, 25, 291-300.
62. Uibu, M., Kuusik, R., Andreas, L., Kirsimäe, K. The CO<sub>2</sub> -binding by Ca-Mg-silicates in direct aqueous carbonation of oil shale ash and steel slag. - *Energy Procedia* **2011**, 4, 925-932.
63. Rendek, E., Ducom, G., Germain, P. Carbon dioxide sequestration in municipal solid waste incinerator (MSWI) bottom ash. - *J. Hazard. Mater.* **2006**, B128, 73-79.
64. Meima, J. A., Van der Weijden, R. D., Eighmy, T. T., Comans, R. N. J. Carbonation processes in municipal solid waste incinerator bottom ash and their effect on the leaching of copper and molybdenum. - *App. Geochem.* **2002**, 17, 1503-1513.
65. Costa, G., Baciocchi, R., Polettini, A., Pomi, R., Hills, C. D., Carey, P. J. Current status and perspectives of accelerated carbonation processes on municipal waste combustion residues. - *Environ. Monit. Assess.* **2007**, 135, 55-75.
66. Fernández-Bertos, B., Simons, S. J. R., Hills, C. D., Carey, P. J. A review of accelerated carbonation technology in the treatment of cement-based materials and sequestration of CO<sub>2</sub>. - *J. Hazard. Mater.* **2004**, B112 193-205.
67. Uibu, M., Velts, O., Kuusik, R. Developments in CO<sub>2</sub> mineral carbonation of oil shale ash. - *J. Hazard. Mater.* **2010**, 174, 209-214.
68. Teir, S., Eloneva, S., Zevenhoven, R. Production of precipitated calcium carbonate from calcium silicates and carbon dioxide. - *Energ. Convers. Manage.* **2005**, 46, 2954-2979.
69. Velts, O., Kindsigo, M., Uibu, M., Kallas, J., Kuusik, R. CO<sub>2</sub> mineralisation: Production of CaCO<sub>3</sub>-type material in a continuous flow disintegrator-reactor. - *Energy Procedia* **2015**, 63, 5904-5911.

70. Velts, O., Uibu, M., Kallas, J., Kuusik, R. Waste oil shale ash as a novel source of calcium for precipitated calcium carbonate: Carbonation mechanism, modeling, and product characterization. - *J. Hazard. Mater.* **2011**, 195, 139-146.
71. Irha, N., Uibu, M., Jefimova, J., Raado, L. M., Hain T., Kuusik, R. Leaching behaviour of Estonian oil shale ash-based construction mortars. - *Oil Shale* **2014**, 31, 4, 394-411.
72. Aavik, J. Tuhavee omaduste selgitamine kaltsiumkarbonaadi seadestustingimuste optimeerimiseks, M.Sc. Thesis. Tallinn University of Technology: Tallinn, Estonia, 2011.
73. Velts, O., Uibu, M., Rudjak, I., Kallas, J., Kuusik, R. Utilization of oil shale ash to prepare PCC: leachability dynamics and equilibrium in the ash-water system. - *Energy Procedia* **2009** 1(1) 4843-4850.
74. VKG Energia Põhja Soojuselektrijaama Tuhaväljaku vastavusse viimise projekt 2010.
75. Pihu, T., Arro, H., Prikk, A., Rootamm, R., Konist, A., Kirsimäe, K., Liira, M., Mõtsep, R. Oil shale CFBC ash cementation properties in ash fields. - *Fuel* **2012**, 93, 172-180.
76. Córdoba, P., Ochoa-Gonzalez, R., Font, O., Izquierdo, M., Querol, X., Leiva, C., López-Antón, M. A., Díaz-Somoano, M., Martínez-Tarazon, R., Fernandez, C., Tomás, A. Partitioning of trace inorganic elements in a coal-fired power plant equipped with a wet Flue Gas Desulphurization system. - *Fuel* **2012** 92, 145-157.
77. Córdoba, P., Castro, I., Maroto-Valer, M., Querol, X. The potential leaching and mobilization of trace elements from FGD-gypsum of a coal-fired power plant under water re-circulation conditions. - *J. Environ. Sci.* **2015**, 32, 72-80.
78. Baba, A., Kaya, A. Leaching characteristics of Fly Ash from Thermal Power Plants of Soma and Tuncbilek, Turkey. - *Environ. Monitor. Assess.* **2004**, 21, 171-181.
79. Komonweeraket, K., Cetin, B., Benson, C. H., Aydilek, A. H., Edil, T. B. Leaching characteristics of toxic constituents from coal fly ash mixed soils under the influence of pH. - *Waste Manage.* **2015**, 38, 174-184.
80. Gunning, P. J., Hills, C. D., Carey, P. J. Accelerated carbonation treatment of industrial wastes. - *Waste Manage.* **2010**, 30, 1081-1090.
81. Elonev, S., Puheloinen, E.M., Kanerv, J., Ekroos, A., Zevenhoven, R., Fogelholm, C. J. Co-utilisation of CO<sub>2</sub> and steelmaking slags for production of pure CaCO<sub>3</sub> – legislative issues. - *J. Clean. Prod.* **2010**, 18, 18, 1833-1839.
82. Chang, E. E, Chiu, A. C., Pan, S. Y., Chen, Y. H., Tan, C. S. Chiang, P. C. Carbonation of basic oxygen furnace slag with metalworking wastewater in a slurry reactor. - *Int. J. Greenh. Gas. Con.* **2013**, 12, 382-389.

83. Environmental Strategy 2030, Ministry of the Environment of the Republic of Estonia, Tallinn, 2007, [http://www.envir.ee/sites/default/files/keskkonnastrateegia\\_inglisek.pdf](http://www.envir.ee/sites/default/files/keskkonnastrateegia_inglisek.pdf), 27.04.15.
84. Tamm, K., Kuusik, R., Uibu, M., Kallas, J. Behaviour of sulfur compounds during aqueous leaching of oil shale ash. *Proceedings of the 4th International Conference on Accelerated Carbonation for Environmental and Materials Engineering*. Nasser, R., Santos, R., Cizer, Ö., Van Gerven, T. (eds.). Leuven, 541 - 544.
85. Tamm, K., Kallaste, P., Uibu, M., Kallas, J., Kuusik, R. Leaching Thermodynamics of Oil Shale Waste Key Components, *Proceedings of the 5th International Conference on Accelerated Carbonation for Environmental and Materials Engineering*, New York City, 2015.
86. Elenurm, A., Oja, V., Tali, E. Tearo, E., Yanchilin, A. Thermal processing of dictyonema argillite and kukersite oil shale: transformation and distribution of sulfur compounds in pilot-scale galoter process. - *Oil shale*, **2008**, 25, 3, 328-334.
87. Bernard, L., Freche, M., Lacout, J. L., Biscans, B. Modeling of the dissolution of calcium hydroxide in the preparation of hydroxyapatite by neutralization. - *Chem. Eng. Sci.* **2000**, 55, 5683-5692
88. Uibu, M., Kuusik, R. Mineral Trapping of CO<sub>2</sub> Via Oil Shale Ash Aqueous Carbonation: Controlling Mechanism of Process Rate and Development of Continuous- Flow Reactor System. - *Oil shale* **2009**, 26, 2, 40-58.
89. Yuan, T., Wang, J., Li, Z. Measurement and modelling of solubility for calcium sulfate dihydrate and calcium hydroxide in NaOH/KOH solutions. - *Fluid Phase. Equilibr.* **2010**, 297, 129-137.
90. Peng, X. Y., Wang, Y. Y., Chai, L. Y., Yu-de Shu, Y. D. Thermodynamic equilibrium of CaSO<sub>4</sub>-Ca(OH)<sub>2</sub>-H<sub>2</sub>O system. - *T. Nonferr. Metal. Soc.* **2009**, 19, 1, 249-252.
91. Wang, W., Zeng, D, Chen, Q., Yin, X., Experimental determination and modeling of gypsum and insoluble anhydrite solubility in the system CaSO<sub>4</sub>-H<sub>2</sub>SO<sub>4</sub>-H<sub>2</sub>O. - *Chem. Eng. Sci.* **2013**, 101, 120-129.
92. Shukla, J., Monhandas, V. P., Kumar, A. Effect of pH on the Solubility of CaSO<sub>4</sub> 2H<sub>2</sub>O in Aqueous NaCl Solutions and Physicochemical Solution Properties at 35°C. - *J. Chem. Eng. Data* **2008**, 53, 2797-2800
93. Kuecher, R., Noack, K., Zorn, T. Investigation of gypsum dissolution under saturated and unsaturated water conditions. - *Ecol. Model.* 2004, 176, 1-2, 1-14.
94. Mölder, L., Elenurm, A., Tamvelius, H. Sulphur Compounds in a Hydraulic ash – Disposal System. - *Proc. Est. Acad. Sci. Chem.* **1995**, 44, (2/3), 207-211.

95. Nielsen, A. H., Vollertsen, J., Hvitved-Jacobsen, T. Determination of kinetics and stoichiometry of chemical sulfide oxidation in wastewater of sewer networks – *Environ. Sci. Technol.* **2003**, 37, (1), 3853-3858.
96. Chen, K. Y., Morris, J. C. Kinetics of Oxidation of Aqueous Sulfide by O<sub>2</sub>. – *Environ. Sci. Technol.* **1972**, 6, (6), 529-537.
97. Almgren, T., Dyrssen, D., Elgquist, B., Johansson, O. Dissociation of hydrogen sulphide in seawater and comparison of pH scale. - *Mar. Chem.* **1976**, 4(3), 289-297.
98. ISO – 6058:1984, ISO 6058:1984, Water quality - Determination of calcium content - EDTA titrimetric method.
99. EKUK Virumaa affiliate Kohta-Järve laboratory of chemistry. 2002. The quality procedure guide TJ 17 – Determination of sulfide in water.
100. ISO – 9963-1: 1994(E)), Water quality -- Determination of alkalinity - Part 1: Determination of total and composite alkalinity.
101. Radleys: <http://www.radleys.com/products>, 24.04.2015.
102. HSC Chemistry® for Windows. Chemical reaction and equilibrium software with extensive thermochemical database. Version 7.1 Pori: Outokumu Research, Licence for Tallinn Technical University 2011.
103. Haario, H. Modest Users Manual, Profmath OY. Helsinki, Finland, 1994.
104. Hindmarsh, A. C. ODEPACK, a systematized collection of ODE solvers. *Scientific Computing: IMACS Transactions on Scientific Computation*, Stepleman, R. S. et al, (eds.), North-Holland, Amsterdam, 1983, 1, 55–64.
105. Aspen Plus User Guide, in 2000.
106. Tamm, K., Kuusik, R., Uibu, M., Kallas, J. Transformations of sulfides during aqueous carbonation of oil shale ash. - *Energy Procedia* 2013, 37, 5905–5912.
107. Tamm, K., Kuusik, R., Uibu, M., Kallas, J. Transformations of sulfur compounds in oil shale ash suspension. *Waste Management and the Environment VI: 6th International Conference on Waste Management and the Environment*, Popov, V., Itoh, H., Brebbia. C.A. (eds.). Wessex Institute of Technology Press, (WIT Transactions on Ecology and the Environment; 163), New Forest, UK, 2012, 25-35.
108. Velts, O., Hautaniemi, M., Kallas, J., Kuusik, R. Modelling calcium dissolution from oil shale ash: Part 1. Ca dissolution during ash washing in a batch reactor. - *Fuel Process. Technol.* 2010, **91**(5), 486-490.
109. Velts, O., Hautaniemi, M., Kallas, J., Kuosa, M., Kuusik, R. Modelling calcium dissolution from oil shale ash: Part 2. Continuous washing of the ash layer. - *Fuel Process Technol.* 2010, **91**(5), 491-495.
110. Estonia – Encyclopedia about Estonia: Nature, Climate, 2012 [http://www.estonica.org/en/Nature/Location and natural conditions/Climate/](http://www.estonica.org/en/Nature/Location%20and%20natural%20conditions/Climate/), 13.12.2015.

## ACKNOWLEDGMENTS

The present research was carried out at the Laboratory of Inorganic Materials, Tallinn University of Technology. The Estonian Science Foundation (Grant No 9334), the Estonian Ministry of Education and Research support (SF0140082s08, IUT33-19) of the Estonian Ministry of Education and Research, graduate school „Functional Materials and Technologies“ received funding from the European Social Fund under project 1.2.0401.09-0079 in Estonia, internationalization programme “DoRa”, activity 8 “Supporting the Participation of Young Researchers in the International Exchange of Knowledge” and the Archimedes Foundation supported this study financially.

I would like to express the attitude to my supervisor’s senior research scientist Rein Kuusik, senior research scientist Mai Uibu and Prof. Emeritus Juha Kallas for their advice, support, guidance and encouragement.

I would like to thank Prof. Kalle Kirsimäe’s team for performing the XRD and XRF measurements, Helle Ehala for carrying out different laboratory analyses, Tõnis Meriste for his valuable consultations, as well as colleagues from the Department of Chemical Engineering for offering the permeability to use their laboratory equipment’s.

I am grateful to all my former and present colleagues in Tallinn University of Technology and University of Tartu. My special thanks belong to Ph.D. Olga Velts-Jänes, MSc Priit Kallaste and Regiina Viires for their helpful support and friendship.

I am also grateful to my relatives and friends who have always encouraged and supported me. My deepest thanks go to my darling husband, Martti and my daughter, Tähe. Thank you for the great backing and love.

# Leaching of the Water-Soluble Calcium Components of Oil Shale Waste Ash

## ABSTRACT

Both the safe disposal of mineral waste and the control of atmospheric emissions are among the most serious problems caused by the use of oil shale for heat and power production as well as shale oil production. Processing two tons of oil shale produces about one ton of mineral residue. Estonia, which processes 20 million tons per year, thus produces vast quantities of mineral waste that is deposited in ash fields using hydrotransportation. The pH of this aqueous system is highly alkaline ( $\text{pH} > 12$ ). The introduction of stricter requirements for pollutants by the EU, the ever increasing size of the waste pile as well as the low rate of recycling (currently 5%) all pose a growing risk to the surrounding environment and people. Yet, these problems may provide new recycling opportunities in the energy sector. Both proposed and upcoming regulations restrict the composition of the mineral residue to mitigate the harmful effects of leaching compounds. This change in legislation will reduce the environmental problems caused by mineral waste, but may also restrict their use as feedstock for new products, and their waste disposal and handling processes.

The aim of this work was to develop a method for calculating the leaching streams from ash fields and the kinetic behavior of various types of oil shale residue for the purpose of designing leaching reactors that can be used to produce precipitated calcium carbonate.

To accomplish this it have been: (i) performed leaching experiments to determine the effective thermodynamic equilibrium of oil shale residues; (ii) determined the equilibrium constants using leaching tests; (iii) measured the leaching dynamics to determine the dissolution of the major components as a function of time; and (iv) found optimal reaction rate constants that are able to reproduce kinetic experimental leaching data. This study focused on the main water-soluble Ca-compounds of various oil shale ashes because these are the compounds that induce a strong alkaline effect ( $\text{pH} > 12$ ). Yet, these potentially harmful leaching waters are also a prerequisite for the production of precipitated calcium carbonate because of their high calcium content.

In order to better understand the impact of the key components on the leaching process, we studied pure components, binary ( $\text{Ca}(\text{OH})_2\text{-CaSO}_4\cdot 2\text{H}_2\text{O-H}_2\text{O}$ ) and ternary ( $\text{Ca}(\text{OH})_2\text{-CaSO}_4\cdot 2\text{H}_2\text{O-CaS-H}_2\text{O}$ ) model systems of pure components, and real process oil shale ashes. The binary and ternary systems were designed to match the composition of the real process ashes to allow for direct comparison. Using a mixture of modeling and experimental work, we determined the leaching mechanisms for three different types of ashes (pulverized firing and circulating fluidized bed ashes from thermal power plants together with solid heat carrier ash from shale oil and gas production) and

developed a mathematical model that is able to reproduce thermodynamic equilibrium and reaction kinetic experimental data.

This dissertation also includes thermodynamic calculations carried out using commercially available programs (HSC Chemistry<sup>®</sup> and ASPEN Plus). These programs helped to predict the ongoing changes in both the aqueous and solid phases in the leaching processes. Proposed leaching models using the Aspen Plus platform was implemented and calculated both the design and operating parameters for various leaching processes (i.e., the composition of contaminated water per year, required reactor volume, and residence time). This work verifies that a single model can be used to model complex technological systems.

In addition, equilibrium relations and mathematical models that describe the dissolution kinetics for the key components within oil shale mineral waste ( $\text{Ca}(\text{OH})_2$ ,  $\text{CaSO}_4 \cdot 2\text{H}_2\text{O}$ , and  $\text{CaS}$ ) have been developed. The model we propose can be used to predict the behavior of other Ca-rich fossil fuel wastes, irrespective of the thermal treatment technology used to create them. This tool could be used to help manage and mitigate the environmental impact of the vast inventory of such waste world-wide.

# Kaltsiumühendite leostumine põlevkivituha vesisüsteemides

## KOKKUVÕTE

Põlevkivil baseeruv elektri- ja õlitootmine tagab küll Eestile energiasõltumatus, kuid sellega kaasnevad mitmed keskkonnavalased probleemid, millest peamised on õhusaaste ja tahked jäätmed.

Eestis töödeldakse aastas pea 20 miljonit tonni põlevkivi ning tekkiv tuhk ladustatakse peaaegu täies ulatuses tuhaväljadele. Eskaleeruv jäätmete ladustamine suurendab koormust keskkonnale ning seega ka mõju inimestele. Selleks, et täita Euroopa Liidu üha karmistuvaid nõudeid atmosfääriheitmetele ja jäätmekäitlusele, tuleb leida uusi keskkonnasäästlikke lahendusi kütuste kasutusahelas. Üheks võimaluseks on vaadelda jäätmeid kui lisaväärtusega ressursi taaskasutuse kontekstis.

Põlevkivi jätkusuutlikuks majandamiseks peab tehnoloogia pidevalt arenema, see omakorda mõjutab nii jäätmete koostist kui ka leostuvate ühendite käitumist. Uute tehnoloogiate kasutuselevõtt võib küll vähendada jäätmete keskkonnoahtlikkust, kuid samas piirata nende taaskasutusvõimalusi.

Uurimistöo eesmärk oli töötada välja meetodika, mille alusel saab simuleerida tuhaväljadel toimuvat ja projekteerida leostusreaktorit sadestatud kaltsiumkarbonaadi tootmise protsessile lähtuvalt eri tüüpi põlevkivijäätmete leostuskineetikast.

Selle saavutamiseks: (1) määrati termodünaamiline tasakaal tuhk–vesi süsteemides; (2) arvutati leostuskatsete tulemuste alusel tasakaalukonstandid; (3) uuriti leostusdünaamikat funktsioonina ajast, et määrata peamiste veeslahustuvate komponentide leostuskineetika; ja (4) leiti optimaalsed reaktsiooni kiiruskonstandid leostusprotsessi reprodutseerimiseks. Antud uuring keskendus põlevkivi mineraalsetes jäätmetes sisalduvatele peamistele veeslahustuvatele Ca-ühenditele, mille leostumine on seotud tugevalt aluselise efektiga ( $\text{pH} > 12$ ), kuid samas on ka sadestatud kaltsiumkarbonaadi tootmise eelduseks.

Põlevkivituhkade leostuskäitumise selgitamiseks kasutati erineva keerukusastmega mudelsüsteeme: võtmekomponendid ( $\text{Ca}(\text{OH})_2$ ,  $\text{CaSO}_4 \cdot 2\text{H}_2\text{O}$  ja  $\text{CaS}$ ), kahe- ( $\text{Ca}(\text{OH})_2$ – $\text{CaSO}_4 \cdot 2\text{H}_2\text{O}$ – $\text{H}_2\text{O}$ ) ja kolmekomponentsed ( $\text{Ca}(\text{OH})_2$ – $\text{CaSO}_4 \cdot 2\text{H}_2\text{O}$ – $\text{CaS}$ – $\text{H}_2\text{O}$ ) mudelsegud vs reaalsed tuhad põlevkivitööstusest. Mudelsüsteemide koostis baseerus reaalsetele tuhkadele (tolmpõletuse ja keevkihi tuhad elektritootmiskateldest ja tahke soojuskandja tuhk põlevkivi õlitootmisest), mis võimaldas otsesest võrdlust. Koostati võtmekomponentide lahustumistasakaalu ning -kineetikat kirjeldavad matemaatilised mudelid. Seejärel määrati leostusmehhanism kolmele eri tüüpi tuhale ja töötati välja matemaatiline mudel, mis reprodutseerib katseandmeid lähtuvalt termodünaamilisest tasakaalust ja reaktsioonikineetikast.

Väitekirjas on välja toodud ka teoreetilised termodünaamikaarvutused HSC Chemistry® ja Aspen Plus programmidega, millega ennustati, leostumise protsessis toimuvaid muutusi nii vesi- kui tahkes faasis. Väljatöötatud leostusmudelit rakendati Aspen Plus platvormil erinevate leostusprotsesside projekteerimis- ja tööparameetrite arvutamiseks (nt. saastunud vee koostis ja reostuskestvus tuhavälja simulatsioonis, viibimisajad ja reaktorite ruumalad leostusreaktori simulatsioonis). Väljatöötatud mudelit saab kohandada analoogsetele kaltsiumiühendeid sisaldavatele tuhadele või muudele tööstusjääkidele.

Töö kinnitab, et ühtse mudeli abil saab modelleerida ka kompleksseid tehnoloogilisi süsteeme ning metoodikat saab kasutada, et hallata ja vähendada mõju keskkonnale sarnaste jäätmete käitlemisel üle maailma.

## APPENDIX A: ORIGINAL PUBLICATIONS

### PAPER I

Uibu, M., *Tamm, K.*, Velts-Jänes, O., Kallaste, P., Kuusik, R., Kallas, J.

Utilization of oil shale combustion wastes for PCC production: Quantifying the kinetics of  $\text{Ca}(\text{OH})_2$  and  $\text{CaSO}_4 \cdot 2\text{H}_2\text{O}$  dissolution in aqueous systems.

*Fuel Processing Technology* 2015, 140, 156-164.





## Research article

Utilization of oil shale combustion wastes for PCC production: Quantifying the kinetics of  $\text{Ca}(\text{OH})_2$  and  $\text{CaSO}_4 \cdot 2\text{H}_2\text{O}$  dissolution in aqueous systems

M. Uibu\*, K. Tamm, O. Velts-Jänes, P. Kallaste, R. Kuusik, J. Kallas

Tallinn University of Technology, Laboratory of Inorganic Materials, Ehitajate tee 5, 19086 Tallinn, Estonia

## ARTICLE INFO

## Article history:

Received 27 April 2015

Received in revised form 2 September 2015

Accepted 5 September 2015

Available online xxxx

## Keywords:

Oil shale ash

Leaching

Kinetics

Portlandite

Modeling

## ABSTRACT

The ash produced during oil shale combustion is classified as waste, however, one could also view it as a low-cost source of lime for the abatement of  $\text{SO}_2$  and  $\text{CO}_2$  emissions as well as for the commercial production of precipitated calcium carbonate (PCC)-type filler material. This study focuses on the dissolution mechanisms of the main water-soluble calcium species in oil shale ash–water systems. Reaction models that describe the dissolution of  $\text{Ca}(\text{OH})_2$  and  $\text{CaSO}_4 \cdot 2\text{H}_2\text{O}$  in water were developed and the kinetic parameters of the proposed system composed of differential equations were estimated by optimizing the model reproduction of experimental data. The dissolution kinetics of  $\text{Ca}(\text{OH})_2$  and  $\text{CaSO}_4 \cdot 2\text{H}_2\text{O}$  were also simulated using the Aspen Plus process modeling platform.

© 2015 Elsevier B.V. All rights reserved.

## 1. Introduction

Both environmentally safe disposal and/or reuse of solid wastes and atmospheric emissions ( $\text{SO}_2$ ,  $\text{CO}_2$ ,  $\text{NO}_x$ , etc.) are among the most serious problems caused by the extensive use of fossil fuels for heat and power production, especially in case of low-grade solid fuels.  $\text{CO}_2$  sequestration by mineral carbonation of alkaline waste residues mitigates both of these problems since the leaching behavior of the alkaline wastes often improves after carbonation [1–7]. In addition, the  $\text{CO}_2$  sequestration process may become economically feasible when considering the possibility of upgrading the carbonized waste materials into commercial products such as precipitated calcium carbonate (PCC) [8,9].

In Estonia about 60% of the country's fuel balance is covered by oil shale (annual mining output 14–16 Mt) and its share in power production exceeds 95% [10,11]. The combustion of oil shale in electric power plants is carried out using circulating fluidized bed combustion and pulverized firing, which generates massive amounts of waste ash (45–48% of the oil shale dry mass [12]) as well as atmospheric emissions ( $\text{SO}_2$ ,  $\text{CO}_2$ ) [13,14]. Only a small percentage of the oil shale ash is utilized, either in the building materials industry, in agriculture as a liming agent, or during road construction. Most of the oil shale ash is still deposited in ash sediment fields near the power plants (6–8 Mt annually) [10]. For transporting the ash to wet open-air deposits, a closed hydraulic system is used in which  $10^7$ – $10^8$  m<sup>3</sup> of  $\text{Ca}^{2+}$ -saturated water is circulating between the plant and the sedimentary ponds [10]. Oil shale ashes from the power plants have been classified as hazardous wastes because of

its high alkalinity according to the Material Safety Data Sheet for Burnt Oil Shale enforced with the EC regulations No 1907/2006 and EU No 453/2010 [15].

The mineral part of oil shale ash consists mainly of  $\text{CaO}$  (30–60%) and  $\text{SiO}_2$  (20–50%), however,  $\text{Al}_2\text{O}_3$ ,  $\text{Fe}_2\text{O}_3$ ,  $\text{K}_2\text{O}$ , and  $\text{MgO}$  are also present [12,16]. Ca is present in multiple forms, primarily as lime (10–25% wt, depending on the combustion technology), anhydrite and calcite, and within glassy matrix as silicates [17–20]. Calcium leaching behavior is associated with the phase composition of the ash. Hydration of oil shale ash involves the slaking of lime to form portlandite ( $\text{Ca}(\text{OH})_2$ ) and anhydrite conversion to gypsum ( $\text{CaSO}_4 \cdot 2\text{H}_2\text{O}$ ) as the main water-soluble calcium compounds [21]. According to Irha et al. [22], the major ions in oil shale ash leachates are  $\text{Ca}^{2+}$ ,  $\text{SO}_4^{2-}$ ,  $\text{K}^+$ , and  $\text{Na}^+$ . They found that  $\text{Ca}^{2+}$  and  $\text{SO}_4^{2-}$  ions are dominant in the leachates and correspond to the content of free lime and sulfates in the ash samples. Izquierdo and Querol [20] also found that the leaching properties of coal ashes depend significantly on the content of calcium compounds. Due to their predominant surface association in fly ash and the marked solubility of most sulfate-bearing compounds, sulfur is the major soluble element in ash along with calcium.

In recent years, our group has studied the leaching behavior of the main soluble compounds in oil shale ash with the aim of obtaining a PCC-type material from the ash and its leaching waters [6,9,21,23,24]. We have determined the equilibrium distribution of calcium between ash–water phases, estimated the internal mass transfer of calcium within ash particles by evaluating the effective diffusion coefficients, and developed mass transfer models that allow one to simulate the dynamics of the calcium dissolution process from the oil shale ash during leaching in a batch as well as a continuous flow reactor [23,24].

\* Corresponding author.

E-mail address: [mai.uibu@ttu.ee](mailto:mai.uibu@ttu.ee) (M. Uibu).

To determine the feasibility of the technologies for upgrading the oil shale ash, one must create mathematical models which define the operating parameters and simulate the leaching of water-soluble oil shale ash components, the binding of CO<sub>2</sub> and SO<sub>2</sub> from flue gases, and the crystallization of solid products in the multi-phase ash leachates – flue gas system. In addition to the calcium leaching dynamics, one must also consider the interactions between different substances (Ca<sup>2+</sup>, SO<sub>4</sub><sup>2-</sup>, K<sup>+</sup>, Na<sup>+</sup>, etc.) leached from the ash. The latter is important when determining whether the environmental safety standards are met or exploring possible co-crystallization effects that could influence the quality of the final product. Thus, the current study investigates the dissolution mechanisms of Ca(OH)<sub>2</sub> and CaSO<sub>4</sub>·2H<sub>2</sub>O as the main water-soluble Ca-species in aqueous oil shale ash systems [21] and proposes modeling algorithms that account for both reaction kinetics and thermodynamic equilibrium.

## 2. Materials and methods

### 2.1. Experimental methods

The dissolution kinetics of calcium hydroxide Ca(OH)<sub>2</sub> (BDH, 95% purity) was determined in a batch reactor. Initially, 0.050 L of deionized water (conductivity 0.05 μS/cm) was stirred in a 0.100 L reactor vessel under N<sub>2</sub> flow at room temperature (25 °C) for 360 s. The temperature remained at 25 °C during the course of all experiments. After the stabilization process, solid Ca(OH)<sub>2</sub> (0.1850 g, 0.0925 g, 0.0463 g, and 0.01982 g corresponding to molar concentrations of 0.0500 M, 0.0250 M, 0.0125 M and 0.0054 M) was quickly added to the water. The pH and temperature of the mixture were measured and recorded every second using a Mettler Toledo electrode DG-112 Pro connected to an automatic titrator T90 under N<sub>2</sub> flow until stabilization.

The dissolution kinetics of CaSO<sub>4</sub>·2H<sub>2</sub>O (Iach:ner, 99% purity) was determined in a batch reactor. Initially, 0.750 L of deionized water (conductivity 0.05 μS/cm) was poured into a 1 L Lara Controlled Lab Reactor. The stirrer was set to revolve at 250 rpm and a thermostat (Huber Unistat 405) kept the entire system at 25 °C during the course of the experiment. A pause control program briefly halted the stirring while solid CaSO<sub>4</sub>·2H<sub>2</sub>O (corresponding to the molar concentrations of 0.0001 M, 0.0015 M, 0.0020 M, 0.0025 M, 0.0040 M, 0.0050 M, 0.0060 M, 0.0080 M, 0.0100 M, 0.0120 M, 0.0150 M, 0.0160 M, 0.0200 M, 0.0250 M, 0.0300 M) was quickly added to the system using a funnel. Each suspension was maintained as a closed system for 1 h.

The particle size distribution of Ca(OH)<sub>2</sub> and CaSO<sub>4</sub>·2H<sub>2</sub>O was determined using Horiba laser scattering particle size distribution analyzer LA-950 (Table 1). The mean size of oil shale fly ashes particles fits in the same range [22].

The system conductivity (Hanna Instruments 9932 Microprocessor Conductivity Meter with HI 92000-5.0.26 software), pH (Knick Portamess 913 pH; pH-meter sensor: Hamilton Polylyte Plus VP360), and temperature were recorded every 10 s.

After each experiment, the suspension was filtered and the filtrate was analyzed for Ca<sup>2+</sup> (ISO-6058:1984), SO<sub>4</sub><sup>2-</sup> (Lovibond Spectro Direct spectrometer, method: Bariumsulfate – turbidity), and alkalinity (ISO-9963-1: 1994(E)).

**Table 1**  
Property data of the tested calcium hydroxide and gypsum samples.

Sample	Mean size	Median size	Particle size distribution		
	μm	μm	x <sub>10</sub> , μm	x <sub>50</sub> , μm	x <sub>90</sub> , μm
Ca(OH) <sub>2</sub> (BDH, 95% purity)	16.45	6.47	2.88	6.47	51.77
CaSO <sub>4</sub> ·2H <sub>2</sub> O (Iach:ner, 99% purity)	29.64	20.51	9.21	20.51	62.81

### 2.2. Modeling software

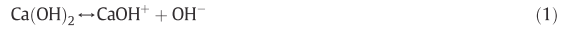
Kinetic calculations were performed using the MODEST 6.1 software package designed to carry out various model building tasks such as simulation, parameter estimation, sensitivity analysis, and optimization [25]. The software consists of a FORTRAN 95/90 library of objective functions, solvers, and optimizers that allow one to link model problem-dependent routines to an objective function. The systems of differential equations were solved by means of linear multi-step methods implemented in ODESSA, which is based on LSODE software [26].

In addition, both equilibrium calculations and process modeling were carried out using ASPEN Plus V8.6 (APV86) software, which is a process modeling tool for conceptual design, optimization, and performance monitoring widely used in the chemical, mining, and solid fuel power generation industries [27].

## 3. Results and discussion

### 3.1. Thermodynamic equilibria of Ca(OH)<sub>2</sub>-H<sub>2</sub>O and CaSO<sub>4</sub>·2H<sub>2</sub>O-H<sub>2</sub>O system

The dissociation equilibria for Ca(OH)<sub>2</sub> and CaSO<sub>4</sub>·2H<sub>2</sub>O in aqueous systems are provided in Eqs. (1)–(3) [28].



The mechanism for lime dissociation can also be presented as a single step reaction system (Eq. (4)).



The thermodynamic equilibrium constants for the dissociation reactions (1)–(3) are:

$$K_1 = [\text{CaOH}^+] \gamma_{\text{CaOH}^+} [\text{OH}^-] \gamma_{\text{OH}^-} \quad (5)$$

$$K_2 = \frac{[\text{Ca}^{2+}] \gamma_{\text{Ca}^{2+}} [\text{OH}^-] \gamma_{\text{OH}^-}}{[\text{CaOH}^+] \gamma_{\text{CaOH}^+}} \quad (6)$$

$$K_3 = \left( [\text{Ca}^{2+}] \gamma_{\text{Ca}^{2+}} \right) \left( [\text{SO}_4^{2-}] \gamma_{\text{SO}_4^{2-}} \right) (\alpha_{\text{H}_2\text{O}})^2 \quad (7)$$

The activity coefficient  $\gamma$  accounts for the nonideality of these electrolyte solutions. By rearranging Eqs. (5) and (6) and considering both the balance of mass and charge, the molarities of CaOH<sup>+</sup>, Ca<sup>2+</sup>, and OH<sup>-</sup> within the Ca(OH)<sub>2</sub>-H<sub>2</sub>O system can be expressed as:

$$[\text{CaOH}^+] = \frac{K_1}{[\text{OH}^-] \gamma_{\text{OH}^-} \gamma_{\text{CaOH}^+}} \quad (8)$$

$$[\text{Ca}^{2+}] = \frac{K_2 [\text{CaOH}^+] \gamma_{\text{CaOH}^+}}{[\text{OH}^-] \gamma_{\text{OH}^-} \gamma_{\text{Ca}^{2+}}} \quad (9)$$

$$[\text{OH}^-]_{\text{total}} = 2[\text{Ca}^{2+}] + [\text{CaOH}^+] + [\text{H}^+] \quad (10)$$

$$[\text{Ca}^{2+}]_{\text{total}} = [\text{Ca}^{2+}] + [\text{CaOH}^+]. \quad (11)$$

The thermodynamic equilibrium constant  $K_1^*$  for the single step reaction system presented in Eq. (4) can be expressed on molar basis as:

$$K_1^* = \frac{[\text{Ca}^{2+}]_{\text{total}} [\text{OH}^-]_{\text{total}}^2}{[\text{Ca}(\text{OH})_2]_{\text{total}}} \quad (12)$$

while the molarity of  $\text{Ca}^{2+}$  in the  $\text{CaSO}_4 \cdot 2\text{H}_2\text{O}-\text{H}_2\text{O}$  system can be expressed as:

$$[\text{Ca}^{2+}] = \frac{K_3}{[\text{SO}_4^{2-}] \gamma_{\pm, \text{CaSO}_4} (\alpha_{\text{H}_2\text{O}})^2} \quad (13)$$

The solubilities of  $\text{Ca}(\text{OH})_2$  and  $\text{CaSO}_4 \cdot \text{H}_2\text{O}$  are equal to the sum of the molarities of the calcium containing species (Eq. (11)). The solubility of portlandite in pure water at 25 °C has been determined in several studies [28–31] and varies within the range of 0.02020–0.02109 m. Nordstrom [31] calculated an average gypsum solubility of  $0.01528 \pm 0.000047$  m at 25 °C by combining the results from several studies. Most recently, Wang et al. [32] determined that gypsum has the solubility of 0.01514 m.

In order to test the capability of the model to predict the solubility of  $\text{Ca}(\text{OH})_2$  and  $\text{CaSO}_4 \cdot 2\text{H}_2\text{O}$ , the Pitzer model embedded in the Aspen Plus platform was employed for the  $\text{Ca}(\text{OH})_2-\text{H}_2\text{O}$  and  $\text{CaSO}_4 \cdot 2\text{H}_2\text{O}-\text{H}_2\text{O}$  systems. An expression for the excess Gibbs free energy [33,34] is expressed by Eq. (14).

$$\frac{G^E}{RT} = n_w \left[ f(I) + \sum_i \sum_j B_{ij} m_i m_j + \sum_i \sum_j \theta_{ij} m_i m_j + 1/2 \sum_i \sum_j \left( \sum_k m_k |z_k| \right) \times C_{ij} m_i m_j + 1/6 \sum_i \sum_j \sum_k \psi_{ijk} m_i m_j m_k \right] \quad (14)$$

The Pitzer model in the Aspen Physical Property System involves user-supplied parameters. These parameters are used in the calculation of binary and ternary parameters for the electrolyte system. The cation–anion parameters  $B_{ij}$  and  $C_{ij}$  are characteristic for an aqueous system containing a single electrolyte.  $B_{ij}$  is expressed as a function of  $\beta_{ij}^0$  and  $\beta_{ij}^1$  or  $\beta_{ij}^0$ ,  $\beta_{ij}^2$ , and  $\beta_{ij}^3$ . The parameters  $\theta_{ij}$  and  $\psi_{ijk}$  are used to define the difference in the interaction of unlike ions of the same sign from the mean interaction of like ions. Because the default parameters of the Pitzer model within Aspen Plus V8.6 did not provide satisfactory results, we included the interaction parameters provided by Yuan et al. [28] using the Methods/Parameters/Binary Interaction form (Table 2).

The Aspen Plus RGibbs reactor model uses a Gibbs free energy minimization technique to determine the composition of each phase. This

was employed to predict the equilibrium composition of both the  $\text{Ca}(\text{OH})_2-\text{H}_2\text{O}$  (Fig. 1a) and  $\text{CaSO}_4 \cdot 2\text{H}_2\text{O}-\text{H}_2\text{O}$  systems (Fig. 2a). Consequently, the equilibrium constants  $K_1$ ,  $K_2$ ,  $K_1^*$  and  $K_3$ , expressed on molar basis in Eqs. (1)–(4), can be computed (Figs. 1b, 2b) together with the equilibrium compositions and material balance, also for dilute solutions as apparent equilibrium (Figs. 1a, 2a).

### 3.2. Building a kinetic model for the $\text{Ca}(\text{OH})_2-\text{H}_2\text{O}$ binary system

The dissolution kinetics of  $\text{Ca}(\text{OH})_2$  has been described by several authors [35,36]. The current study was focused on building kinetic reaction models that without further modifications could be applied for process modeling with ASPEN Plus to upscale the processes and estimate the feasibility of the proposed method.

#### 3.2.1. Determining the dissolution kinetics of $\text{Ca}(\text{OH})_2$ in a batch reactor

Kinetic models of the  $\text{Ca}(\text{OH})_2-\text{H}_2\text{O}$  system were constructed using experimental data. The dissolution kinetics of  $\text{Ca}(\text{OH})_2$  was determined in a batch reactor by measuring pH profiles at different concentrations of  $\text{Ca}(\text{OH})_2(\text{s})$  (Fig. 3). The temperature of the  $\text{Ca}(\text{OH})_2$  aqueous mixtures remained at 25 °C throughout all experiments. The molar concentration of  $\text{OH}^-$  was calculated at every point in time based on the pH measurements of the solution using the activity coefficient,  $\gamma_{\text{OH}^-}$ . A value for  $\gamma_{\text{OH}^-}$  was calculated using the Debye–Hückel equation (Eq. (15)) for  $0.01 < I < 0.1$ , where  $\gamma_i$  is activity coefficient of species  $i$ ,  $d_i$  is effective diameter of the hydrated ion (nm),  $z_i$  is the charge on species  $i$ , and  $I$  is the ionic strength of solution.

$$\log \gamma_i = - \frac{0.51 \cdot z_i^2 \sqrt{I}}{1 + 3.3 \cdot d_i \sqrt{I}} \quad (15)$$

#### 3.2.2. $\text{Ca}(\text{OH})_2$ two-step dissolution model

Two dissolution models were constructed to describe the  $\text{Ca}(\text{OH})_2-\text{H}_2\text{O}$  system using respective kinetics parameters. In the more complex approach, the mechanism of lime dissolution in an aqueous batch system was expressed as a two-step first order reaction system (Eqs. (16)–(17)).



**Table 2**

Pitzer model interaction parameters for  $\text{Ca}(\text{OH})_2-\text{H}_2\text{O}$  and  $\text{CaSO}_4 \cdot 2\text{H}_2\text{O}-\text{H}_2\text{O}$  system.

System	Component i	Component j	Parameters	Value	Reference	
$\text{Ca}(\text{OH})_2-\text{H}_2\text{O}$	$\text{CaOH}^+$	$\text{OH}^-$	$\beta_{ij}^0$	$a_1$	0.13618	[28]
			$a_2$	0.03584		
			$\beta_{ij}^1$	$a_1$	−0.36923	[28]
			$a_2$	−0.06441		
			$C_{ij}$	$a_1$	−0.04982	[28]
			$a_2$	−0.05177		
$\text{CaSO}_4 \cdot 2\text{H}_2\text{O}-\text{H}_2\text{O}$	$\text{CaOH}^+$	$\text{Ca}^{2+}$	$\theta_{ij}$	$a_1$	−10.0032	[28]
			$a_2$	0.00014		
			$\beta_{ij}^0$	$a_1$	13.1654	[28]
			$a_2$	−0.13683		
			$\beta_{ij}^1$	$a_1$	0	APV86 PITZER
			$a_2$	0		
	$\beta_{ij}^2$	$a_1$	−55.7	APV86 PITZER		
	$a_2$	−0.516				
	$\beta_{ij}^3$	$a_1$	2.65	APV86 PITZER		
	$a_2$	0.0546				
	$C_{ij}$	$a_1$	−192.276	[28]		
	$a_2$	2.13099				

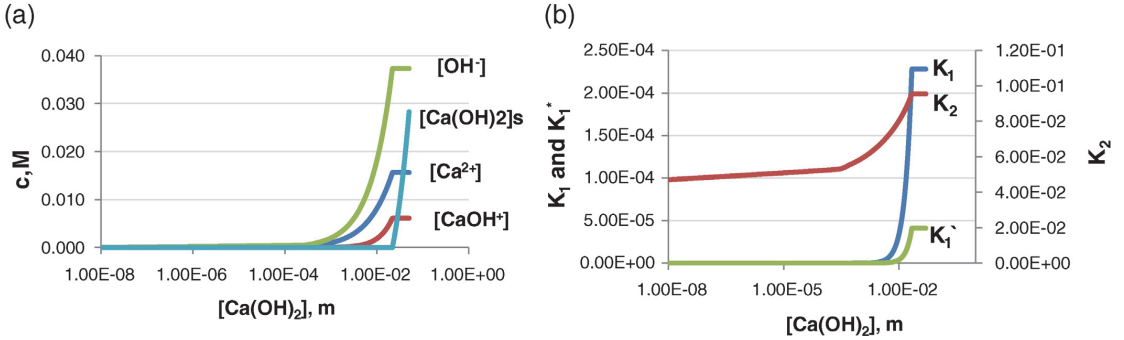


Fig. 1. Thermodynamic equilibria of the Ca(OH)<sub>2</sub>-H<sub>2</sub>O binary system at 25 °C according to the Pitzer model in Aspen Plus V8.6 together with the interaction parameters provided in Table 2: (a) equilibrium composition and (b) equilibrium constants K<sub>1</sub>, K<sub>2</sub> and K<sub>1</sub><sup>\*</sup> expressed on molar basis: K<sub>1</sub> = [CaOH<sup>+</sup>][OH<sup>-</sup>]; K<sub>2</sub> = [Ca<sup>2+</sup>][OH<sup>-</sup>]/[CaOH<sup>+</sup>]; K<sub>1</sub><sup>\*</sup> = [Ca<sup>2+</sup>]<sub>Total</sub>[OH<sup>-</sup>]<sub>Total</sub><sup>2</sup>.



Using this dissolution model, the dynamic concentration profiles of the characteristic species that participate in the lime dissolution process can be modeled using the differential equations presented in Eqs. (18)–(21):

$$\frac{d[\text{OH}^-]}{dt} = k_{11}[\text{Ca}(\text{OH})_2] - k_{12}[\text{CaOH}^+][\text{OH}^-] + k_{21}[\text{CaOH}^+] - k_{22}[\text{Ca}^{2+}][\text{OH}^-] \quad (18)$$

$$\frac{d[\text{Ca}^{2+}]}{dt} = k_{21}[\text{CaOH}^+] - k_{22}[\text{Ca}^{2+}][\text{OH}^-] \quad (19)$$

$$\frac{d[\text{CaOH}^+]}{dt} = k_{11}[\text{Ca}(\text{OH})_2] - k_{12}[\text{CaOH}^+][\text{OH}^-] - k_{21}[\text{CaOH}^+] + k_{22}[\text{Ca}^{2+}][\text{OH}^-] \quad (20)$$

$$\frac{d[\text{Ca}(\text{OH})_2]}{dt} = -k_{11}[\text{Ca}(\text{OH})_2] + k_{12}[\text{CaOH}^+][\text{OH}^-]. \quad (21)$$

Values for the backward reaction rate constants, k<sub>12</sub> and k<sub>22</sub>, may be expressed in terms of the forward reaction rate constants and the equilibrium constants as k<sub>11</sub>[Ca(OH)<sub>2</sub>]<sub>i</sub>/K<sub>1</sub> and k<sub>21</sub>/K<sub>2</sub> respectively, where

[Ca(OH)<sub>2</sub>]<sub>i</sub> is the Ca(OH)<sub>2</sub> concentration at the time moment t during dissolution. The equilibrium constants K<sub>1</sub> and K<sub>2</sub> were calculated from the equilibrium composition (Fig. 1).

The reaction rate constants, k<sub>11</sub> and k<sub>21</sub>, were evaluated using a parameter estimation procedure utilizing the proposed model equations together with the experimental data obtained in batch experiments at various concentrations of Ca(OH)<sub>2</sub>. The correlation coefficients for all data sets were greater than 0.98. Based on these results, average values for the reaction rate constants, k<sub>11</sub> and k<sub>21</sub>, were estimated to be 0.0345 s<sup>-1</sup> and 0.0544 L(mol s)<sup>-1</sup>, respectively. Next, we simulated the dissolution process using average values for the rate constants. We confirmed the accuracy of the proposed dissolution model (R<sup>2</sup> > 90%) by comparing the results of process simulation with experimental data that was not used during the parameter evaluation step (Fig. 3). The concentration profiles of the relative species are given in Fig. 4 for various concentrations of the Ca(OH)<sub>2</sub> suspension. These results indicate that the two-step Ca(OH)<sub>2</sub> dissolution model is more accurate at higher concentrations (Fig. 4b, c, d versus a).

### 3.2.3. Ca(OH)<sub>2</sub> one-step dissolution model

The Ca(OH)<sub>2</sub> dissolution mechanism can also be presented as a simplified one-step first order reaction system:



Thus, dissolution of Ca(OH)<sub>2</sub> in aqueous solutions can be modeled using the following differential equations for each of the three different

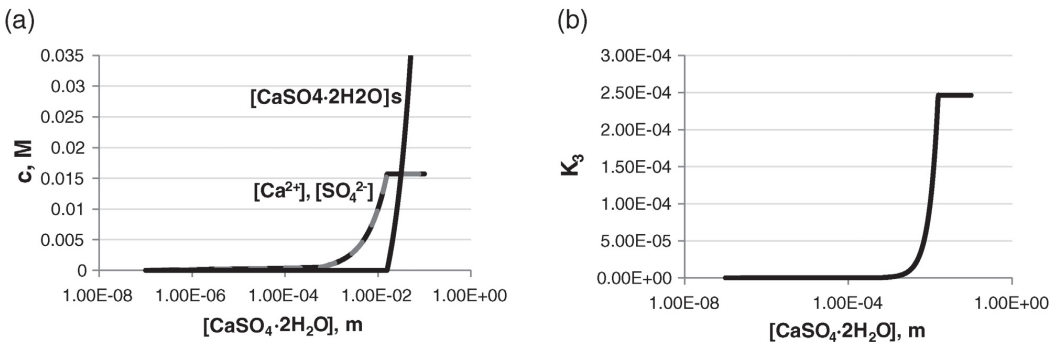


Fig. 2. Thermodynamic equilibria of CaSO<sub>4</sub>·2H<sub>2</sub>O-H<sub>2</sub>O binary system at 25 °C according to Pitzer model in Aspen Plus V8.6 together with the interaction parameters provided in Table 2: (a) equilibrium composition and (b) equilibrium constant K<sub>3</sub> expressed on molar basis: K<sub>3</sub> = [Ca<sup>2+</sup>][SO<sub>4</sub><sup>2-</sup>].

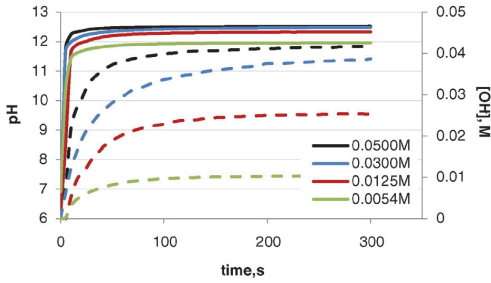


Fig. 3. Experimental pH (—) and  $[\text{OH}^-]$  (---) vs time plot for  $\text{Ca}(\text{OH})_2\text{-H}_2\text{O}$  batch system at 25 °C.

species:

$$\frac{d[\text{OH}^-]}{dt} = 2.0 \times (k_{11}^* [\text{Ca}(\text{OH})_2] - k_{12}^* [\text{Ca}^{2+}] [\text{OH}^-]^2) \quad (23)$$

$$\frac{d[\text{Ca}^{2+}]}{dt} = k_{11}^* [\text{Ca}(\text{OH})_2] - k_{12}^* [\text{Ca}^{2+}] [\text{OH}^-]^2 \quad (24)$$

$$\frac{d[\text{Ca}(\text{OH})_2]}{dt} = -k_{11}^* [\text{Ca}(\text{OH})_2] + k_{12}^* [\text{Ca}^{2+}] [\text{OH}^-]^2 \quad (25)$$

The value of the backward reaction rate constant,  $k_{12}^*$  may be expressed in terms of the equilibrium constant as  $k_{12}^* = k_{11}^* [\text{Ca}(\text{OH})_2]_{\text{eq}} / K^*$ . The concentrations in Eqs. (23)–(25) are expressed in molar units. The

equilibrium constant  $K^*$  was calculated from the equilibrium composition (Fig. 1b).

The reaction rate constant  $k_{11}^*$  was evaluated ( $R^2 > 92\%$ ) using the differential Eqs. (23)–(25) and was found to have a value of  $0.0282 \text{ s}^{-1}$ . The model was verified by comparing the predictions of the changes in concentration of the reactive species ( $\text{Ca}^{2+}$ ,  $\text{OH}^-$ ,  $\text{Ca}(\text{OH})_2$ ) with the experimental data. Plots of the experimental and simulated concentration profiles are provided in Fig. 5. The results indicate that the one-step  $\text{Ca}(\text{OH})_2$  dissolution model is more accurate for dilute solutions (Fig. 5a, b, c versus d). The shift to two-step model takes place at saturated solutions (Fig. 5d vs d), as the share of  $\text{CaOH}^+$  (Fig. 1a) and its effect on  $\text{Ca}(\text{OH})_2$  dissolution kinetics increases.

Although the two-step model elaborates the  $\text{Ca}(\text{OH})_2$  dissolution mechanism in more detail, the simplified one-step model also fits with the experimental results and is easier to handle and compare with real systems. The current models are built on the first order kinetics which considers the reduction of specific surface area in proportion to the decreasing solid phase. Modifications to include also the effect of particle size into the Ca dissolution model are planned for the next step.

### 3.3. Building a $\text{CaSO}_4 \cdot 2\text{H}_2\text{O}\text{-H}_2\text{O}$ kinetic model

#### 3.3.1. Determining the dissolution kinetics of $\text{CaSO}_4 \cdot 2\text{H}_2\text{O}$ in a batch reactor

A kinetic model of the  $\text{CaSO}_4 \cdot 2\text{H}_2\text{O}\text{-H}_2\text{O}$  system was constructed using experimental data. The dissolution kinetics of gypsum was determined in a batch reactor by measuring the EC profiles at different  $\text{CaSO}_4 \cdot 2\text{H}_2\text{O}(\text{s})$  concentrations (Fig. 6). The molar concentration of  $\text{Ca}^{2+}$  at each time point was calculated using the EC measurements. The correlation between the measured concentrations of EC and  $\text{Ca}^{2+}$  ( $R^2 = 0.99$ ) is presented in Fig. 7.

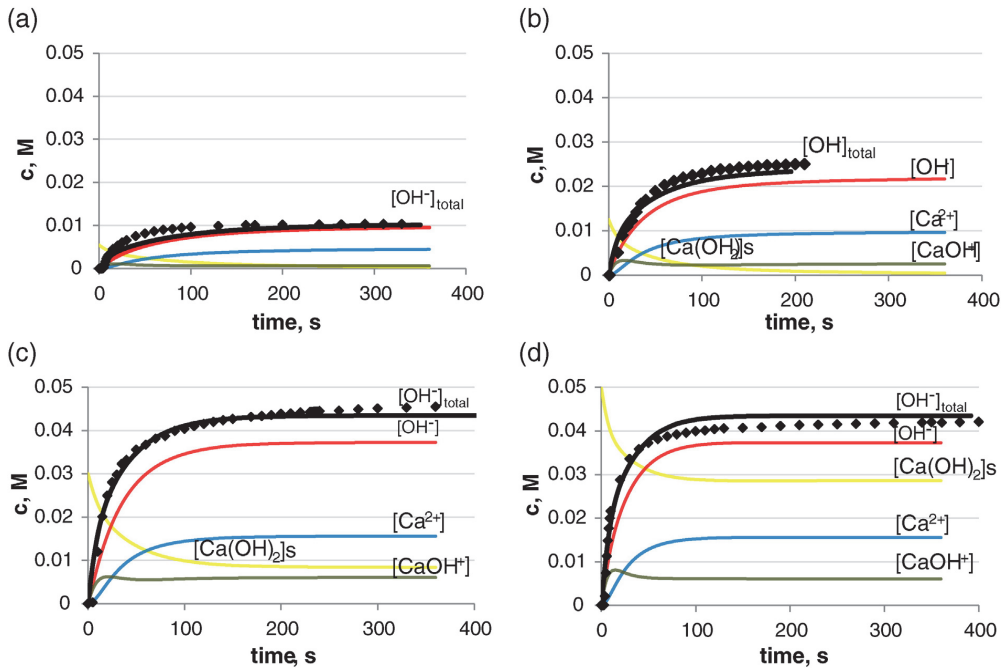


Fig. 4. Modeling of  $\text{Ca}(\text{OH})_2$  2-step dissolution kinetics in  $\text{Ca}(\text{OH})_2\text{-H}_2\text{O}$  batch system: experimental ( $\blacklozenge$   $[\text{OH}^-]_{\text{total}}$ ) vs simulated (— by Modest 6.1 and Aspen Plus V8.6) concentration profiles ( $[\text{OH}^-]_{\text{total}} = 2[\text{Ca}^{2+}] + [\text{CaOH}^+] + [\text{H}^+]$ ) at (a) 0.0054 M  $\text{Ca}(\text{OH})_2(\text{s})$ ; (b) 0.0125 M  $\text{Ca}(\text{OH})_2(\text{s})$ ; (c) 0.0300 M  $\text{Ca}(\text{OH})_2(\text{s})$ ; and (d) 0.0500 M  $\text{Ca}(\text{OH})_2(\text{s})$ .

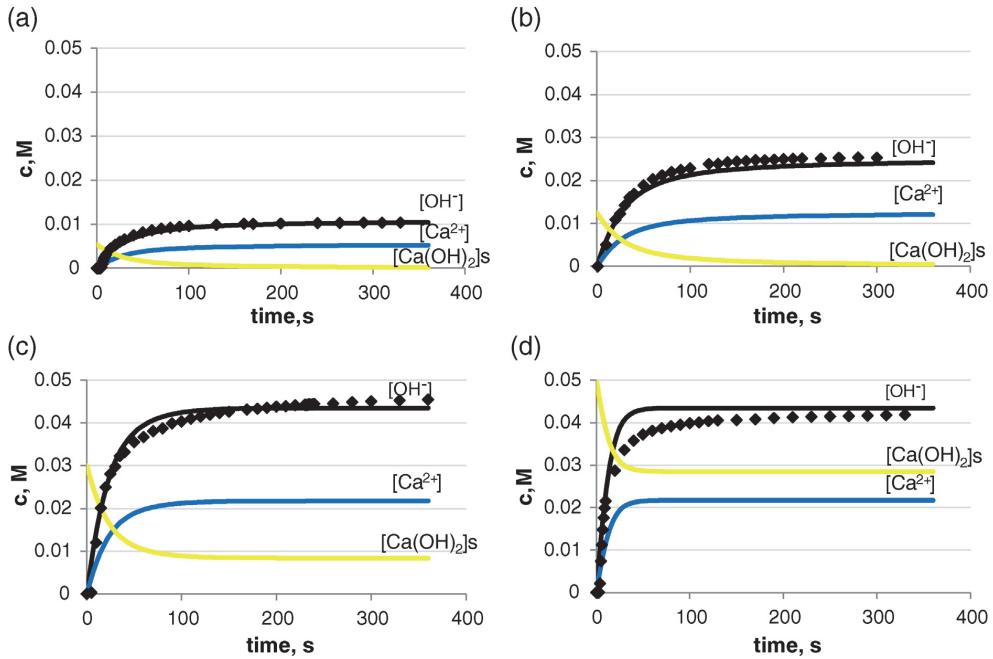


Fig. 5. Modeling of  $\text{Ca(OH)}_2$  1-step dissolution kinetics in  $\text{Ca(OH)}_2\text{-H}_2\text{O}$  batch system: experimental ( $\blacklozenge$   $[\text{OH}^-]$ ) vs simulated (— by Modest 6.1 and Aspen Plus V8.6) concentration profiles. (a) 0.0054 M  $\text{Ca(OH)}_2(\text{s})$ ; (b) 0.0125 M  $\text{Ca(OH)}_2(\text{s})$ ; (c) 0.0300 M  $\text{Ca(OH)}_2(\text{s})$ ; and (d) 0.0500 M  $\text{Ca(OH)}_2(\text{s})$ .

3.3.2.  $\text{CaSO}_4\cdot 2\text{H}_2\text{O}$  dissolution model

The dissolution of gypsum in water can be expressed as follows:



Using this dissolution model, the concentration profiles of all the three species can be modeled by the following differential Eqs. (27)–(29):

$$\frac{d[\text{SO}_4^{2-}]}{dt} = k_{31}[\text{CaSO}_4] - k_{32}[\text{Ca}^{2+}][\text{SO}_4^{2-}] \quad (27)$$

$$\frac{d[\text{Ca}^{2+}]}{dt} = k_{31}[\text{CaSO}_4] - k_{32}[\text{Ca}^{2+}][\text{SO}_4^{2-}] \quad (28)$$

$$\frac{d[\text{CaSO}_4]}{dt} = -k_{31}[\text{CaSO}_4] + k_{32}[\text{Ca}^{2+}][\text{SO}_4^{2-}] \quad (29)$$

The value of the reverse reaction rate constant  $k_{32}$  can be expressed in terms of the equilibrium constant (Fig. 2) as  $k_{31}[\text{CaSO}_4]_e/K_3$ .

The reaction rate constant  $k_1$  was evaluated ( $R^2 > 95\%$ ) from the differential Eqs. (27)–(29) using several experimental data sets for comparison. The average value of the reaction rate constant was found to be  $0.051 \text{ s}^{-1}$ . The model-predicted and experimental concentration profiles of the relative species are well matched for different concentrations of the gypsum suspension (Fig. 8). The remaining solid

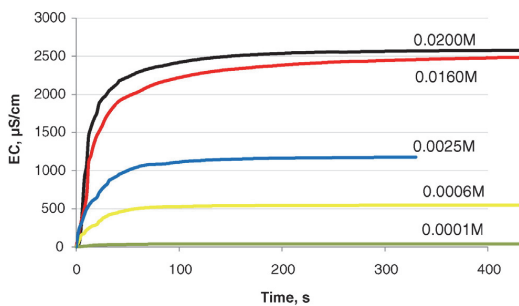


Fig. 6. Plot of electrical conductivity (EC) versus time for the  $\text{CaSO}_4\cdot 2\text{H}_2\text{O-H}_2\text{O}$  batch system at  $25^\circ\text{C}$ .

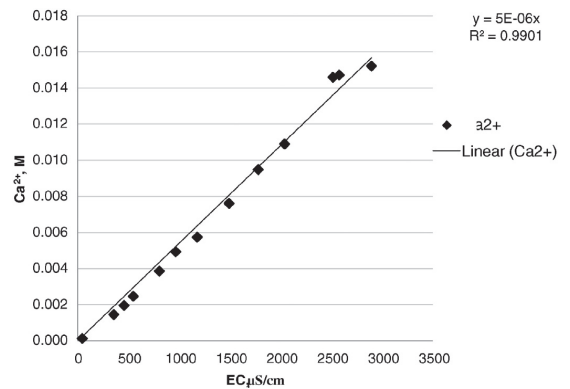


Fig. 7. Correlation between the electrical conductivity EC and the concentration of  $\text{Ca}^{2+}$  in the  $\text{CaSO}_4\cdot 2\text{H}_2\text{O-H}_2\text{O}$  system at  $25^\circ\text{C}$ .

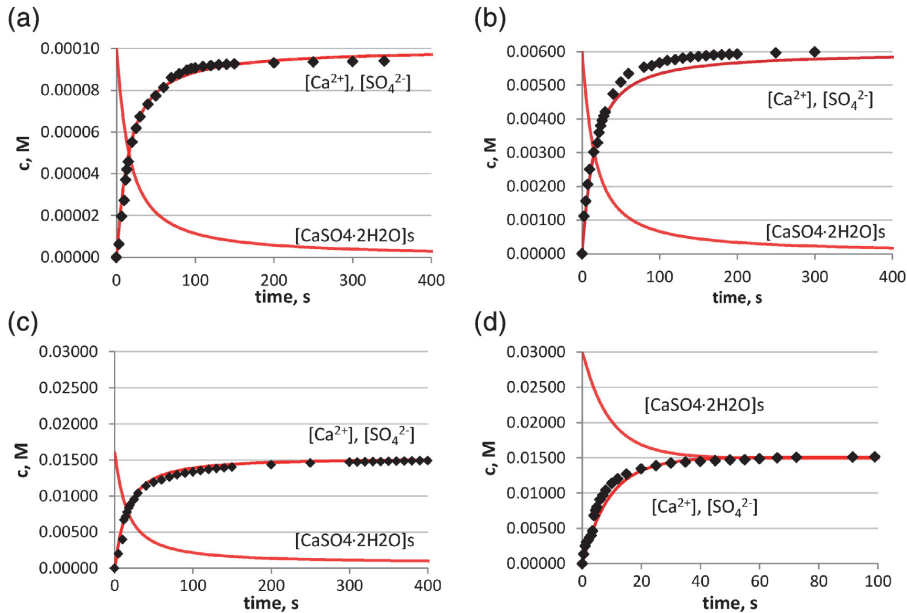


Fig. 8. Modeling of  $\text{CaSO}_4 \cdot 2\text{H}_2\text{O}$  dissolution kinetics in  $\text{CaSO}_4 \cdot 2\text{H}_2\text{O}$ – $\text{H}_2\text{O}$  batch system: experimental ( $\blacklozenge$   $[\text{OH}^-]$ ) vs simulated (— by Modest 6.1 and Aspen Plus V8.6) concentration profiles. (a) 0.0001 M  $\text{CaSO}_4 \cdot 2\text{H}_2\text{O}$ (s); (b) 0.0060 M  $\text{CaSO}_4 \cdot 2\text{H}_2\text{O}$ (s); (c) 0.0160 M  $\text{CaSO}_4 \cdot 2\text{H}_2\text{O}$ (s); and (d) 0.0300 M  $\text{CaSO}_4 \cdot 2\text{H}_2\text{O}$ (s).

$\text{CaSO}_4 \cdot 2\text{H}_2\text{O}$  indicates that the ionic concentrations have reached their maximum values.

### 3.4. Implementing the dissolution kinetics of $\text{Ca}(\text{OH})_2$ and $\text{CaSO}_4 \cdot 2\text{H}_2\text{O}$ within Aspen plus

Kinetic dissolution models for the aqueous  $\text{Ca}(\text{OH})_2$  and  $\text{CaSO}_4 \cdot 2\text{H}_2\text{O}$  systems were implemented within the Aspen Plus simulation platform by inserting the dissociation reactions and corresponding kinetic constants for each system into the RBatch reactor model ( $t = 25^\circ\text{C}$ ,  $P = 1$  bar,  $Q = 0$  Gcal/h). For the two-step  $\text{Ca}(\text{OH})_2$  model we inserted Eqs. (16) and (17) together with kinetic constants  $k_{11}$ ,  $k_{12}$ ,  $k_{21}$ , and  $k_{22}$  while the one-step model required Eq. (22) together with  $k^*_{11}$  and  $k^*_{12}$ . The  $\text{CaSO}_4 \cdot 2\text{H}_2\text{O}$  dissolution model defined in Eq. (26) was inserted together with parameters  $k_{31}$  and  $k_{32}$ . The validity of each model was confirmed by comparing simulated concentration profiles with profiles obtained using Modest 6.1 and experimental data

measured at different  $\text{Ca}(\text{OH})_2$  and  $\text{CaSO}_4 \cdot 2\text{H}_2\text{O}$  concentrations. As seen in Figs. 4, 5 and 8, the simulation results obtained by Aspen Plus V6.8 and Modest 6.1 coincided.

The kinetic parameters  $k^*_{11}$  and  $k^*_{12}$  for the simplified  $\text{Ca}(\text{OH})_2$ – $\text{H}_2\text{O}$  system were also inserted into a CSTR reactor model ( $t = 25^\circ\text{C}$ ,  $P = 1$  bar,  $Q = 0$  Gcal/h) to estimate the residence time and reactor volume required for continuous extraction of  $\text{Ca}^{2+}$  from the oil shale ash. We performed this calculation with respect to one Mt. of oil shale ash per year (114 t/h; 16.27%  $\text{Ca}(\text{OH})_2$ ) and the results are presented in Fig. 9.

As it can be seen from Fig. 9, the degree of  $\text{Ca}(\text{OH})_2$  leaching and the degree of  $\text{Ca}^{2+}$  saturation in the leachate are governed by the solid to liquid ratio (1/10, 1/50 and 1/100) and depend on the residence time of the CSTR. Due to the low solubility of  $\text{Ca}(\text{OH})_2$ , either a very large leaching reactor or repetitive extraction may be required to maximize both the  $\text{Ca}(\text{OH})_2$  leaching from ash and  $\text{Ca}^{2+}$  saturation in the solution. As an example, a reactor volume of about 200  $\text{m}^3$  is required to extract

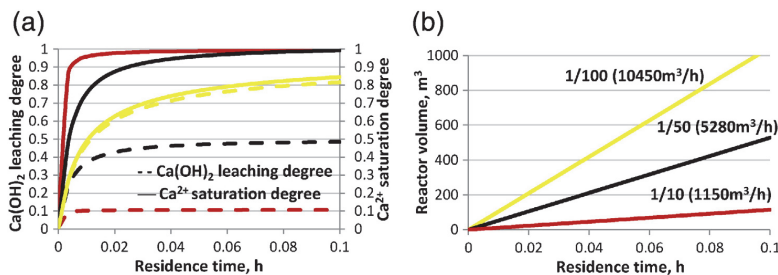


Fig. 9. Continuous model of  $\text{Ca}^{2+}$  extraction from oil shale ash (1 Mt oil shale ash/year = 114 t/h; 16.27%  $\text{Ca}(\text{OH})_2$ ): dependence of  $\text{Ca}(\text{OH})_2$  leaching degree (---) and leachate  $\text{Ca}^{2+}$  saturation degree (—) on residence time (a) or reactor volume needed for respective residence time (b) at given solid to liquid ratios (1/10 – red; 1/50 – black; 1/100 – yellow). (For interpretation of the references to color in this figure legend, the reader is referred to the web version of this article.)

50% of the calcium from the  $\text{Ca}(\text{OH})_2$  system using 1 Mt of oil shale ash per year (114 t/h) with a solid to liquid ratio of 1/50. However, in the current plant approximately  $10^7$ – $10^8$  m<sup>3</sup> of alkaline water (pH 12–13) is circulating in a hydraulic system between the plant and the sedimentary pond [10] which has a high degree of  $\text{Ca}^{2+}$  saturation. Direct utilization of this water is expected to be more economical than processing ash directly; however, a detailed assessment of this is out of the scope of the current publication.

#### 4. Conclusions

We have investigated the dissolution mechanisms and kinetics of the main water-soluble calcium species in two oil shale ash–water systems ( $\text{Ca}(\text{OH})_2$  and  $\text{CaSO}_4 \cdot 2\text{H}_2\text{O}$ ). The thermodynamic equilibrium for the  $\text{Ca}(\text{OH})_2$ – $\text{H}_2\text{O}$  and  $\text{CaSO}_4 \cdot 2\text{H}_2\text{O}$ – $\text{H}_2\text{O}$  binary systems were modeled using the Pitzer model embedded within the Aspen Plus platform. The kinetic reaction models of the binary systems were constructed using experimental data. Two approaches were applied to describe the  $\text{Ca}(\text{OH})_2$ – $\text{H}_2\text{O}$  system at 25 °C. The more complex approach modeled portlandite dissolution in an aqueous batch system as a two-step first order reaction system:  $\text{Ca}(\text{OH})_2 \rightarrow \text{CaOH}^+ + \text{OH}^-$  and  $\text{CaOH}^+ \rightarrow \text{Ca}^{2+} + \text{OH}^-$ . By using an optimization approach we determined values for the reaction rate constants in both the two-step ( $0.0345 \text{ s}^{-1}$  and  $0.0544 \text{ L}(\text{mol s})^{-1}$ ) and one-step ( $0.0282 \text{ s}^{-1}$ ) dissolution models ( $\text{Ca}(\text{OH})_2 \rightarrow \text{Ca}^{2+} + 2\text{OH}^-$ ). The two-step model elaborates the dissolution mechanism in more detail; however, the simplified one-step model fits with the experimental results as well and is easier to handle in practice. The average value of the reaction rate constant for gypsum dissolution was found to be  $0.051 \text{ s}^{-1}$ . We confirmed the accuracy of the proposed dissolution models ( $R^2 > 90\%$ ) by comparing simulation results with experimental data that was not used during the optimization process.

Both  $\text{Ca}(\text{OH})_2$  and  $\text{CaSO}_4 \cdot 2\text{H}_2\text{O}$  dissolution kinetics were implemented for the first time within the Aspen Plus simulation platform. Using the capacity of 1 Mt of oil shale ash per year as a basis, we calculated both the residence times and reactor volumes of three solid to liquid ratios (1/10, 1/50, 1/100) for continuous  $\text{Ca}^{2+}$  extraction from oil shale ash in a CSTR. According to the simulation, large leaching pools or repetitive leaching of ash is needed in order to enhance  $\text{Ca}^{2+}$  extraction and utilization of oil shale ash for PCC production. The models proposed are very general and can be applied for other lime and gypsum/anhydrite consisting combustion or industrial waste streams.

#### List of symbols

$B_{ij}, C_{ij}$	the interaction parameters
$d_i$	effective diameter of hydrated ion (nm)
EC	electrical conductivity, $\mu\text{S}/\text{cm}$
$G^E$	excess of Gibbs free energy
$I$	ionic strength of solution, $I(I) = \text{an electrostatic term as a function of ionic strength}$
$i, j, k$	cations and anions of the solution
$K$	equilibrium constant
$k$	rate constant
$M$	molarity of species ( $\text{mol L}^{-1}$ )
$m$	molarity of species ( $\text{mol kg H}_2\text{O}^{-1}$ )
$n_i$	the number of moles of the solution constituent
$P$	pressure (bar)
$Q$	duty (Gcal/h)
$T$	temperature (K)
$t$	temperature (°C)
$z_i$	a charge on species $i$
$\alpha_{\text{H}_2\text{O}}$	the activity of water
$\beta_{ij}^0, \beta_{ij}^1, \beta_{ij}^2, \beta_{ij}^3$	the interaction and mixing parameters

$\theta_{ij}, \psi_{ijk}$   
 $\gamma$  the activity coefficient of component

#### Acknowledgments

We gratefully acknowledge the financial support provided by the Archimedes Foundation (project 3.2.0501.10.0002), institutional research funding IUT (IUT33–19), of the Estonian Ministry of Education and Research, and the Estonian Science Foundation (Grant No. 9334).

#### References

- [1] T. Van Gerven, E. Van Keer, S. Aricx, M. Jaspers, G. Wauters, C. Vandecasteele, Carbonation of MSWI-bottom ash to decrease heavy metal leaching, in view of recycling, *Waste Manag.* 25 (2005) 291–300.
- [2] E. Rendek, G. Ducom, P. Germain, Carbon dioxide sequestration in municipal solid waste incinerator (MSWI) bottom ash, *J. Hazard. Mater.* B128 (2006) 73–79.
- [3] J.A. Meima, R.D. van der Weijden, T.T. Eighty, R.N.J. Comans, Carbonation processes in municipal solid waste incinerator bottom ash and their effect on the leaching of copper and molybdenum, *Appl. Geochem.* 17 (2002) 1503–1513.
- [4] G. Costa, R. Baciocchi, A. Polettini, R. Pomi, C.D. Hills, P.J. Carey, Current status and perspectives of accelerated carbonation processes on municipal waste combustion residues, *Environ. Monit. Assess.* 135 (2007) 55–75.
- [5] B. Fernández Bertos, S.J.R. Simons, C.D. Hills, P.J. Carey, A review of accelerated carbonation technology in the treatment of cement-based materials and sequestration of  $\text{CO}_2$ , *J. Hazard. Mater.* B112 (2004) 193–205.
- [6] M. Uibu, O. Velts, R. Kuusik, Developments in  $\text{CO}_2$  mineral carbonation of oil shale ash, *J. Hazard. Mater.* 174 (2010) 209–214.
- [7] M. Uibu, M. Uus, R. Kuusik,  $\text{CO}_2$  mineral sequestration in oil-shale wastes from Estonian power production, *J. Environ. Manag.* 90 (2009) 1253–1260.
- [8] S. Teir, S. Eloneva, R. Zevenhoven, Production of precipitated calcium carbonate from calcium silicates and carbon dioxide, *Energy Convers. Manag.* 46 (2005) 2954–2979.
- [9] O. Velts, M. Uibu, J. Kallas, R. Kuusik, Waste oil shale ash as a novel source of calcium for precipitated calcium carbonate: carbonation mechanism, modeling, and product characterization, *J. Hazard. Mater.* 195 (2011) 139–146.
- [10] R. Kuusik, M. Uibu, K. Kirsimäe, R. Mõtlep, T. Meriste, Open-air deposition of Estonian oil shale ash: formation, state of art, problems and prospects for the abatement of environmental impact, *Oil Shale* 29 (2012) 376–403.
- [11] World Energy Outlook 2010, Executive summary, International Energy Agency, <http://www.iea.org/Textbase/npsum/weo2010sum.pdf>, in, 2010 (accessed in Apr. 24, 2015).
- [12] H. Buerst, V. Kattai, Kukersite oil shale, *Geology and Mineral Resources of Estonia*, in: A. Raukas, Teedumäe, A. (Eds.) (Ed.), Estonian Academy Publishers, Tallinn, (1997) 313–327.
- [13] Eesti Energia Annual Report 2013, Environmental Report, [https://www.energia.ee/-/doc/10187/pdf/concern/annual\\_report\\_2013\\_eng.pdf](https://www.energia.ee/-/doc/10187/pdf/concern/annual_report_2013_eng.pdf) (accessed in Apr. 24, 2015).
- [14] Greenhouse gas emissions in Estonia 1990–2005, National Inventory report to the UNFCCC secretariat in Ministry of the Environment, Tallinn, 2007.
- [15] Material Safety Data Sheet for Burnt Oil Shale according to EC regulations no 1907/2006 and EU no 453/2010, [https://www.energia.ee/-/doc/10187/pdf/concern/Burnt\\_Oil\\_Shale\\_eng.pdf](https://www.energia.ee/-/doc/10187/pdf/concern/Burnt_Oil_Shale_eng.pdf) (accessed in July 24, 2015).
- [16] M. Laja, G. Urb, N. Irha, J. Reinik, U. Kirso, Leaching behaviour of ash fractions from oil shale combustion by fluidized bed and pulverized firing process, *Oil Shale* 22 (2005) 453–465.
- [17] R. Kuusik, M. Uibu, K. Kirsimäe, Characterization of oil shale ashes formed at industrial scale boilers, *Oil Shale* 22 (2005) 407–420.
- [18] M. Liira, K. Kirsimäe, R. Kuusik, R. Mõtlep, Transformation of calcareous oil-shale circulating fluidized-bed combustion boiler ashes under wet conditions, *Fuel* 88 (2009) 712–718.
- [19] L. Bityukova, R. Mõtlep, K. Kirsimäe, Composition of oil shale ashes from pulverized firing and circulating fluidized-bed boiler in Narva Thermal Power plants, Estonia, *Oil Shale* 27 (2010) 339–353.
- [20] M. Izquierdo, X. Querol, Leaching behaviour of elements from coal combustion fly ash: an overview, *Int. J. Coal Geol.* 94 (2012) 54–66.
- [21] K. Tamm, P. Kallaste, M. Uibu, J. Kallas, R. Kuusik, Leaching thermodynamics of oil shale waste key components, in: Proceedings of the 5th International Conference on Accelerated Carbonation for Environmental and Materials Engineering, New York City, June 21–24, 2015.
- [22] N. Irha, M. Uibu, J. Jefimova, L.-M. Raado, T. Hain, R. Kuusik, Leaching behaviour of Estonian oil shale-based construction mortars, *Oil Shale* 31 (2014) 394–411.
- [23] O. Velts, M. Hautaniemi, J. Kallas, R. Kuusik, Modeling calcium dissolution from oil shale ash: part 1. Ca dissolution during ash washing in a batch reactor, *Fuel Process. Technol.* 91 (2010) 486–490.
- [24] O. Velts, M. Hautaniemi, J. Kallas, M. Kuosa, R. Kuusik, Modeling calcium dissolution from oil shale ash: part 2: continuous washing of the ash layer, *Fuel Process. Technol.* 91 (2010) 491–495.
- [25] H. Haario, Modest User Manual, Profmath OY, Helsinki, Finland, 1994.
- [26] A.C. Hindmarsh, ODEPACK, a systematized collection of ODE solvers, Scientific Computing: IMACS Transactions on Scientific Computation 1 (1983) 55–64.
- [27] Aspen Plus User Guide, 2000.

- [28] T. Yuan, J. Wang, Z. Li, Measurement and modelling of solubility for calcium sulfate dihydrate and calcium hydroxide in NaOH/KOH solutions, *Fluid Phase Equilib.* 297 (2010) 129–137.
- [29] M.J.G.M. Lito, M.F.F.C. Camões, A. Covington, Equilibrium in saturated  $\text{Ca}(\text{OH})_2$  solutions: parameters and dissociation constants, *J. Solut. Chem.* 27 (1998) 925–933.
- [30] J. Duchesne, E.J. Reardon, Measurement and prediction of portlandite solubility in alkali solutions, *Cem. Concr. Res.* 25 (1995) 1043–1053.
- [31] D.K. Nordstrom, Improving internal consistency of standard state thermodynamic data for sulfate ion, portlandite, gypsum, barite, celestine, and associated ions, *Procedia Earth and Planetary Science* 7 (2013) 624–627.
- [32] W. Wang, D. Zeng, Q. Chen, X. Yin, Experimental determination and modeling of gypsum and insoluble anhydrite solubility in the system  $\text{CaSO}_4\text{--H}_2\text{SO}_4\text{--H}_2\text{O}$ , *Chem. Eng. Sci.* 101 (2013) 120–129.
- [33] K.S. Pitzer, Thermodynamics of electrolytes. I. Theoretical basis and general equations, *The Journal of Physical Chemistry* 77 (1973) 268–277.
- [34] Aspen Physical Property System, *Physical Property Methods*, Aspen Tech., 2009.
- [35] K. Johannsen, S. Rademacher, Modelling the kinetics of calcium hydroxide dissolution in water, *Acta Hydrochim. Hydrobiol.* 27 (1999) 72–78.
- [36] D.E. Giles, I.M. Ritchie, B.-a. Xu, The kinetics of dissolution of slaked lime, *Hydrometallurgy* 32 (1992) 119–128.



## **PAPER II**

*Tamm, K., Uibu, M., Kallas, J., Kallaste, P., Velts-Jänes, O., Kuusik, R.*

Thermodynamic and kinetic study of CaS in aqueous systems.

*Fuel Processing Technology* 2016, 142, 242-249.





## Research article

## Thermodynamic and kinetic study of CaS in aqueous systems



Kadriann Tamm\*, Mai Uibu, Juha Kallas, Priit Kallaste, Olga Velts-Jänes, Rein Kuusik

Tallinn University of Technology, Laboratory of Inorganic Materials, 5 Ehitajate Str., Tallinn 19086, Estonia

## ARTICLE INFO

## Article history:

Received 1 April 2015

Received in revised form 16 September 2015

Accepted 19 October 2015

Available online 25 October 2015

## Keywords:

Calcium sulfide

Oil shale ash

HSC chemistry

Sulfide oxidation

Sulfur ions leachability

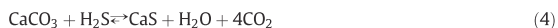
## ABSTRACT

One of the main sources of sulfide in fuel combustion ashes is the hazardous compound calcium sulfide (CaS), which decomposes in water and releases sulfide compounds into the environment. In order to safely use hydrotransport and open air deposition of wet ash, as well as to treat alkaline ash transportation waters, it is important to know the dissolution behavior of CaS, in this regard, several values of both CaS solubility and equilibrium constants of dissolution reactions are illustrated in the scientific literature. To reconcile these differences, both kinetics and equilibrium of CaS dissolution reactions under inert and air conditions at 25 °C were studied. The water solubility of CaS under an inert atmosphere (with N<sub>2</sub> treated water) is lower ( $2.29 \cdot 10^{-3}$  mol/L) than under air ( $2.74 \cdot 10^{-3}$  mol/L). A more complex reaction mechanism for open air dissolution, elucidated using HSC Chemistry® 7.1 simulations, was also presented. Various reaction mechanisms as well as equilibrium and rate constants were evaluated to model CaS dissolution data. The relatively small deviations between calculated values and experimental data confirm that the suggested models could be employed to describe CaS dissolution under both atmospheric and inert conditions.

© 2015 Elsevier B.V. All rights reserved.

## 1. Introduction

With regard to atmospheric emissions (e.g. CO<sub>2</sub>, SO<sub>2</sub>), the most serious problem caused by the extensive use of oil shale is the safe disposal of the related mineral waste (8.0 MT in 2013) [1]. The sulfur content (<2% in Estonian oil shale) in oil shale power plant ash depends on the combustion technology and operating parameters such as boiler temperature and pressure as well as the presence of reductive and oxidative zones. More sulfur is bound into power plant ash as CaSO<sub>4</sub> using circulating fluidized bed (CFB) technology (up to 10.9 wt.%) compared with pulverized firing (PF) technology (up to 5.4 wt.%). CaS concentrations values are typically <0.2 wt.%; however concentration values up to 0.7 wt.% can be found in CFB ash [2,3,4] and almost up to 3 wt.% is found in the solid waste from shale oil production [5,6]. CaS is the most hazardous sulfur based compound for the environment [7,8], it forms during both ash sulfation and fuel combustion as well as thermal processing over both calcium oxide (Eqs. (1)–(2)) and carbon (Eqs. (3)–(4)) [8,9].



CaS is chemically unstable in open air and also disintegrates at the ash dump site during leaching. Upon hydration, CaS decomposes releasing sulfides into the environment and generates toxic H<sub>2</sub>S under acidic conditions [4]. To mitigate its environmental impact, one must understand the behavior of CaS in a complex mixture of leachable substances within both power plant ashes and shale oil production ash during both hydrotransport or while treating ash leachates with CO<sub>2</sub> containing gas to reduce its alkalinity and produce precipitated CaCO<sub>3</sub> as a commercial by-product [4,10]. Accurate thermodynamic measurements are prerequisite to this goal.

Literature information about CaS leaching is currently ambiguous. Since the dissolution mechanism is complex, different values have been given for the CaS solubility (Table 1). This study aims to resolve this discrepancy by investigating the dissolution mechanisms of CaS on the basis of both thermodynamic equilibrium and reaction kinetics. The new proposed mathematical models simulate the CaS dissolution process under various conditions and enable to both predict the dynamics of CaS leaching at ash dumping sites and optimize operating conditions to avoid H<sub>2</sub>S emissions during the precipitation of CaCO<sub>3</sub> from oil shale ash.

More specifically, the current paper presents reaction models built for the CaS–H<sub>2</sub>O system under both an inert and air atmosphere using experimentally determined CaS solubility data as well as reactions kinetics.

\* Corresponding author.

E-mail address: [kadriann.tamm@ttu.ee](mailto:kadriann.tamm@ttu.ee) (K. Tamm).

**Table 1**  
Values for water solubility of CaS.

Temp. (°C)	Input data	mol/L	Reference
20	0.212 g per 1 L	$2.94 \cdot 10^{-3}$	Riesenfeld and Feld (1921) [11]
Room temperature	0.02 parts per 100 parts in water; decomposing	$2.77 \cdot 10^{-3}$	Dean (1999) [12]
Room temperature	0.02 parts per 100 parts in water; decomposing	$2.77 \cdot 10^{-3}$	CRC Handbook (2006) [13]
25	1.733 mmol/L	$1.73 \cdot 10^{-3}$	Zekker et al. (2011) [14]
25	0.1 wt.%	$1.38 \cdot 10^{-2}$	Licht (1988) [15]
25	<1 g/L; decomposes	$<1.38 \cdot 10^{-2}$	Perry and Green (1999) [16]
15	0.01 g per 100 cm <sup>3</sup> solution	$1.39 \cdot 10^{-3}$	Linke (1958) [17]

## 2. CaS dissolution mechanism – generalization of literature data

### 2.1. CaS–H<sub>2</sub>O system under an inert environment

CaS leaching under inert conditions corresponds to the dissolution environment in the deeper layers within ash piles. The CaS dissolution reaction, Eq. (5), and thermodynamic equilibrium constant  $K_1$ , Eq. (6), of calcium sulfide (CaS) can be defined as follows [7,14,18–19]:



$$K_1 = [\text{Ca}^{2+}] \times [\text{S}^{2-}] \quad (6)$$

Mölder et al. (1995) [7] reported that the first order rate constants for CaS hydrolysis are 0.0467 and 0.0936 h<sup>-1</sup> at 20 °C and 40 °C, respectively.

CaS dissolution determines with a noticeable change in the system pH due to the formation of HS<sup>-</sup> and H<sub>2</sub>S as S<sup>2-</sup> dissociation products (Eqs. (7) and (9)). The dissociation of S<sup>2-</sup> can be characterized by the basicity constants  $K_{b2}$  and  $K_{b1}$  (Eqs. (8) and (10)) [14].



$$K_{b2} = \frac{[\text{HS}^-] \times [\text{OH}^-]}{[\text{S}^{2-}]} \quad (8)$$



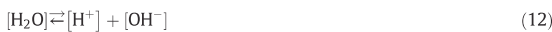
$$K_{b1} = \frac{[\text{H}_2\text{S}] \times [\text{OH}^-]}{[\text{HS}^-]} \quad (10)$$

Equilibrium between the phases of molecular sulfide can be given as follows [20]:



The equilibrium between the water-soluble hydrogen sulfide and gas form is set by Henry–Dalton's law as  $x(g) = k_H \cdot p(g)$ , where  $x(g)$  – the concentration of gas in solution expressed through the mole fraction (the number of gas moles divided by the total number of moles of the solution),  $k_H$  – Henry constant, the gas mole fraction in the solution, Pa<sup>-1</sup> and  $p(g)$  – the partial pressure of the gas above the solution, Pa. Carroll and Mather [21] presented the proportionality coefficient ( $k_H$ ) value for H<sub>2</sub>S at 25 °C as 0.018 mol frac/MPa.

Water autoprotolysis (H<sub>2</sub>O dissociation) must also be taken into account:



The ion-product constant of water,  $K_w$  is expressed as follows [14, 22]:

$$K_w = [\text{H}^+] \times [\text{OH}^-] = 10^{-14} \quad (13)$$

The activity coefficients in CaS water system were expected approximately equal to 1 and have therefore been excluded.

According to CaS dissolution mechanism described above, the solubility product ( $K_{sp}$ ) (Eq. (14)) is calculated as a product of ions in the saturated solution from Eq. (6), using the concentrations of total sulfide [ $S_{\text{sulfide}} = [\text{S}^{2-}] + [\text{HS}^-] + [\text{H}_2\text{S}(aq)]$ ] and calcium [ $\text{Ca}^{2+}$ ]:

$$K_{sp} = [\text{Ca}^{2+}] \times [S^{2-}]_{\text{tot}} = [\text{Ca}^{2+}] \times [\text{Ca}^{2+}] \quad (14)$$

Since the solution contains equal amount of calcium and sulfide ions, the value of  $K_1$  can be expressed as the square of Ca-ion content.

The dissolution of CaS can also be described by hydrolysis, excluding S<sup>2-</sup> formation [7] (Eq. (15)), and the reaction equilibrium can be calculated as the ion-product  $K_s$ , Eq. (16):



$$K_s = [\text{Ca}^{2+}] \times [\text{HS}^-] \times [\text{OH}^-] \quad (16)$$

As a quotient of  $K_s$  to the second basicity constant ( $K_{b2}$ ) [14], which simplifies to Eq. (6):

$$K_s / K_{b2} = [\text{Ca}^{2+}] \times [\text{S}^{2-}] = K_1 \quad (17)$$

The above equation is used in the current study for describing the dissociation equilibrium of CaS.

### 2.2. CaS–H<sub>2</sub>O system under an oxidizing environment

Although the oxidation of sulfides has been extensively studied [7, 19,20,23–25], uncertainties regarding oxidation rates, mechanisms, and formation of products still remain. Several processes have been proposed for sulfide oxidation in aqueous systems. Both the reaction mechanism and the nature of the products strongly depend on the water system pH [7,25–28]. The formation of sulfur and polysulfides is unlikely under alkaline conditions (pH > 9) [29] and when the sulfur-oxygen ratio is small [25]. The following simplified chain of oxidation reactions was proposed for deeply alkaline systems by Mölder et al. (1995) [7], where HS<sup>-</sup> is the main reacting sulfide species and the most stable reduced sulfide oxidation forms are thiosulfate (Eq. (18)) and sulfate (Eq. (19)):



It was assumed that reactions (18) and (19) display first order kinetics and proceed simultaneously. Mölder et al. (1995) [7] investigated

both the hydrolysis and oxidation of CaS and reported rate constants of  $0.0272$  and  $0.0119 \text{ h}^{-1}$  at  $20 \text{ }^\circ\text{C}$  for Eqs. (18) and (19), respectively. Thiosulfate is very stable at pH values higher than 11 and further oxidation of thiosulfate to sulfate proceeds very slowly [7,29].

### 3. Materials and methods

Chemical transformations within CaS aqueous systems were studied using a combination of experimental and modeling techniques. A CaS dissolution model was made using experimentally determined CaS solubility data, equilibrium composition, and kinetic measurements.

#### 3.1. Experimental procedure

##### 3.1.1. CaS–H<sub>2</sub>O system under N<sub>2</sub> atmosphere

Pure CaS (Alfa Aesar) was used for the batch experiments and the concentrations values were chosen based on literature data for the solubility of CaS (Table 1). Deionized water (750 mL) was poured into a 1 L computer controlled “Lara Controlled Lab Reactor (LCLR)” (Scheme 1).

N<sub>2</sub> was bubbled through the water for 0.3 h to remove oxygen; the absence of dissolved oxygen (DO) in an aqueous system was confirmed by oxygen-meter Marvet Junior MJ2000 (Elke Sensor, Estonia); during the pause in the control program, a specific mass of CaS, in the range of 0.021 g–0.200 g, was added into the system using a funnel. The CaS suspension was continuously stirred in a closed system at 250 rpm at constant temperature of  $25 \text{ }^\circ\text{C}$  (step time 10 min) for 3 h. The system temperature was automatically kept constant within  $\pm 0.1^\circ$  of accuracy and observed with a temperature probe. The conductivity (Hanna instruments 9932 Microprocessor Conductivity Meter with HI 92000-5.0.26 software), pH (Knick Portamess 913 pH; pH-meter sensor: Hamilton Polylyte Plus VP360) and temperature of this solution were continuously monitored during the test. The Radleys Control Software was used to observe the system parameter in real-time during the kinetics experiments. In addition, the amount of H<sub>2</sub>S, O<sub>2</sub>, CO<sub>2</sub>, and SO<sub>2</sub> in the gaseous phase was unceasingly analyzed using a flue gas analyzer (Testo 350-S/XI). After each experiment, the suspension was filtered under vacuum and the chemical composition of the filtrate was analyzed to determine (i) Ca<sup>2+</sup> (ISO – 6058:1984) [30], (ii) total sulfide (sum of dissolved H<sub>2</sub>S, HS<sup>−</sup> and S<sup>2−</sup>) and SO<sub>4</sub><sup>2−</sup> (Lovibond Spectro Direct spectrometer, method: DPD/Catalyst, Bariumsulfate – Turbidity), (iii) total reduced sulfur (total sulfide and other sulfide intermediate

oxidative forms) iodometrically [31] and (iv) alkalinity (ISO – 9963-1:1994(E)) [32].

##### 3.1.2. CaS–H<sub>2</sub>O system in air

The leaching behavior of CaS was also studied under an air environment based on our previous work [4,33] the developed systems ranged in the concentration values  $3.35 \cdot 10^{-4}$ – $4.50 \cdot 10^{-3}$  mol CaS per L H<sub>2</sub>O. In each test, an equilibrium state was achieved by stirring the solution for 3 h in a shaker at  $25 \text{ }^\circ\text{C}$  and atmospheric pressure. Experiments to measure the reaction kinetics were carried out using the LCLR. Each CaS suspension was constantly mixed at 250 rpm under an air environment at  $25 \text{ }^\circ\text{C}$  for 3 h. The system pH and conductivity were continuously monitored during the experiments and the composition of the liquid phase (Ca<sup>2+</sup>, SO<sub>4</sub><sup>2−</sup>, total sulfide, total reduced sulfur and alkalinity) was analyzed every 0.3 h.

#### 3.2. Modeling

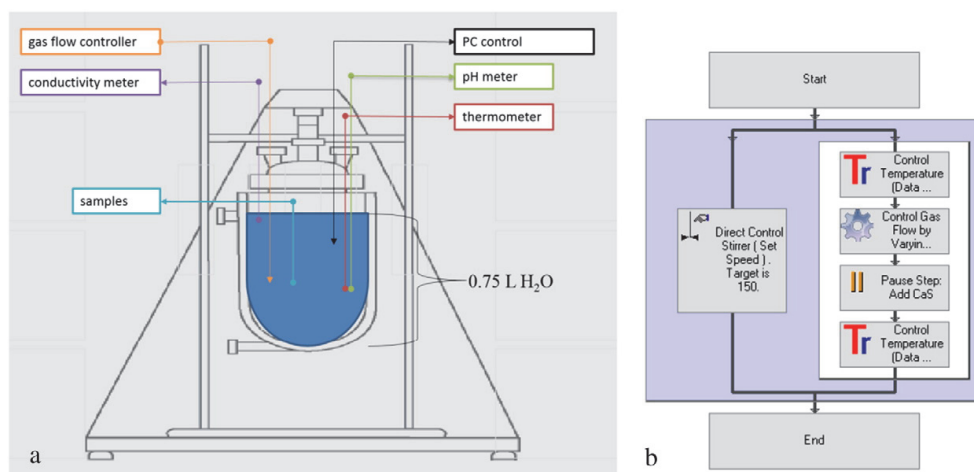
The phase equilibrium (solid, liquid, gas) in the CaS system under both inert (N<sub>2</sub>) and oxidizing (air) environments was also investigated using the Hsc Chemistry® 7.1 thermodynamic program [34]. In this regard, the simulations were carried out by uses of the equilibrium calculation module which is based on a Gibbs Energy Minimization method. Kinetic calculations and dissolution process simulations were performed utilizing the MODEST 6.1 software package [35], it is designed for various model building tasks such as simulation, parameter estimation, sensitivity analysis, and optimization. The software consists of a FORTRAN 95/90 library of objective functions, solvers and optimizers linked to model problem-dependent routines as well as objective function. Each system of differential equations was solved by means of linear multi-step methods implemented in ODESSA (which is based on LSODE software [36]).

### 4. Results and discussion

#### 4.1. CaS dissolution equilibrium in aqueous systems

##### 4.1.1. Thermodynamic calculations

In reactions (7) and (9) the anions are Brønsted bases which implies that distribution of the sulfide species strongly depends on the aqueous system conditions (e.g. pH, temperature, pressure). Sun et al. (2008) [22] compared the calculated with the experimental values for  $K_{b1}$ ;



Scheme 1. Batch reactor system (a) and the recipe of experimental procedures (b).

they find out that all calculated values for  $K_{b1}$  (the two average values presented in Table 2) well agree with the experimental results and can be used for predicting of the metal-sulfide solubility. The same author suggested that using  $K_{b2}$  to calculate the concentration of sulfide species and predict the solubility of metal-sulfide should be avoided because of the uncertainty in the available data.

A wide range (a 7-orders of magnitude variation) of values for  $K_{b2}$  have been reported [14,20,22], this is thought to be due to the difficulty of accurately measuring the  $\text{HS}^-$  and  $\text{S}^{2-}$  concentration in water systems [22]. Zekker et al. (2011) [14] used a value of 15.20 for the  $K_{b2}$  value of  $\text{S}^{2-}$ , this value was chosen on the basis of a relatively wide scope of data from different authors.

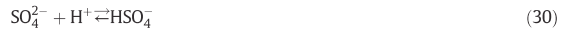
According to the equilibrium HsC calculations, different forms of sulfide ( $\text{S}^{2-}$ ,  $\text{HS}^-$ ,  $\text{H}_2\text{S}(\text{a})$ ) are pH dependent in aqueous systems (Fig. 1). The module uses the Gibbs Energy Minimization method, which takes into account all the possible chemical reactions automatically. The chemical system and the initial composition of model were specified at time zero and the program calculates the amounts of products for equilibrium state at isothermal and isobaric conditions. The inert CaS– $\text{H}_2\text{O}$  system included gas ( $\text{N}_2(\text{g})$ ,  $\text{H}_2\text{S}(\text{g})$ ,  $\text{H}_2\text{O}(\text{g})$ ); liquid ( $\text{Ca}^{2+}$ ,  $\text{Ca}(\text{HS})_2(\text{a})$ ,  $\text{Ca}(\text{OH})_2(\text{a})$ ,  $\text{CaHS}^+$ ,  $\text{CaOH}^+$ ,  $\text{CaS}(\text{a})$ ,  $\text{H}^+$ ,  $\text{H}_2\text{O}$ ,  $\text{H}_2\text{S}(\text{a})$ ,  $\text{HS}^-$ ,  $\text{HS}_2^-$ ,  $\text{HS}_3^-$ ,  $\text{HS}_4^-$ ,  $\text{HS}_5^-$ ,  $\text{HS}_6^-$ ,  $\text{OH}^-$ ,  $\text{S}^{2-}$ ,  $\text{S}_2^{2-}$ ,  $\text{S}_3^{2-}$ ,  $\text{S}_4^{2-}$ ,  $\text{S}_5^{2-}$ ,  $\text{S}_6^{2-}$ ), and solid phase ( $\text{CaS}$ ,  $\text{Ca}(\text{HS})_2$ ,  $\text{Ca}(\text{OH})_2$ ). The content of CaS was varied at a constant amount of water ( $\text{OH}^-$  equaled  $\text{H}^+$  ( $1 \cdot 10^{-7}$ ) at time zero). The pH of CaS– $\text{H}_2\text{O}$  system under inert  $\text{N}_2$  (0.1 mol) environment was modeled by adding  $\text{HCl}(\text{a})$  or  $\text{NaOH}(\text{a})$ , at 25 °C. The pH value for no extra acid or base added is called *normal pH* (Fig. 1). The equilibrium values calculated as a function of pH and presented in Fig. 1 are in good accordance with experimentally determined values (Fig. 4).

For comparison,  $K_{b2}$  (0.0653 mol/L) and  $K_{b1}$  ( $1.11 \cdot 10^{-7}$  mol/L) values were derived from the HsC calculations at the experimentally determined equilibrium concentration of  $2.29 \cdot 10^{-3}$  mol/L CaS. Comparative calculations with  $1.73 \cdot 10^{-3}$  mol/L, one of the more recently published CaS solubility values [14], indicated that the *normal pH* ( $11.26 \pm 0.011$ ) and  $\text{HS}^-$  concentration ( $1.69 \pm 0.01$  mmol/L), are in good accordance with the HsC results (*normal pH* 11.22 and concentration of  $\text{HS}^-$  1.68 mmol/L) (Fig. 1). The  $\text{Ca}^{2+}$  at equilibrium was lower compared to the  $S_{\text{sulfide}}$  concentration due to the formation of calcium hydroxide (2.2% of the  $\text{Ca}^{2+}$ ) at higher pH values. The concentration of others species (e.g.  $\text{CaHS}^+$  and  $\text{Ca}(\text{HS})_2$ ) remained out of the range (Fig. 1), therefore these have been excluded from the present work.

The CaS– $\text{H}_2\text{O}$  system was also investigated over a large oxidative range by varying the content of air. The oxygen, carbonates and oxidized species of sulfur were included into the calculation platform. To determine the thermodynamic equilibrium of the CaS– $\text{H}_2\text{O}$  system we used standard atmospheric composition, however, over a larger oxidative range at 25 °C, the distribution of the main sulfur species and system pH changes (Fig. 2), which indicates that the equilibrium state and system pH depends on the consumption of oxygen.

The oxidation of sulfides in an aqueous system is a complex process which may involve parallel reactions. Even if the exact sequences of reaction steps are difficult to obtain [23–25,29,37–38], the equilibrium calculation model (Fig. 2) helps one to describe the reaction mechanism

(Eq. (29)–(31) together with Eqs. (5) and (8)). CaS oxidation takes place over the formation of  $\text{HS}^-$  (which agrees with literature [7]) and generates polysulfides at low oxidation ratios ( $\text{O}_2/\text{CaS}$  0.0–0.5). The main products are  $\text{S}_2^{2-}$  and  $\text{S}_3^{2-}$  with pH values ranging from 11.4 and 11.15 (Eqs. (20)–(21)) [25], while  $\text{S}_5\text{O}_3^{2-}$  forms according to Eqs. (22)–(23) with pH values  $\sim 11.2$ . In the region  $\text{O}_2/\text{CaS}$  0.80–1.25,  $\text{S}_3\text{O}_3^{2-}$  predominates (Eqs. (24)–(25)). At higher oxidative rates ( $\text{O}_2/\text{CaS}$  1.25–2.00),  $\text{SO}_4^{2-}$  forms over several intermediates (Eqs. (26)–(28)), and becomes the main oxidative species that ultimately leads to the sharp decrease in pH (which supports the findings of our previous works [4]). Finally,  $\text{HSO}_4^-$  and  $\text{HSO}_3^-$  react with additional  $\text{O}_2$  forming  $\text{H}_2\text{SO}_8^-$  (Eq. (31)), thereby increasing the pH which then stabilizes at  $\sim 11.2$ .



#### 4.1.2. Experimental data

The CaS solubility experiments showed a clear linear dependence between the  $\text{Ca}^{2+}$  concentration and conductivity (Fig. 3); it means that  $\text{Ca}^{2+}$  concentration values could be calculated on the basis of conductivity (E) measurements (see Eq. (32) under inert conditions ( $R^2 = 0.97$ ) and Eq. (33) in air ( $R^2 = 0.93$ )). The initial concentrations of the CaS suspensions in air and in inert environment were  $3.35 \cdot 10^{-4}$ – $4.50 \cdot 10^{-3}$  mol/L and  $5.54 \cdot 10^{-4}$ – $2.77 \cdot 10^{-3}$  mol/L, respectively.

$$[\text{Ca}^{2+}] = 2.22 \cdot 10^{-6} \times E \quad (32)$$

$$[\text{Ca}^{2+}] = 2.91 \cdot 10^{-6} \times E \quad (33)$$

**Table 2**  
CaS solubility equilibrium constants in CaS– $\text{H}_2\text{O}$  in inert system at 25 °C.

Equilibrium constant	Experimental mol/L	HsC cal.	Reference
$K_1$	9.79 · 10 <sup>-7</sup> (used experimental $K_{b2}$ ) 8.95 · 10 <sup>-8</sup> (used HsC $K_{b2}$ )	1.65 · 10 <sup>-7</sup>	8.60 · 10 <sup>-6</sup> Riesenfeld and Feld (1921) [11] 7.943 · 10 <sup>-7</sup> Licht (1988) [15]
$K_{b2}$	3.84 · 10 <sup>-10</sup> (used Zekker et al. $K_{b2}$ ) 5.97 · 10 <sup>-3</sup>	6.53 · 10 <sup>-2</sup>	3.49 · 10 <sup>-10</sup> Zekker et al. (2011) [14] 0.0708 Zavodnov et al. (1960) [39] 0.0275 Kubli (1946) [40] 0.01 Su et al. (1997) [41]
$K_{b1}$		1.11 · 10 <sup>-7</sup>	1.04 · 10 <sup>-7</sup> Sun et al. (2008) [22] 1.02 · 10 <sup>-7</sup> Almgren et al. (1976) [26]

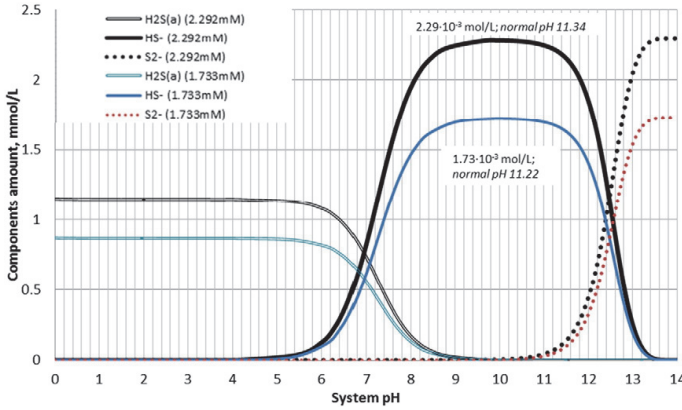


Fig. 1. HsC calculations of CaS–H<sub>2</sub>O inert system showing changes in sulfide forms over a large pH range.

In the CaS–H<sub>2</sub>O system [Ca<sup>2+</sup>] equals [S<sub>total</sub>]. On the basis of the experimental results, the formation of H<sub>2</sub>S in the gas phase was negligible over the concentration range of 2.98 · 10<sup>-4</sup>–2.77 · 10<sup>-3</sup> mol/L and formed up to 1 ppm at pH > 10. The HsC calculations (Fig. 1) also confirm that the [H<sub>2</sub>S] concentrations are very low under these conditions. The mass-balance in the inert system can thus be expressed as follows:

$$[Ca^{2+}] = [S_{total}] = [HS^-] + [S^{2-}] \quad (34)$$

Applying to the ionic charge balance, the electroneutrality condition must be fulfilled:

$$2[Ca^{2+}] + [H^+] = 2[S^{2-}] + [HS^-] + [OH^-] \quad (35)$$

Eqs. (34) and (35) can be used to calculate the approximate values for [HS<sup>-</sup>] and [S<sup>2-</sup>]

$$[HS^-] = [OH^-] - [H^+] \quad (36)$$

$$[S^{2-}] = [Ca^{2+}] - [OH^-] + [H^+] \quad (37)$$

Therefore, according to Eqs. (36) and (37), [HS<sup>-</sup>] and [S<sup>2-</sup>] could be individually determined from pH and [Ca<sup>2+</sup>] data. The value of K<sub>b2</sub> could be calculated on the basis of OH<sup>-</sup> and sulfide species concentrations according to Eq. (8) (Table 2).

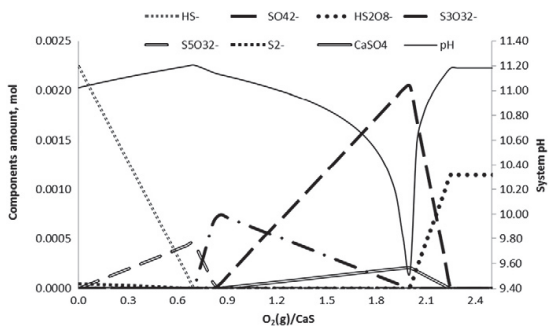


Fig. 2. HsC calculation of CaS–H<sub>2</sub>O (2.292 mM) in air system at 25 °C showing changes in sulfur components and system pH over a large oxidative range.

The pH profiles related to the CaS–H<sub>2</sub>O system under both inert and oxidizing environments show that the system pH (initial pH of water phase was about 6), which depends on the amount of solid phase added, stabilizes during the first few minutes at pH > 11 and pH > 10 (Fig. 4). The oxidation of sulfides promotes the pH decrease in the CaS–H<sub>2</sub>O system under oxidizing conditions (Fig. 2) because sulfates are weaker bases and increase the concentration of H<sup>+</sup>. The OH<sup>-</sup> and H<sup>+</sup> concentration values, determined from the system pH, were in good accordance with the thermodynamic calculations (Fig. 1).

A correlation between the measured concentrations of Ca<sup>2+</sup> and S<sub>total</sub> (R<sup>2</sup> = 0.98) is shown in Fig. 5.

The content of polysulfides [20] in the system in air investigated was considered when determining the total reduced sulfur iodometrically.

The biggest difference between measured and calculated values is shown in oxidative environment concerning the different forms of sulfur; this occurs because the experiments were performed for a 3 h period while the HsC program considers an infinite time period when performing equilibrium calculations and in the absence of a specific endpoint all sulfur would be oxidized according to Eqs. (18) and (19), (Fig. 6).

The measured concentration values of Ca<sup>2+</sup> and S<sub>total</sub> were used to determine the solubility of CaS in aqueous systems (Fig. 6). The vertical dashed lines refer to the solubility points under inert (2.29 · 10<sup>-3</sup> mol/L) and air (2.74 · 10<sup>-3</sup> mol/L), respectively. Oxygen provokes the solubility when CaS is present in a solid phase, because the content of sulfide ions would be restored by further CaS hydrolysis. This was also evident

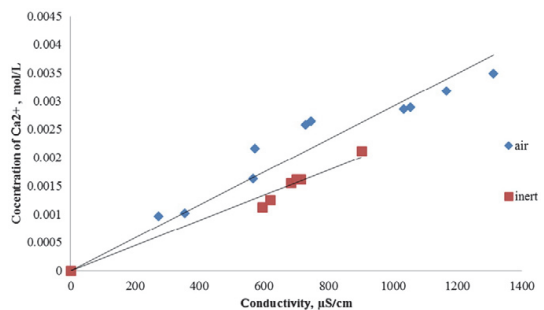


Fig. 3. Relationship between Ca<sup>2+</sup>-ion concentration and conductivity in air and in inert CaS–H<sub>2</sub>O system.

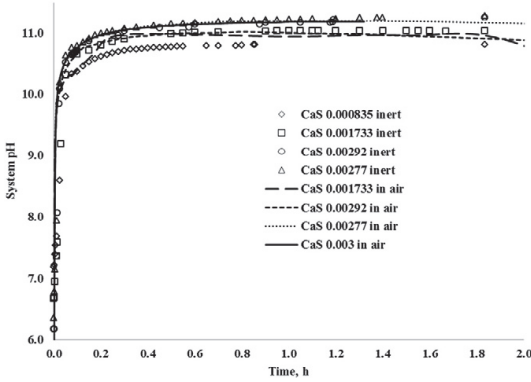


Fig. 4. The experimental system pH in CaS–H<sub>2</sub>O system in inert and in air environment at 25 °C.

from the decreasing of DO in the aqueous phase. While in inert conditions the content of DO was 0, in case of in air environment, the content of DO decreased. The calculated equilibrium compositions (Fig. 2) well agree with the experimental results (system pH,  $S_{total}$ ,  $Ca^{2+}$ ), (Fig. 6).

The HSC calculated solubility results correspond to the inserted values of CaS. This is due to the fact that the calculation process is not limited by fixed solubility values. This characteristic is described with a continuous diagonal in air system on Fig. 6. The water solubility of CaS in inert system,  $2.29 \cdot 10^{-3}$  mol/L achieved experimentally (part 4.1.2), was inserted to the HSC database. The calculated concentration values are related with latter, which correspond to the horizontal part of line (Fig. 6), are related to latter.

Equilibrium constants for the CaS aqueous system were determined from measured concentrations of  $Ca^{2+}$ ,  $S_{sulfide}$  and  $OH^-$  using Eqs. (8), (14) and (17) and illustrated in Table 2.

CaS dissociates in water (Eq. (15)), while its oxidation behavior in the solid phase is negligible [7]. The 3 h dissolution concentrations provided in Fig. 6 show that oxidized sulfur compounds in aqueous systems accelerate the dissociation of CaS due to the oxidation of  $HS^-$  (Eqs. (18) and (19)).

#### 4.2. CaS dissolution kinetics in the CaS–H<sub>2</sub>O system

Two approaches were applied to describe the CaS–H<sub>2</sub>O system and to establish the kinetic parameters. The mechanism of CaS dissolution in an inert aqueous system can be presented by three step reaction systems where Eq. (5) is first order and Eqs. (7) and (9) are second order

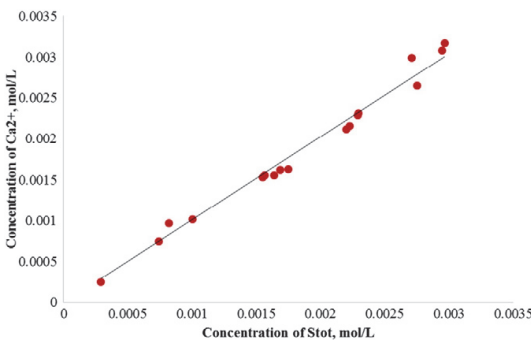


Fig. 5. Relationship between  $Ca^{2+}$  and  $S_{total}$  concentration in CaS–H<sub>2</sub>O system.

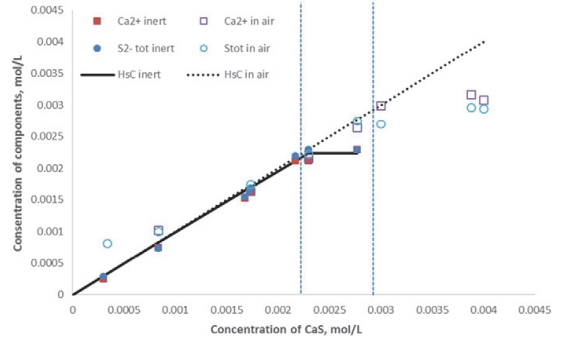


Fig. 6. Measured and calculated concentrations for calcium-ions and sulfide-ions in CaS–H<sub>2</sub>O inert and in air system, at 25 °C.

reactions that take water into account. The equilibrium constants  $K_1$ ,  $K_{b2}$ , and  $K_{b1}$ , were calculated from experimentally measured concentration values (Table 2).

The concentration profiles of characteristic species taking part to the CaS dissolution process can be modeled as a function of time using a system of differential equations namely:

The system of equations was solved with the following boundary and initial conditions:  $t = 0 \dots t = \infty$ ;  $CaS(s)_t = 0 = CaS(s)_{input}$ ;  $pH = 6.5$ ;  $Ca^{2+}/S^{2-} = 0$ .

$$\frac{d[CaS]}{dt} = -k_1[CaS(s)] + \frac{k_1}{K_1}[CaS(s)][Ca^{2+}][S^{2-}] \quad (38)$$

$$\frac{d[Ca^{2+}]}{dt} = k_1[CaS(s)] - \frac{k_1}{K_1}[CaS(s)][Ca^{2+}][S^{2-}] \quad (39)$$

$$\frac{d[OH^-]}{dt} = k_2[S^{2-}] - \frac{k_2}{K_{b2}}[HS^-][OH^-] + k_3[HS^-] - \frac{k_3}{K_{b1}}[OH^-] \times [H_2S(aq)] \quad (40)$$

$$\frac{d[S^{2-}]}{dt} = k_1[CaS(s)] - \frac{k_1}{K_1}[CaS(s)][Ca^{2+}][S^{2-}] - k_2[S^{2-}] + \frac{k_2}{K_{b2}}[HS^-][OH^-] \quad (41)$$

$$\frac{d[H_2S]}{dt} = k_3[HS^-] + \frac{k_3}{K_{b1}}[OH^-][H_2S(aq)] \quad (42)$$

$$\frac{d[HS^-]}{dt} = k_2[CaS(s)][S^{2-}] - \frac{k_2}{K_{b2}}[HS^-][OH^-] + k_3[HS^-] - \frac{k_3}{K_{b1}}[OH^-] \times [H_2S(aq)] \quad (43)$$

The reaction rate constants,  $k_1$ – $k_3$ , were determined using a parameter estimation procedure that iteratively solved the proposed model equations and minimized the difference between these predictions and experimental data obtained in batch experiments over a range of CaS concentrations. The correlation coefficients in all data sets were greater than 0.98. Average values for the reaction rate constants,  $k_1$ ,  $k_2$ , and  $k_3$  were equal to  $1.49 \cdot 10^{-3}$ , 2.77, and  $4.49 \text{ s}^{-1}$ , respectively. The values of the backward reactions  $k_{-1}$ ,  $k_{-2}$  and  $k_{-3}$  can be calculated from the equilibrium constants and can be expressed as  $k_1/K_1$ ,  $k_2/K_{b2}$  and  $k_3/K_{b1}$ , respectively. A simulation procedure was performed with the values of the rate constants. The accuracy of the proposed dissolution model ( $R^2 > 99\%$ ) was confirmed by comparing the results of simulation process with the experimental data.

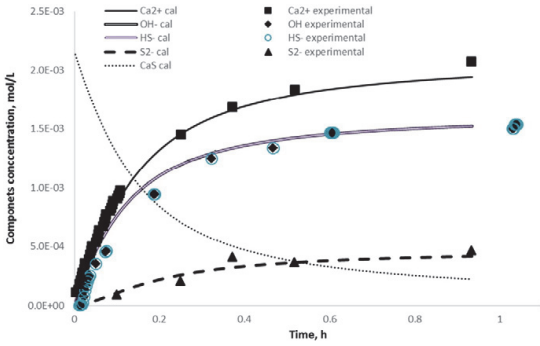


Fig. 7. The comparison of the experimental and modeling (Modest 6.1) results (2.292 mM) in inert system, at 25 °C.

The concentration values of  $\text{Ca}^{2+}$ ,  $\text{OH}^-$ ,  $\text{HS}^-$  and  $\text{S}^{2-}$ , as function of time, (for  $2.29 \cdot 10^{-3}$  mol/L concentrations of the CaS–H<sub>2</sub>O system) are reported in Fig. 7.

The mechanism of CaS dissolution in an aqueous oxidative system is more complex. Observed changes in both the pH and the conductivity of the suspension (Figs. 4 and 8) can be explained by considering a CaS dissolution reactions mechanism. After CaS dissociation, the resulting sulfides bind protons according to Eqs. (5) and (7). In the region where conductivity increases but pH remains stable thiosulfates are formed (Eq. (18)). This observation agrees with the results determined by Carcia-Calzada et al. [19], they detected thiosulfates mainly when CaS was still present in a solid form. Further on, when conductivity and pH begin to decrease, sulfates are formed (Eq. (19)).

It was suggested that the concentration (expressed in molar units) can be modeled through the following differential equations together with Eqs. (38)–(42):

$$\frac{d[\text{HS}^-]}{dt} = -k_4[\text{HS}^-] - k_5[\text{HS}^-] + k_2[\text{S}^{2-}] - \frac{k_2}{K_{b2}}[\text{HS}^-][\text{OH}^-] - k_3[\text{HS}^-] + \frac{k_3}{K_{b1}}[\text{OH}^-][\text{H}_2\text{S}(aq)] \quad (44)$$

$$\frac{d[\text{S}_2\text{O}_3^{2-}]}{dt} = 0.5k_4[\text{HS}^-] \quad (45)$$

$$\frac{d[\text{SO}_4^{2-}]}{dt} = k_5[\text{HS}^-] \quad (46)$$

The reaction rate constants,  $k_4$  and  $k_5$ , were evaluated for a CaS concentration ranged from  $3.35 \cdot 10^{-4}$  mol/L to  $4.50 \cdot 10^{-3}$  mol/L. For each data set, the correlation coefficient between measured and predicted data was found to be greater than 0.94. The average estimated values of the rate constants  $k_4$  and  $k_5$  ( $2.01 \cdot 10^{-4} \text{ s}^{-1}$  and  $8.66 \cdot 10^{-5} \text{ s}^{-1}$ )

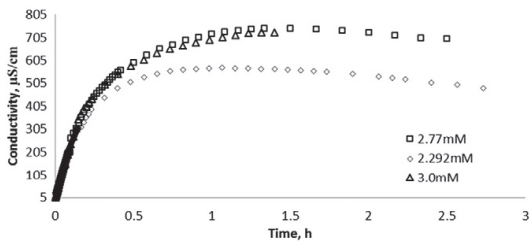


Fig. 8. Conductivity change in time of CaS–H<sub>2</sub>O in air system, at 25 °C.

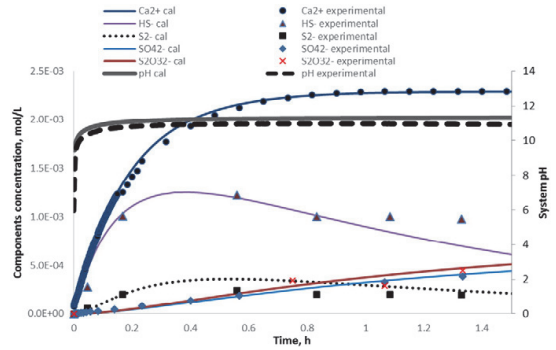


Fig. 9. The comparison of the experimental and modeling (Modest 6.1) results (2.292 mM) in air system, at 25 °C.

are one order of magnitude higher than these obtained by results of Mölder et al. (1995) [7], they reported values of  $1.2 \cdot 10^{-5} \text{ s}^{-1}$  and  $9.0 \cdot 10^{-6} \text{ s}^{-1}$ , for  $k_4$  and  $k_5$ . Comparing plots of the model predicted concentration values of the main ions ( $\text{S}_2\text{O}_3^{2-}$  = total reduced sulfur – total sulfide) and pH change of the system and of the experimental data are presented in Fig. 9.

The relatively small deviations between the calculated and experimental data confirm that the two suggested models can be used to adequately describe the CaS dissolution process under both inert and atmospheric conditions.

### 5. Conclusions

We studied both the thermodynamics and kinetics of the CaS–H<sub>2</sub>O system at 25 °C under inert as well as atmospheric conditions in order to assess the CaS leaching behavior during the processing and disposal of oil shale waste. A mechanism of CaS dissolution based on experimental data and thermodynamic calculations (HsC Chemistry® 7.1) was also suggested. CaS solubility was experimentally determined under an inert atmosphere ( $2.29 \cdot 10^{-3}$  mol/L) and a higher solubility was evaluated under atmospheric conditions ( $2.74 \cdot 10^{-3}$  mol/L) (after 3 h of dissolution). Oxygen provokes the solubility when CaS is present in a solid phase, because the content of sulfide ions would be restored by further CaS dissociation. The experimental equilibrium constants for the dissolution reactions ( $K_1 = 9.79 \cdot 10^{-7}$  and  $K_{b2} = 5.97 \cdot 10^{-3}$ ) were found to be in good agreement with the HsC simulation results. Mathematical dynamics model for CaS dissolution was proposed with the reaction rate constants in inert system ( $k_1 = 1.49 \cdot 10^{-3} \text{ s}^{-1}$ ,  $k_2 = 2.77 \text{ s}^{-1}$  and  $k_3 = 4.49 \text{ s}^{-1}$ ) and in air system together with oxidation reactions ( $k_4 = 2.01 \cdot 10^{-4} \text{ s}^{-1}$  and  $k_5 = 8.66 \cdot 10^{-5} \text{ s}^{-1}$ ). These values were confirmed by simulating both dissolution equilibrium and its dynamics and compared these predictions with experimental values. The simulated concentration profiles for our batch reactor are in good agreement with the experimental data for the inert system and provide a satisfactory representation of the CaS–H<sub>2</sub>O system under atmospheric conditions. The proposed kinetic models could serve as the basis for designing more complex and safe waste handling schemes.

### Acknowledgments

This research was supported by European Social Fund's Doctoral Studies (ESF 1.2.0401.09-0079) and Internationalisation Programme DoRa (T8), Estonian Ministry of Education and Research (SF0140082s08), Estonian Science Foundation (Grant No 9334), institutional research funding IUT (IUT33-19), which are gratefully acknowledged.

## References

- [1] Eesti Energia, 2013 Annual Report of the Eesti Energia, 2013 Retrieved from [https://www.energia.ee/-/doc/10187/pdf/concern/annual\\_report\\_2013\\_eng.pdf](https://www.energia.ee/-/doc/10187/pdf/concern/annual_report_2013_eng.pdf)
- [2] R. Kuusik, M. Uibu, K. Kirsimäe, Characterization of oil shale ashes formed at industrial scale boilers, *Oil Shale* 22 (4 Special) (2005) 407–419.
- [3] L. Bityukova, R. Mõtlep, K. Kirsimäe, Composition of oil shale ashes from pulverized firing and circulating fluidized-bed boiler in narva thermal power plants, Estonia, *Oil Shale* 27 (4) (2010) 339–353.
- [4] K. Tamm, R. Kuusik, M. Uibu, J. Kallas, Transformations of sulfur compounds in oil shale ash suspension, in: waste management and the environment VI, WIT Trans. Ecol. Environ. 163 (2012) 25–35.
- [5] R. Mõtlep, K. Kirsimäe, P. Talviste, E. Puura, J. Jürgenson, Mineral composition of Estonian oil shale semi-coke sediments, *Oil shale* 24 (3) (2007) 405–422.
- [6] A. Elenurm, V. Oja, E. Tali, E. Tearo, A. Yanchilin, Thermal processing of dictyonema argillite and kukersite oil shale: transformation and distribution of sulfur compounds in pilot-scale galoter process, *Oil Shale* 25 (3) (2008) 328–334.
- [7] L. Mõlder, A. Elenurm, H. Tamvelius, Sulphur compounds in a hydraulic ash – disposal system, *Proc. Est. Acad. Sci. Chem.* 44 (2/3) (1995) 207–211.
- [8] E.J. Anthony, L. Jia, A.P. Iribarne, G. Welford, J. Wang, O. Trass, Calcium sulphide in FBC boilers and its fate using liquid water reactivation, *Fuel* 85 (2006) 1871–1879.
- [9] S. Wu, M.A. Uddin, S. Nagamine, E. Sasaoka, Role of water vapor in oxidative decomposition of calcium sulfide, *Fuel* 83 (2004) 671–677.
- [10] O. Velts, M. Uibu, J. Kallas, R. Kuusik, Waste oil shale ash as a novel source of calcium for precipitated calcium carbonate: carbonation mechanism, modeling, and product characterization, *J. Hazard. Mater.* 195 (2011) 139–146.
- [11] E.H. Riesenfeld, H. Feld, Die Löslichkeit von Calciumsulfid bei Gegenwart von Schwefelwasserstoff, *Z. Anorg. Allg. Chem.* 116 (1) (1921) 213–227.
- [12] J.A. Dean, *Lange's Handbook of Chemistry*, 15th ed. McGraw-Hill, New York, 1999.
- [13] D.R. Lide (Ed.), *CRC Handbook of Chemistry and Physics*, 88th ed. CRC press, Boca Raton, FL, 2008.
- [14] I. Zekker, T. Tenno, A. Selberg, K. Uiga, Dissolution modeling and experimental measurement of CaS-H<sub>2</sub>O binary system, *Chin. J. Chem.* 29 (11) (2011) 2327–2336.
- [15] S. Licht, Aqueous solubilities, solubility products and standard oxidation-reduction potentials of the metal sulfides, *J. Electrochem. Soc.* 135 (12) (1988) 2971–2975.
- [16] R.H. Perry, D.W. Green, *Perry's Chemical Engineers' Handbook*, 7th ed. McGraw-Hill book Company, New York, 1999.
- [17] W.F. Linke, *Solubilities of Inorganic and Metal-organic Compounds*, 4th ed. ACS, 1958.
- [18] M. de Beer, J.P. Maree, L. Liebenberg, F.J. Doucet, Conversion of calcium sulphide to calcium carbonate during the process of recovery of elemental sulphur from gypsum waste, *Waste Manag.* 34 (11) (2014) 2373–2381.
- [19] M. Garcia-Calzada, G. Marban, A.B. Fuentes, Decomposition of CaS particles at ambient conditions, *Chem. Eng. Sci.* 55 (2000) 1661–1674.
- [20] J.W. Morse, F.J. Millero, J.C. Cornwell, D. Rickard, The chemistry of the hydrogen sulfide and iron sulfide systems in natural waters, *Earth Sci. Rev.* 24 (1) (1987) 1–42.
- [21] J.J. Carroll, A.E. Mather, The solubility of hydrogen sulphide in water from 0 to 90 °C and pressures to 1 MPa, *Geochim. Cosmochim. Acta* 53 (6) (1989) 1163–1170.
- [22] W. Sun, S. Nešić, D. Young, R.C. Woollam, Equilibrium expressions related to the solubility of the sour corrosion product mackinawite, *Ind. Eng. Chem. Res.* 47 (5) (2008) 1738–1742.
- [23] V.J. Šuklytė, E. Rinkeviciėnė, V. Zelionkaitė, The chemistry of sulfur in anoxic zones of the Baltic sea, *Environ. Res. Eng. Manag.* 3 (21) (2002) 55–60.
- [24] A.H. Nielsen, J. Vollertsen, T. Hvitved-Jacobsen, Determination of kinetics and stoichiometry of chemical sulfide oxidation in wastewater of sewer networks, *Environ. Sci. Technol.* 37 (1) (2003) 3853–3858.
- [25] K.Y. Chen, J.C. Morris, Kinetics of oxidation of aqueous sulfide by O<sub>2</sub>, *Environ. Sci. Technol.* 6 (6) (1972) 529–537.
- [26] T. Almgren, D. Dyrssen, B. Elgquist, O. Johansson, Dissociation of hydrogen sulphide in seawater and comparison of pH scale, *Mar. Chem.* 4 (1976) 289–297.
- [27] F.J. Millero, T. Plese, M. Fernandez, The dissociation of hydrogen sulfide in seawater, *Limnol. Oceanogr.* 22 (33) (1988) 296–274.
- [28] J.D. Cline, F.A. Richards, Oxygenation of hydrogen sulfide in seawater at constant salinity, temperature and pH environmental, *Sci. Technol.* 3 (9) (1969) 838–843.
- [29] B.J. Lefers, T.K. Wicher, P.M.V.S. Willibrordus, The oxidation of sulphide in aqueous solutions, *Chem. Eng. J.* 15 (1978) 111–120.
- [30] ISO – 6058, ISO 6058:1984, Water Quality – Determination of Calcium Content – EDTA Titrimetric Method, 1984.
- [31] EKUK Virumaa affiliate Kohta-Järve laboratory of chemistry, The Quality Procedure Guide TJ 17 – Determination of Sulfide in Water, 2002.
- [32] ISO – 9963-1, Water quality - Determination of Alkalinity – Part 1: Determination of Total and Composite Alkalinity, 1994.
- [33] K. Tamm, R. Kuusik, M. Uibu, J. Kallas, Behaviour of sulfur compounds during aqueous leaching of oil shale ash, Proceedings of the 4th International Conference on Accelerated Carbonation for Environmental and Materials Engineering ACEME 2013, Leuven Belgium 2013, pp. 541–544.
- [34] HSC Chemistry® for Windows, Chemical reaction and equilibrium software with extensive thermochemical database, Version 7.1 Pori: Outokumu Research, Licence for Tallinn Technical University, 2011.
- [35] H. Haario, Modest User Manual, Profmath OY, Helsinki, Finland, 1994.
- [36] A.C. Hindmarsh, ODEPACK, a systematized collection of ODE solvers, Scientific computing: IMACS transactions on scientific computation, 1 1983, pp. 55–64.
- [37] D.J. O'Brien, F.B. Birkner, Kinetics of oxygenation of reduced sulfur species in aqueous solution, *Environ. Sci. Technol.* 11 (12) (1977) 1114–1120.
- [38] M.R. Hoffman, B.C. Lim, Kinetics and mechanism of the oxidation of sulfide by oxygen: catalysis by homogeneous metal-phthalocyanine complexes, *Environ. Sci. Technol.* (1979) 1406–1414.
- [39] S.S. Zavodnov, P.A. Kryukov, The value of the second dissociation constant of hydrogen sulfide, *Otdelene Khim. Nauk* 9 (1960) 1704–1706.
- [40] H. Kubli, Die dissociation von schwefelwasserstoff, *Helv. Chim. Acta* 29 (1946) 1962–1973.
- [41] Y.S. Su, K.L. Cheng, Y.C. Jean, Amplified potentiometric determination of pK<sub>00</sub>, pK<sub>0</sub>, pK<sub>1</sub> and pK<sub>2</sub> of hydrogen sulfides with Ag<sub>2</sub>S ISE, *Talanta* 44 (1997) 1757–1763.

### **PAPER III**

*Tamm, K., Kallaste, P., Uibu, M., Kallas, J., Velts-Jänes, O., Kuusik, R.*

Leaching Thermodynamics and Kinetics of Oil Shale Waste Key Components.

*Oil Shale*, 2016, 30, 1, 80-99.



## LEACHING THERMODYNAMICS AND KINETICS OF OIL SHALE WASTE KEY COMPONENTS

KADRIANN TAMM\*, PRIIT KALLASTE, MAI UIBU,  
JUHA KALLAS, OLGA VELTS-JÄNES, REIN KUUSIK

Laboratory of Inorganic Materials, Tallinn University of Technology, Ehitajate tee 5, 19086 Tallinn, Estonia

**Abstract.** Estonia is strongly dependent on locally mined oil shale which is the main fuel for power and oil production. Vast amounts of solid wastes are formed from circulating fluidized bed (CFB), pulverized firing (PF), and solid heat carrier (SHC) technologies, and are currently wet deposited in open-air fields. Both the utilization of newly produced ash and the management of historical deposits require an accurate thermodynamic modelling of complex mixtures. The authors investigated the leaching of the main water-soluble Ca-compounds from three types of oil shale mineral waste and developed a kinetic model that was used to determine the equilibrium constants and kinetic parameters of dissolution reactions for all three ash-water systems over a wide range of solid-to-liquid (S/L) ratio. For this, we prepared binary  $(Ca(OH)_2-CaSO_4 \cdot 2H_2O-H_2O)$  and ternary  $(Ca(OH)_2-CaSO_4 \cdot 2H_2O-CaS-H_2O)$  model systems that reflect the composition of the three different ashes, and measured the kinetics of dissolution for both the model systems and industrial ash. Thermodynamic calculations were performed using HsC Chemistry<sup>®</sup> 7.1 and Aspen Plus V8.6 while the leaching kinetics was simulated employing the MODEST 6.1 software package. By comparing the results obtained for our model systems with those obtained for industrial oil shale ash-water systems the authors were able to both verify that the model results coincided to a satisfactory degree with simulation data, and also propose models that may aid one to design shale ash processing technologies.

**Keywords:** oil shale ash, HsC chemistry, calcium compounds, sulfur compounds.

### 1. Introduction

About 60% of Estonia's fuel balance is covered by local low-grade oil shale (OS), which is mainly used to produce heat, power, and shale oil. Oil shale

---

\* Corresponding author: e-mail [kadriann.tamm@ttu.ee](mailto:kadriann.tamm@ttu.ee)

processing generates vast amounts of solid waste of varying composition depending on both the composition of raw OS and processing conditions [1]. 45–48% of OS dry matter remains as solid waste [2].

The oil shale ash (OSA) from thermal power plants contains mainly free lime ( $\text{CaO}_{\text{free}}$ ), Ca-sulfate, secondary Ca(Mg)-silicate minerals, and an amorphous Al-Si glass phase [3–5]. Both the high temperatures and thermal processing conditions as well as combustion conditions ( $> 750\text{ }^{\circ}\text{C}$ , residence time, combustion regime – pulverized firing (PF) or circulating fluidized bed (CFB) combustion) ensure that all of the organic matter (mainly kerogen) in OS (up to 65% [6]) is burnt out [1].

Gaseous heat carrier (GHC) and solid heat carrier (SHC) retorts are used to produce shale oil. In the SHC process, OS is heated in the absence of oxygen by continuously mixing the combusted retorting residue at about  $800\text{ }^{\circ}\text{C}$  [7, 8]. During the last stage of the process, the retorting residue is combusted in an aero furnace at temperatures up to  $950\text{ }^{\circ}\text{C}$ . The resulting solid residue consists mainly of calcite, quartz, K-feldspar, and dolomite, with only trace amounts of  $\text{CaO}_{\text{free}}$ . The composition of this residue is similar to that of ash produced in the circulating fluidized bed furnaces at thermal power plants, but contains up to a few percent of unburnt organic matter due to the short residence time in the combustion stage [8, 9].

Eesti Energia, Estonia's major power company, deposited 7.9 Mt of OSA and emitted 12.8 Mt of  $\text{CO}_2$  in 2014 [10]. At the same time, the largest OS retorting company, VKG OIL Ltd., processed 2.9 Mt of OS and produced 433,000 t of shale oil [11]. In 2013, VKG processed 2.8 Mt of OS and generated approximately 1.48 Mt of ash and about 0.9 MT of semicoke type retorting waste [12]. The safe disposal and/or reuse of OS ash waste, together with atmospheric emissions ( $\text{CO}_2$ ,  $\text{SO}_2$ ,  $\text{NO}_x$ , etc.), are among the most serious environmental problems in Estonia.

Today, about 90% of oil shale ash is wet deposited in ash fields near the power plants. Only a small percentage of OSA is utilized, either in the building materials industry, in agriculture as a liming agent, or in road construction [5]. OSA is classified as a "hazardous waste" mainly due to the high alkalinity of leachates (pH values 12–13), contributed by the dissolution of free lime (up to 30 wt%). However, this property makes OSA (or OSA leachates) an attractive material for  $\text{CO}_2$  mineralization [13, 14] or producing precipitated calcium carbonate (PCC) [15, 16]. Currently, the lack of kinetic process data, including that characterizing leaching, impedes the implementation of more effective waste valorization and environmental pollution control methods.

The current study investigates the dissolution mechanisms of OS mineral waste. In order to better understand the behavior and impact of the waste's key components on the leaching process, both binary and ternary model systems were prepared to match the composition of OS processing ashes and investigated for comparison. The aim of the study was to elaborate the leaching equilibriums and dynamics of the main water-soluble Ca-compounds of

OSAs, as a basis for mathematical models, which simulate the processes of leaching. The results provide a basis for designing a complete OSA neutralization and/or carbonation process.

## 2. Materials and methods

### 2.1. Characterization of materials

Three types of ash were used as Ca-rich raw materials. The circulating fluidized bed ash mixture (taken from the common silo) and pulverized firing cyclone ash were collected from Eesti Power Plant of Narva Power Plants in 2011. The SHC ash was collected in 2012 from the final residue resulting from the shale oil production process at the VKG retorting plant.

Each ash sample was analyzed using both X-ray fluorescence spectroscopy (XRF, Rigaku Primus II) and quantitative X-ray diffraction (XRD, Bruker D8 Advanced) methods at the Institute of Geology, University of Tartu (UT). The contents of free lime ( $\text{CaO}_{\text{free}}$ ) (ethylene glycol method) [17], different forms of sulfur (sulfate and sulfide) [18], total carbon (TC) and inorganic carbon (TIC) (Electra CS - 580 Carbon/ Sulfur Determinator) were determined. The BET specific surface area (SSA) was determined using a Kelvin 1042 sorptometer. The chemical and mineral composition as weight percentages together with the SSA values of the three ashes are provided in Table 1.

Of the three ashes, PF ash is characterized by the highest free lime content. The sulfates in CFB ash are present mainly in the form of anhydrite ( $\text{CaSO}_4$ ), which in water systems crystallizes into gypsum ( $\text{CaSO}_4 \cdot 2\text{H}_2\text{O}$ ). In both the CFB and PF ashes the content of sulfides (mainly CaS) is relatively low. SHC ash is characterized by high sulfide content. This ash also contains organic matter with a chemical oxygen demand of  $99 \pm 10$  mg/L as measured according to the method described in [19], which is present because the residence time in the final burner at the oil factory is insufficient to ensure complete pyrolysis. The presence of organics also causes the high porosity and surface area of the retorted ashes [20]. The SSA of both CFB and SHC ashes is more than ten times that of PF ash (Table 1). Under ambient conditions the sulfides from each of these ashes can be emitted into the atmosphere as gaseous  $\text{H}_2\text{S}$ , generating atmospheric pollution. Sulfides, which remain in the aqueous phase, may also induce toxic effects depending on the pH of the suspension [21].

**Table 1. The composition and SSA of OS ashes in wt% and  $m^2 \cdot g^{-1}$** 

Chemical composition	CFB	PF	SHC
CaO <sub>free</sub>	12.31	22.37	1.89
SO <sub>4</sub> <sup>2-</sup>	7.90	5.24	1.82
S <sup>2-</sup>	0.64	0.064	1.22
TC	3.03	0.30	7.82
TIC	3.03	0.30	6.45
TOC	0	0	1.37
Mineral composition	CFB	PF	SHC
Quartz (SiO <sub>2</sub> )	11.40	4.40	14.10
K-feldspar (KAlSi <sub>3</sub> O <sub>8</sub> )	10.20	3.90	12.70
Calcite (CaCO <sub>3</sub> )	27.70	3.30	29.40
Lime (CaO)	9.30	28.30	3.00
Portlandite (Ca(OH) <sub>2</sub> )	1.10	0	–
Anhydrite (CaSO <sub>4</sub> )	10.10	8.60	0.70
Periclase (MgO)	2.70	5.10	8.70
Dolomite (CaMg(CO <sub>3</sub> ) <sub>2</sub> )	1.40	0	10.00
Wollastonite (CaSiO <sub>3</sub> )	1.20	3.70	1.90
Belite (Ca <sub>2</sub> SiO <sub>4</sub> )	6.70	24.00	–
Alite (Ca <sub>3</sub> SiO <sub>5</sub> )	1.40	0	–
Merwinite (Ca <sub>3</sub> Mg(SiO <sub>4</sub> ) <sub>2</sub> )	0.80	6.30	1.30
Melilite ((CaMg) <sub>2</sub> (MgAl)(SiAl) <sub>3</sub> O <sub>7</sub> )	2.50	8.20	1.20
Brownmillerite (4CaO·Al <sub>2</sub> O <sub>3</sub> ·Fe <sub>2</sub> O <sub>3</sub> )	1.30	2.40	2.20
Hematite/magnetite (Fe <sub>2</sub> O <sub>3</sub> /Fe <sub>3</sub> O <sub>4</sub> )	2.20	1.30	1.60
Jasmondite (Ca <sub>11</sub> (SiO <sub>4</sub> ) <sub>4</sub> O <sub>2</sub> S)	1.70	0	–
Calcium ferrite (2CaO·Fe <sub>2</sub> O)	1.30	0	–
Yeelimite (Ca <sub>4</sub> Al <sub>6</sub> (SO <sub>4</sub> )O <sub>12</sub> )	0.60	0	–
Albite (NaAlSi <sub>3</sub> O <sub>8</sub> )	–	–	1.60
Rankinite (Ca <sub>3</sub> Si <sub>2</sub> O <sub>7</sub> )	–	–	0.90
Illite (K <sub>y</sub> Al <sub>4</sub> (Si <sub>3-y</sub> Al <sub>y</sub> )O <sub>20</sub> (OH) <sub>4</sub> )	6.40	0	3.40
Ca-Al pyroxene (CaAl <sub>2</sub> SiO <sub>6</sub> )	2.50	8.20	1.20
Physical characteristic	CFB	PF	SHC
SSA, $m^2 \cdot g^{-1}$	6.30	0.40	7.44

## 2.2. Experimental procedure

All experiments with CFB, PF and SHC ash-water systems as well as the corresponding binary (Ca(OH)<sub>2</sub>-CaSO<sub>4</sub>·2H<sub>2</sub>O-H<sub>2</sub>O) and ternary (Ca(OH)<sub>2</sub>-CaSO<sub>4</sub>·2H<sub>2</sub>O-CaS-H<sub>2</sub>O) model systems were performed at room temperature and atmospheric pressure. The selected ash-to-water ratios ranged from 0.004–0.200 and were selected based on the results of previous studies [22], and the parameters (ash-to-water ratio of 1.20) used in the hydrotransport of OSA. Model binary and ternary ash mixtures were made of pure Ca(OH)<sub>2</sub> (BDH, 95% purity), CaSO<sub>4</sub>·2H<sub>2</sub>O (Iach:ner, 99% purity), and CaS (Alfa Aeser, 99.9% purity) as sources of Ca<sup>2+</sup>, SO<sub>4</sub><sup>2-</sup> and S<sup>2-</sup> ions. For a comparative study the proportions of components in model systems were chosen according to their content in the respective OSAs.

To achieve an equilibrium state, the systems under study were kept in closed centrifuge tubes for 3 h in an overhead shaker (GFL 3025) at 45 rpm

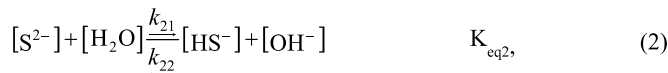
throughout the experiment. The suspensions were prepared in 50 mL tubes sealed with airtight caps beforehand. The pH (MT SevenGo pH) and electrical conductivity of the suspensions (MT SevenGo Duo Pro) were measured immediately after a 3 h experiment. The dissolution kinetics of these systems was determined in a batch reactor. For this, 0.750 L of deionized water (conductivity 0.05  $\mu\text{S}/\text{cm}$ ) was poured into a 1 L Lara Controlled Lab Reactor. The stirrer was set to revolve at 250 rpm and a thermostat (Huber Unistat 405) kept the entire system at 25 °C in the course of the experiment. A pause control program momentarily halted the stirring while the solid phase was quickly added to the system using a funnel. Each suspension was maintained as a closed system for one hour. The conductivity (Mettler Toledo SevenGO Duo Pro with LabX software), pH (Knick Portamess 913 pH; Hamilton Polylyte Plus VP360 pH-meter sensor) and temperature of the solution were continuously monitored during the experiment. The resulting suspensions were then filtered using a vacuum filter (Munktell filter paper, 100 g/m<sup>2</sup>). The contents of calcium ( $\text{Ca}^{2+}$  ions), total reduced sulfur, and alkalinity ( $\text{OH}^-$ ,  $\text{CO}_3^{2-}$  and  $\text{HCO}_3^-$  ions) were determined using titration methods, the ISO-6058:1984 method [23], iodometric titration [24], and the ISO-9963-1:1994(E) method [25], respectively. The content of total sulfide was determined as the sum of dissolved sulfide ( $\text{S}^{2-}$ ,  $\text{HS}^-$ ,  $\text{H}_2\text{S}$ ) and  $\text{SO}_4^{2-}$  ions, using a Lovibond Spectro Direct spectrometer, and DPD/Catalyst and barium sulfate turbidity methods, respectively.

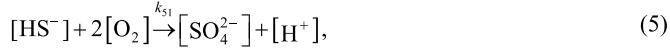
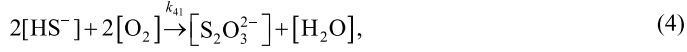
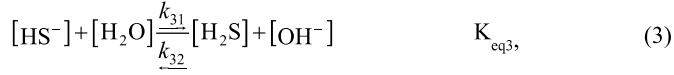
### 2.3. Modeling software

The equilibrium calculations were carried out using thermodynamic programs based on the Gibbs free energy minimization technique. The Aspen Plus RGibbs reactor model, which employs the ELECNRTL model together with the Aspen Plus V8.6 default databases, and the HsC Chemistry<sup>®</sup> 7.1 program were applied to both determine the composition of each phase and predict the equilibrium composition of ternary systems according to the composition of the three ashes (CFB, PF, SHC). The equilibrium composition of the real CFB ash-water system was also investigated using the HsC program.

### 2.4. Process chemistry

Equations (1)–(7) represent a simplified dissociation (equilibriums (1)–(3) and (6)–(7)) for OSA and ternary ( $\text{Ca}(\text{OH})_2$ - $\text{CaSO}_4 \cdot 2\text{H}_2\text{O}$ - $\text{CaS}$ - $\text{H}_2\text{O}$ ) model systems:





where  $K_{\text{eq}1}$ – $K_{\text{eq}3}$  and  $K_{\text{eq}6}$ – $K_{\text{eq}7}$  are the equilibrium constants expressed on a molar basis,  $k_{11}$ – $k_{71}$  (in the numerator) are the forward reaction rate constants, and  $k_{12}$ – $k_{72}$  (in the denominator) are the reverse reaction rate constants,  $\text{s}^{-1}$ .

The  $\text{Ca}(\text{OH})_2$  dissolution mechanism is presented as a one-step reaction system for a more universal approach [26]. The formation of gaseous  $\text{H}_2\text{S}$  is not included in the proposed model. As a more complex approach, a two-step reaction system for lime dissolution ( $\text{Ca}(\text{OH})_2 \leftrightarrow \text{CaOH}^+ + \text{OH}^-$ ;  $\text{CaOH}^+ \leftrightarrow \text{Ca}^{2+} + \text{OH}^-$ ) and further hydrolysis of sulfide are included in the Aspen Plus ternary and HsC Chemistry<sup>®</sup> (also the formation of gaseous  $\text{H}_2\text{S}$ ) models (in all OSA based ternary systems and the CFB ash system).

### 3. Results and discussion

The following section will discuss the results of thermodynamic and kinetic calculations for ternary model systems and the solubility results for the experimentally measured binary and ternary models as well as OS ash-water systems.

#### 3.1. Simulation approach

The thermodynamic calculations show that at the equilibrium state the unstable compounds are bound to the steady phase (Fig. 1). Its final composition indicates mineral changes to have taken place in OSA after leaching for an unlimited period of time. At equilibrium, quartz does not occur, and therefore, Ca-silicate minerals dominate, oxides are present as their hydrated forms, also gypsum is formed from the original anhydrate.

Both the binary and ternary tests were carried out using  $\text{Ca}(\text{OH})_2$  and  $\text{CaSO}_4 \cdot \text{H}_2\text{O}$  as the main  $\text{Ca}^{2+}$  and  $\text{SO}_4^{2-}$  ion sources in OS ash-water systems. Thermodynamic calculations show the results obtained using Aspen Plus V6.8 and HsC Chemistry<sup>®</sup> 7.1 to coincide (Fig. 2).

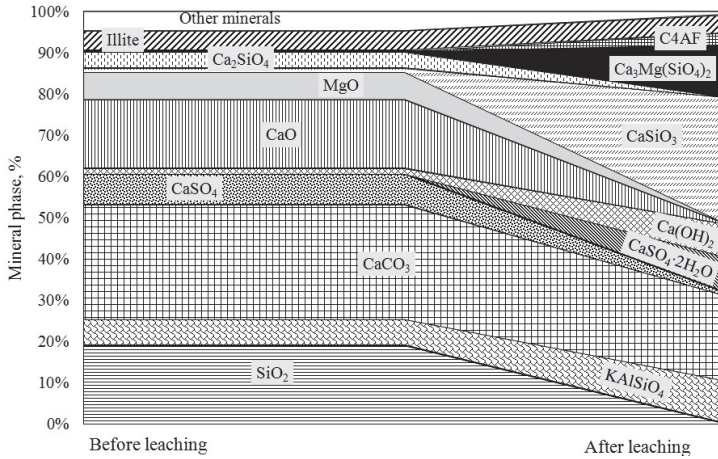


Fig. 1. The composition of theoretical CFB ash (S/L 1:10) and mineral changes in it during the leaching process (HsC Chemistry<sup>®</sup> 7.1).

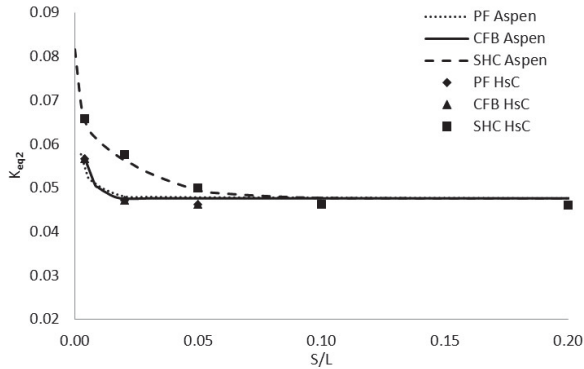


Fig. 2. Apparent equilibrium of ternary model systems (Aspen Plus V8.6 and HsC Chemistry<sup>®</sup> 7.1 simulation).

The simulation results revealed that the equilibrium state of the ion distribution was achieved for the most oversaturated systems ( $S/L$  ratio  $\geq 0.1$ ). Both the CFB and PF ash-water systems had similar equilibrium concentrations of the observed species.

The equilibrium constant  $K_{eq2}$  for Equation (2) was calculated from the simulated equilibrium composition for the OS ash-water model systems (Fig. 2).  $K_{eq2}$  was calculated from the results of both the Aspen Plus V8.6 and HsC Chemistry<sup>®</sup> 7.1 simulations, which coincided, and this value was

used to determine the distribution of sulfide forms in both the model and real OS ash-water systems.

To compare experimental results, the sum of  $\text{Ca}^{2+}$  ( $\text{Ca}^{2+} + \text{CaOH}^+$ ) and  $\text{OH}^-$  ( $\text{OH}^- + \text{CaOH}^+$ ) ions, and  $S_{\text{sulfide}}$  ( $\text{S}^{2-} + \text{HS}^- + \text{H}_2\text{S}$ ) were used to determine the equilibrium constants ( $K_{\text{eq}1}$ ,  $K_{\text{eq}6}$  and  $K_{\text{eq}7}$ ) for Equations (1), (6) and (7).

The equilibrium constant  $K_{\text{eq}3}$  (reported as  $1 \times 10^{-7}$  in [27, 28]) for Equation (3) was calculated from the equilibrium concentration of pure CaS.

### 3.2. Solubility results

By varying the content of the model components of OS ash-water systems according to the ash-to-water ratios from 0.004 to 0.200 and allowing the batch experiments to achieve equilibrium, we were able to determine the system pH, conductivity, and the concentration of the main ion species ( $\text{Ca}^{2+}$ ,  $\text{SO}_4^{2-}$ ,  $S_{\text{sulfide}}$ ) in the liquid phase. The leaching equilibrium of the three types of ashes and the corresponding ternary model systems are shown in Figure 3. The average pH and conductivity (E) were determined based on the experimentally measured values of the equilibrium state model and ash-water systems.

The pH values (12.31–12.66) of saturated binary and ternary systems coincided with those of real OS ash-water systems. The highest pH values occurred in the PF ash based system because this ash contained the highest amount of initial free lime.

The conductivity values determined at saturation for CFB and SHC ash model systems were higher (up to 9.97 mS/cm) than that for the PF ash model system, which tended to stabilize at lower values (up to 9.58 mS/cm). This indicates that the high initial CaS content has a stronger influence on the conductivity of the ions that remain in the aqueous phase than the other components. In real OS ash-water systems, the lowest conductivity values occurred in the SHC ash-water system (10.35 mS/cm) while the PF ash-water system had the highest conductivity (up to 12.25 mS/cm), which in this case was driven by the higher content of free lime and Ca-silicate phases.

At saturation, both  $\text{Ca}^{2+}$  and  $\text{SO}_4^{2-}$  ions were present in similar concentrations in all model systems (0.033–0.035 and 0.014–0.015 mol/L, respectively). At the same time, the respective values were slightly higher in the ternary model systems due to the dissolution of CaS (Eqs. (1)–(3)) and the oxidation of sulfide ions to intermediate forms (Eq. (4)) and sulfate (Eq. (5)). Due to the similarity in leaching mechanism between the binary and ternary model systems, the small ion concentration variations of about 0.001 mol/L can be neglected, hence, the results of binary model systems are not shown in Figure 3. The concentrations of  $\text{Ca}^{2+}$  and  $\text{SO}_4^{2-}$  ions (ca 0.034 and 0.009 mol/L, respectively) were lower in the SHC ash-water system than in both the CFB and PF ash-water systems (ca 0.040 and 0.016 mol/L, respectively). The latter is related to the original composition of the ashes (Table 1). In the ash of the SHC system, the content of leachable  $\text{SO}_4^{2-}$  and  $\text{Ca}^{2+}$  ions was lower than in PF and CFB ashes.

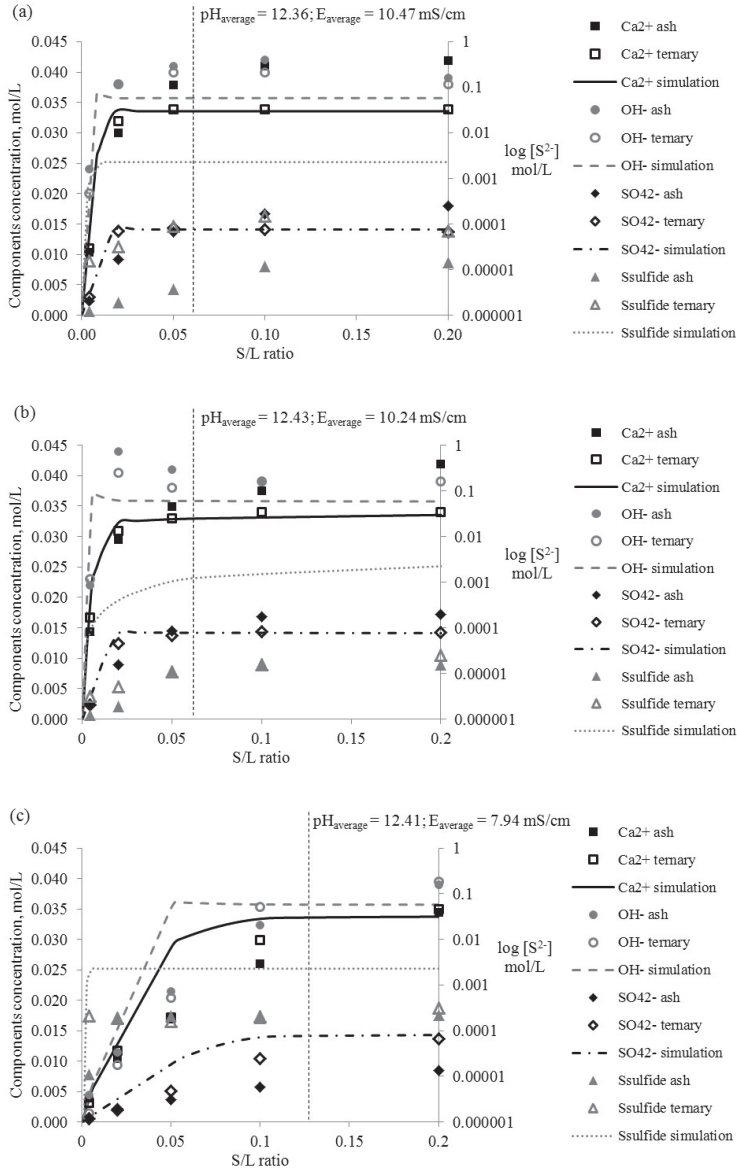


Fig. 3. Experimental vs simulation dissolution data for OSA from: (a) CFB; (b) PF; (c) SHC.

The SHC ash-water system with the highest initial CaS content can also be clearly distinguished by the leaching of sulfides. The total sulfide concentration in the SHC ternary model system was up to  $5.6 \times 10^{-4}$  mol/L, which is notably higher compared with both the CFB and PF ternary model systems ( $7.9 \times 10^{-5}$  and  $2.1 \times 10^{-5}$  mol/L, respectively). Total sulfide concentrations in the leachates of CFB and PF ash-water systems remained at  $1.5 \times 10^{-5}$  mol/L, and were up to 20 times that in the SHC ash-water system, which stayed at  $2.2 \times 10^{-4}$  mol/L (the equilibrium concentration was not reached under our experimental conditions). Though there was no remarkable difference in initial CaS content between the ashes compared, the leaching of CaS was favored in the SHC ash-water system.

The parameters of the ternary ash-water model and real OS ash-water systems were well comparable. The small differences observed were caused by other water-soluble OS ash components (Table 1). Consequently, the OS ash leaching scheme can be modeled using our ternary model system.

The predicted dissociation results for the OS ash-water systems (Eqs. (1)–(7)) were compared with the experimental data (Fig. 3). The relatively small differences in the measured and predicted data confirm the ability of the proposed model to describe accurately the dissolution process of OS ash-water systems. The variability in sulfide concentrations is largely due to uncertainties in the experimentally determined solubility of pure CaS. In our previous work [29], the CaS solubility was determined after three hours of dissolution under both an inert atmosphere ( $2.29 \times 10^{-3}$  mol/L) and atmospheric conditions ( $2.74 \times 10^{-3}$  mol/L). The experimental results show a

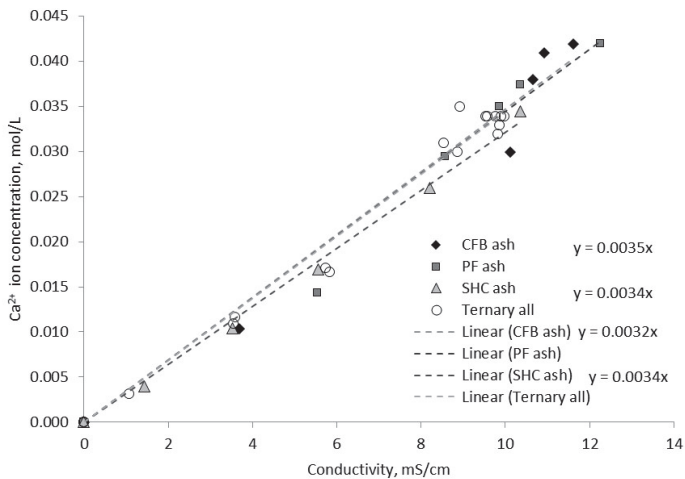


Fig. 4. Relationship between  $\text{Ca}^{2+}$  ion concentration and conductivity in ternary model and OSA based water systems.

strong relationship between the  $\text{Ca}^{2+}$  ion concentration and conductivity (E) of the solution for all of the OS ash-water systems, including the ternary  $(\text{Ca}(\text{OH})_2\text{-CaSO}_4\cdot 2\text{H}_2\text{O-CaS})$  model ( $R^2 = 0.986$ ), and CFB, PF and SHC ash-water systems (Fig. 4).

Including the experimentally determined pH values of the solutions as a main parameter in addition to E did not improve significantly the correlation coefficient, therefore the correlation is expressed as the following averaged equation (8) ( $R^2 = 0.982$ ):

$$[\text{Ca}^{2+}] = 0.003375 \cdot E, \quad (8)$$

where  $\text{Ca}^{2+}$  is the concentration of calcium ions expressed in mol/L and E is the system conductivity in mS/cm.

The earlier studies have shown that  $\text{Ca}^{2+}$  and  $\text{SO}_4^{2-}$  are the main leachable ions in OS ash leachates, the leachability of  $\text{K}^+$  is one order of magnitude lower and  $\text{Na}^+$ ,  $\text{Al}^{3+}$  and  $\text{Mg}^{2+}$  have been detected at minor levels [1, 30]. Also, the presence of other anions ( $\text{Cl}^-$ ,  $\text{S}^{2-}$ ,  $\text{SO}_3^{2-}$ ,  $\text{S}_2\text{O}_3^{2-}$  and  $\text{PO}_4^{3-}$ ) in small concentrations has been detected [31–33]. However, the sum of  $\text{Ca}^{2+}$ ,  $\text{SO}_4^{2-}$  and  $\text{OH}^-$  ions corresponds to 90–95% of the electroneutrality condition. Based on optimal linear approximation (Eq. (8)), the concentration of  $\text{Ca}^{2+}$  ions can be determined for OS ash-water systems from conductivity measurements and compared with the predictions from the kinetic model. This approach may aid in optimizing an industrial PCC process using OS ash-water systems as a feedstock.

The equilibrium constants were calculated from the experimental data using the thermodynamic model and are presented as average values in Table 2. These results indicate that the experimental and predicted values of  $K_{\text{eq}6}$  and  $K_{\text{eq}7}$  ( $K_{\text{eq}6} = 6.37 \times 10^{-5}$ ,  $K_{\text{eq}7} = 5.21 \times 10^{-4}$  and  $K_{\text{eq}6} = 4.28 \times 10^{-5}$ ,  $K_{\text{eq}7} = 4.73 \times 10^{-4}$ , respectively) agree for the ternary model systems quite well. Comparison of the results of ternary model (experimental and simulated) and OS ash-water systems shows the  $K_{\text{eq}6}$  and  $K_{\text{eq}7}$  values for real OS ash-water systems to be higher due to the presence of additional ash components that could provide  $\text{Ca}^{2+}$  and  $\text{SO}_4^{2-}$  ions into the solution. The value of  $K_{\text{eq}6}$  ( $5.24 \times 10^{-5}$ ) reveals the largest discrepancy from the result of

**Table 2. Equilibrium constants of the systems under study**

$K_{\text{eq}}$ OSA, mol/L	Experimental				Simulated (Aspen ternary)			
	$K_{\text{eq}1}$	$K_{\text{eq}2}$	$K_{\text{eq}6}$	$K_{\text{eq}7}$	$K_{\text{eq}1}$	$K_{\text{eq}2}$	$K_{\text{eq}6}$	$K_{\text{eq}7}$
CFB system	$4.05 \times 10^{-7}$	$4.61 \times 10^{-2}$	$6.66 \times 10^{-5}$	$6.52 \times 10^{-4}$	$7.68 \times 10^{-5}$	$4.76 \times 10^{-2}$	$4.28 \times 10^{-5}$	$4.73 \times 10^{-4}$
PF system	$5.36 \times 10^{-7}$	$4.61 \times 10^{-2}$	$7.21 \times 10^{-5}$	$6.18 \times 10^{-4}$				
SHC system	$7.52 \times 10^{-6}$	$4.61 \times 10^{-2}$	$5.24 \times 10^{-5}$	$2.93 \times 10^{-4}$				

the SHC model system ( $5.45 \times 10^{-5}$ ), which indicates that in SHC ash, the balance between calcium and hydroxide ions affects the concentration of all the main components. The value of  $K_{eq7}$  found for the ternary model matches better with that established for the CFB and PF ash-water systems because the concentration of  $SO_4^{2-}$  ions does not reach equilibrium in the real SHC ash-water system. The oxidation reactions (Eqs. (4) and (5)) are expressed as unidirectional because the backward reactions do not occur during the initial combustion processes. However, oxidation in aqueous suspensions takes place as long as sulfide ions are present as “combustible matter”. Considering this, our 3 h experiments do not reflect the endpoint of sulfide oxidation in the suspension. The values of  $K_{eq1}$  for OS ash-water and ternary model systems are also comparable, agreeing with that for the PF ash-water system that has low sulfide content. However, these values significantly differ from the respective simulation figures because our model currently takes into consideration the solubility of CaS in pure water. Consequently, the  $Ca(OH)_2$ - $CaSO_4 \cdot 2H_2O$ - $CaS$ - $H_2O$  model system should be adjusted according to the new experimental data.

Although the ashes of the three types of OS ash-water systems differ in both chemical and physical structure (Table 1) but yet remain comparable with the results for our model ash, we can state that the proposed model can be implemented for describing the leaching behavior of the three key Ca-compounds:  $Ca(OH)_2$ ,  $CaSO_4 \cdot 2H_2O$ , and CaS.

The value of the equilibrium constant  $K_{eq3}$ ,  $1.11 \times 10^{-7}$ , presented in Table 2 was calculated using the equilibrium concentration of pure CaS. The value reported here, together with Equation (17), can be used to develop utilization schemes for more complex OS ash-water systems that involve chemical reactions and also to treat similar alkaline waste materials.

### 3.3. Dissolution kinetics in OS ash-water systems

The dissolution kinetics of  $Ca(OH)_2$  [34, 35] together with the mechanism of CaS dissolution [29, 31, 32, 36] has been described by several authors. In our previous studies [22, 37, 38], the main characteristics of the Ca dissolution process for OS ash were established on the basis of mass transfer mechanisms. In the current study, the leaching behavior of the main components in OS mineral wastes was investigated using the reaction kinetics approach.

Both the kinetic calculations and dissolution process simulations were performed using the MODEST 6.1 software package [39]. The software consists of a FORTRAN 95/90 library of objective functions, solvers and optimizers linked to model problem-dependent routines and the objective function. Each system of differential equations was solved by the means of linear multi-step methods implemented in ODESSA (a systematized collection of the ordinary differential equations solver), which is based on LSODE (Livermore Solver for Ordinary Differential Equations) software [40].

Using the dissolution model (Eqs. (1)–(7)), the dynamic concentration profiles of the characteristic species that participate in the OSA dissolution process can be modeled employing the differential equations presented below:

$$\frac{d[\text{CaS}]}{dt} = -k_{11}[\text{CaS}] + \frac{k_{11}}{K_1}[\text{CaS}][\text{Ca}^{2+}][\text{S}^{2-}]. \quad (9)$$

$$\begin{aligned} \frac{d[\text{Ca}^{2+}]}{dt} &= k_{11}[\text{CaS}] - \frac{k_{11}}{K_1}[\text{CaS}][\text{Ca}^{2+}][\text{S}^{2-}] + k_{61}[\text{Ca}(\text{OH})_2] \\ &- \frac{k_{61}}{K_6}[\text{Ca}(\text{OH})_2][\text{Ca}^{2+}][\text{OH}^-]^2 + k_{71}[\text{CaSO}_4] - \frac{k_{71}}{K_7}[\text{CaSO}_4][\text{Ca}^{2+}][\text{SO}_4^{2-}]. \end{aligned} \quad (10)$$

$$\begin{aligned} \frac{d[\text{OH}^-]}{dt} &= k_{21}[\text{S}^{2-}] - \frac{k_{21}}{K_2}[\text{OH}^-][\text{HS}^-] + k_{31}[\text{HS}^-] - \frac{k_{31}}{K_3}[\text{OH}^-][\text{H}_2\text{S}] \\ &+ 2k_{61}[\text{Ca}(\text{OH})_2] - \frac{k_{61}}{K_6}[\text{Ca}(\text{OH})_2][\text{Ca}^{2+}][\text{OH}^-]^2. \end{aligned} \quad (11)$$

$$\begin{aligned} \frac{d[\text{HS}^-]}{dt} &= k_{41}[\text{HS}^-] - k_{51}[\text{HS}^-] + k_{21}[\text{S}^{2-}] - \frac{k_{21}}{K_2}[\text{HS}^-][\text{OH}^-] - k_{31}[\text{HS}^-] \\ &+ \frac{k_{31}}{K_3}[\text{OH}^-][\text{H}_2\text{S}]. \end{aligned} \quad (12)$$

$$\frac{d[\text{S}_2\text{O}_3^{2-}]}{dt} = 0.5k_{41}[\text{HS}^-]. \quad (13)$$

$$\frac{d[\text{SO}_4^{2-}]}{dt} = k_{51}[\text{HS}^-] + k_{71}[\text{CaSO}_4] - \frac{k_{71}}{K_7}[\text{CaSO}_4][\text{Ca}^{2+}][\text{SO}_4^{2-}]. \quad (14)$$

$$\frac{d[\text{S}^{2-}]}{dt} = k_{11}[\text{CaS}] - \frac{k_{11}}{K_1}[\text{CaS}][\text{Ca}^{2+}][\text{S}^{2-}] - k_{21}[\text{S}^{2-}] + \frac{k_{21}}{K_2}[\text{HS}^-][\text{OH}^-]. \quad (15)$$

$$\frac{d[\text{Ca}(\text{OH})_2]}{dt} = -k_{61}[\text{Ca}(\text{OH})_2] + \frac{k_{61}}{K_6}[\text{Ca}(\text{OH})_2][\text{Ca}^{2+}][\text{OH}^-]^2. \quad (16)$$

$$\frac{d[\text{CaSO}_4]}{dt} = -k_{71}[\text{CaSO}_4] + \frac{k_{71}}{K_7}[\text{CaSO}_4][\text{Ca}^{2+}][\text{SO}_4^{2-}]. \quad (17)$$

The values of the reverse reaction rate constants ( $k_{x2}$ ,  $x = 1-3, 6-7$ ) may be expressed through the equilibrium constants as  $k_{x1}/K_x$ ,  $x = 1-3, 6-7$ , accordingly. The concentrations in Equations (9)–(17) are expressed in

molar units. The concentration of  $H^+$  ions can be found from the concentration of hydroxide ions ( $[H^+] = K_w/[OH^-]$ ) or by using the pH ( $[H^+] = 10^{-pH}$ ).

The reaction rate constants used in Equations (9)–(17) were estimated in the modeling of OS ash-water dissolution processes (the reaction rate constants  $k_{11}$ – $k_{51}$  were used in all systems and were based on the pure CaS system). The estimated values of the rate constants  $k_{41}$  ( $2.01 \times 10^{-4} s^{-1}$ ) and  $k_{51}$  ( $8.66 \times 10^{-5} s^{-1}$ ) were one order of magnitude higher than the results reported by Mölder et al. [36] who investigated the rate of hydrolysis and oxidation (saturating the suspension with air) of CaS in a hydraulic ash disposal system. They reported rate constants for reactions (4) and (5) to be about  $1 \times 10^{-5} s^{-1}$  and approximately  $4 \times 10^{-6} s^{-1}$ , respectively. The reaction rate constants  $k_{61}$  and  $k_{71}$  at S/L ratios ranging from 0.004 to 0.2 were determined using the parameter estimation procedure that iteratively solved the proposed model equations and minimized the difference between these predictions and data obtained in batch experiments. For all data sets the correlation coefficient was greater than 0.87. The correlation coefficient of undersaturated model systems differed most from that of other model systems. In case of OS ash-water and ternary systems,  $k_{61}$  for the PF ash-water system and  $k_{71}$  for the SHC ash-water system agreed best.

As the next step, the simulation procedure was performed using the average values of rate constants (Table 3).

The accuracy of the proposed dissolution model ( $R^2 > 90\%$ ) was confirmed by comparing the results of process simulations with experimental data. The concentration profiles, pH (Fig. 5), and the relative concentration of species for the OS ash-water and ternary model systems (S/L 0.004 and 0.1) resulting from modeling are shown in Figure 6.

The pH profile of the CFB ash-water model system follows the trend of the PF ash-water model system, the  $Ca(OH)_2$  dissolution (Eq. 6) gives the highest alkaline reaction. In the SHC ternary system, the values of pH are

**Table 3. Reaction rate constants for the systems under study**

Reaction rate constant, $s^{-1}$		System	
		Ash	Ternary
In all systems	$k_{11}$	0.00149	
	$k_{21}$	2.7700	
	$k_{31}$	8.4874	
	$k_{41}$	0.000201	
	$k_{51}$	0.0000866	
CFB	$k_{61}$	0.0171	0.0326
	$k_{71}$	0.0072	0.0214
PF	$k_{61}$	0.0294	0.0232
	$k_{71}$	0.0029	0.0175
SHC	$k_{61}$	0.0091	0.0340
	$k_{71}$	0.0266	0.0330

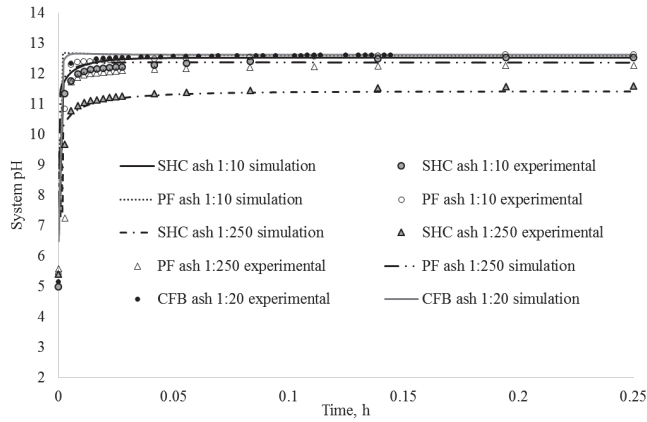


Fig. 5. Modeling of OSA dissolution: experimental vs simulated system pH.

higher (comparing  $\text{Ca}(\text{OH})_2$  contents in CFB and PF systems) due to the proton capture of sulfides, releasing the  $\text{OH}^-$  ions into the solution (Eqs. (2) and (3)).

The experimental results and simulated data in Figure 5 show that the pH of the system depends on the amount of the solid phase added because a greater amount of OS ash generates a faster increase in pH. The rate at which the equilibrium pH was reached differed between the selected ashes: it was slower for the real SHC ash system while the real PF ash system reached equilibrium more rapidly (Fig. 5). This implies that PF ash contains more compounds (Ca and Mg oxides) which ensure (dissolution of their hydrated forms) a fast basic reaction. This can also be seen from the reaction rate constants reported in Table 3, the value of the reaction constant for Equation (6) for the one-step ( $0.0282 \text{ s}^{-1}$ ) pure  $\text{Ca}(\text{OH})_2$  dissolution model [41] matches with the rate constant ( $0.0294 \text{ s}^{-1}$ ) for the PF ash system. The best accordance between OSA and ternary systems was achieved for  $k_{61}$  for the PF ash-water system and for  $k_{71}$  for the SHC ash-water system.

The experimental and model-predicted results for the pH and main ion concentrations agreed very well in the S/L ratio range of 1:10 to 1:250.

Plots of experimental and simulated concentration profiles for various S/L ratios for the PF ash-water system are presented in Figure 6. The sulfide content of SHC ash is two orders of magnitude higher than that of other ashes.

With regard to the calcium, sulfate and sulfide ions, the experimental results for the OS ash-water systems agree with simulated profiles. The PF ash-water system becomes saturated with calcium more rapidly than the others (Fig. 6a) because it has the highest content of  $\text{CaO}_{\text{free}}$  (22.37 wt%). The dissolution profiles of sulfate are rather similar in both the PF and CFB

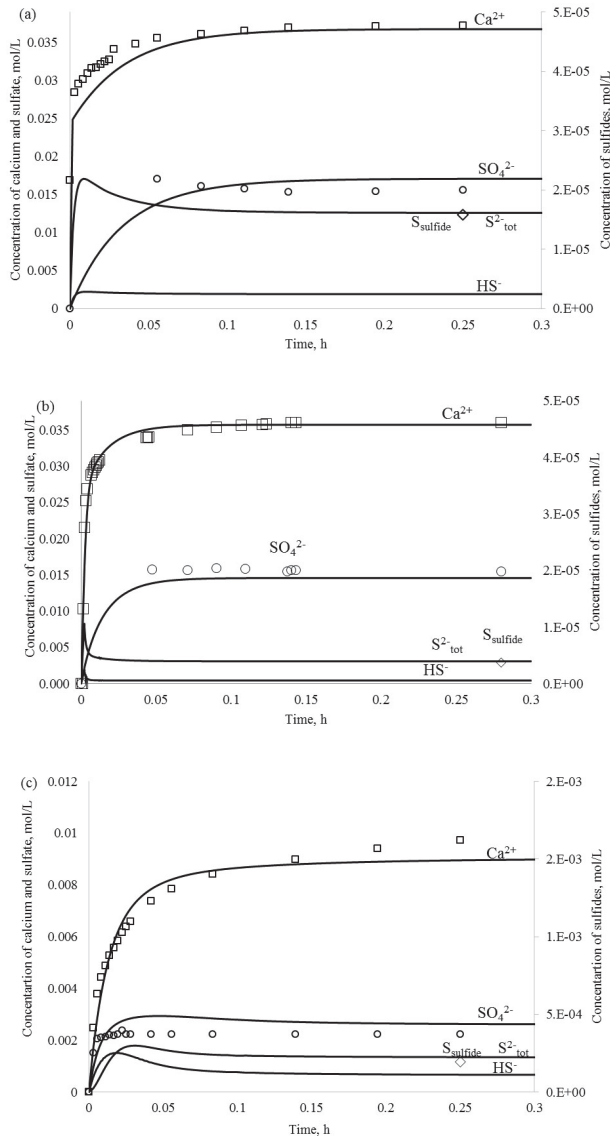


Fig. 6. Experimental vs MODEST 6.1 simulated leaching dynamics of key components of OSA from: (a) PF – S/L 1:10; (b) CFB – S/L 1:20; (c) SHC – S/L 1:50). (tot = total).

ash systems (Figs. 6a and 6b, respectively). However, due to the higher content of initial  $\text{CaSO}_4$  (10.10 wt%) in raw CFB ash, the CFB ash-water system becomes saturated with sulfate more rapidly, as seen from the reaction rate constant  $k_{71}$  presented in Table 3. Regarding the SHC ash-water system, sulfate reaches equilibrium most rapidly, which is due to the oxidation of sulfides (Eq. (5)) present in a relatively high amount. The dissolution profiles of sulfides are related to the content of sulfides in the initial ash. The greater the amount of initial CaS added to the water system, the greater the concentration of sulfides in the liquid phase.

#### 4. Conclusions

The leaching behavior of the main Ca-compounds in OS ash-water systems, which can be viewed as sorbents for both  $\text{CO}_2$  mineralization and PCC production, were studied in order to provide a better understanding of the behavior of OS ash suspensions and leachates especially by wet deposition.

Based on the comparative equilibrium 3 h batch experiments, the thermodynamic results for the aqueous systems of three different types of OSAs (CFB, PF and SHC) as well as the corresponding model systems were obtained.

The results indicate that the provided OS ash leaching model simulations were in good agreement with experimental data, confirming its accuracy. The measured values of pH, conductivity, and the concentration of  $\text{Ca}^{2+}$  ions of OS ash-water systems were slightly higher than those of ternary model systems because the real OS ash contains other water-soluble components.

The authors also determined, according to the 3 h equilibrium concentrations, the thermodynamic equilibrium constants  $K_{\text{eq}1}$ – $K_{\text{eq}3}$  and  $K_{\text{eq}6}$ – $K_{\text{eq}7}$  for the dissolution reactions of  $\text{Ca}(\text{OH})_2$ ,  $\text{CaSO}_4 \cdot 2\text{H}_2\text{O}$  and CaS in OS ash-water systems and proposed an empirical equation to calculate the concentration of  $\text{Ca}^{2+}$  ions as the dominating cation in OS ash leachates from conductivity measurements.

Furthermore, a kinetic reaction model, which incorporates dissolution mechanisms of  $\text{Ca}(\text{OH})_2$ ,  $\text{CaSO}_4 \cdot 2\text{H}_2\text{O}$  and CaS, was constructed to describe OS ash-water systems.

Although the three types of OS ashes studied differ in chemical and physical structure, it was found that a single model provided results that were in good agreement with experimental data, and can therefore be used to describe the leaching behavior of the key Ca-compounds in OS ash.

The equilibrium constants determined can be used, firstly, to estimate the kinetics of dissolution and create a complete OS ash-water leaching model and, secondly, to design a pilot-scale OS ash-water carbonation reactor. The latter could significantly reduce the environmental impact of using oil shale and other Ca-rich fossil fuels in the energy sector.

The model constructed for the OS ash-water systems incorporates mechanisms of dissolution of  $\text{Ca}(\text{OH})_2$ ,  $\text{CaSO}_4 \cdot 2\text{H}_2\text{O}$  and  $\text{CaS}$ . This model can be used to simulate all three types of OS ash (CFB, PF and SHC), which notably differ in chemical and physical structure. The proposed model and estimated parameters are thus suitable for describing the leaching of various types of ash that originate from the oil shale industry.

## Acknowledgements

This research was supported by the European Social Fund's Doctoral Studies and Internationalization Program Kristjan Jaak, the Estonian Ministry of Education and Research (SF0140082s08, IUT33-19) and the Estonian Science Foundation (Grant No 9334), which are gratefully acknowledged. The authors express their gratitude to Dr Peeter Somelar who performed the XRD measurements.

## REFERENCES

1. Ots, A. Oil Shale Fuel Combustion. Tallinna Raamatutrükikoda, Tallinn, 2006.
2. Bauert, H., Kattai, V. Kukersite oil shale. In: *Geology and Mineral Resources of Estonia* (Raukas, A., Teedumäe, A., eds.). Estonian Academy Publishers, Tallinn, 1997, 313–327.
3. Kuusik, R., Uibu, M., Kirsimäe, K. Characterization of oil shale ashes formed at industrial-scale CFBC boilers. *Oil Shale*, 2005, **22**(4S), 407–419.
4. Bitjukova, L., Mõtsep, R., Kirsimäe, K. Composition of oil shale ashes from pulverized firing and circulating fluidized-bed boiler in Narva Thermal Power Plants, Estonia. *Oil Shale*, 2010, **27**(4), 339–353.
5. Kuusik, R., Uibu, M., Kirsimäe, K., Mõtsep, R., Meriste, T. Open-air deposition of Estonian oil shale ash: formation, state of art, problems and prospects for the abatement of environmental impact. *Oil Shale*, 2012, **29**(4), 376–403.
6. Kattai, V., Saadre, T., Savitski, L. *Estonian Oil Shale: Geology, Resource, Mining Conditions*. Geological Survey of Estonia, Tallinn, 2000, 226 pp (in Estonian).
7. Golubev, N. Solid oil shale heat carrier technology for oil shale retorting. *Oil Shale*, 2003, **20**(3S), 324–332.
8. Reinik, J., Irha, N., Steinnes, E., Piirisalu, E., Aruoja, V., Schultz, E., Leppänen, M. Characterization of water extracts of oil shale retorting residues form gaseous and solid heat carrier processes. *Fuel Process. Technol.*, 2015, **131**, 443–451.
9. Talviste, P., Sedman, A., Mõtsep, R., Kirsimäe, K. Self-cementing properties of oil shale solid heat carrier retorting residue. *Waste Manage. Res.*, 2013, **31**(6), 641–647.
10. *Eesti Energia Annual Report 2014*. [https://www.energia.ee/-/doc/10187/pdf/concern/annual\\_report\\_2014\\_eng.pdf](https://www.energia.ee/-/doc/10187/pdf/concern/annual_report_2014_eng.pdf) (accessed in August 2015).
11. *VKG Yearbook 2014. Viru Keemia Grupp*. <http://www.vkg.ee/cms-data/upload/juhatus/vkg-aastaraamat-eng-2014.pdf> (accessed in August 2015).

12. VKG Yearbook 2013. *Viru Keemia Grupp*. <http://www.vkg.ee/cms-data/upload/juhatus/vkg-aastaraamat-eng-2013.pdf> (accessed in August 2015).
13. Uibu, M., Uus, M., Kuusik, R. CO<sub>2</sub> mineral sequestration in oil-shale wastes from Estonian power production. *J. Environ. Manage.*, 2009, **90**(2), 1253–1260.
14. Sanna, A., Uibu, M., Caramanna, G., Kuusik, R., Maroto-Valer, M. M. A review of mineral carbonation technologies to sequester CO<sub>2</sub>. *Chem. Soc. Rev.*, 2014, **43**, 8049–8080.
15. Velts, O., Uibu, M., Kallas, J., Kuusik, R. Waste oil shale ash as a novel source of calcium for precipitated calcium carbonate: carbonation mechanism, modeling, and product characterization. *J. Hazard. Mater.*, 2011, **195**, 139–146.
16. Velts, O., Uibu, M., Kallas, J., Kuusik, R. CO<sub>2</sub> mineralisation: concept for co-utilization of oil shale energetics waste streams in CaCO<sub>3</sub> production. *Energy Procedia*, 2013, **37**, 5912–5928.
17. Reisper, H. J., Determination of free CaO content in oil shale ash. *Transact. Tallinn Polytechnical Institute*, series A, 1966, No 245, 73–76 (in Estonian).
18. EVS 664:1995. *Solid Fuels. Sulphur content. Determination of total sulphur and its bonding forms*.
19. APHA - American Public Health Association, American Water Works Association, Water Environment Federation. *Standard methods for examination of water and wastewater*, 21st ed., Washington DC, USA, 2005, 1368.
20. Külaots, I., Goldfarb, J., L., Suuberg, E., M. Characterization of Chinese, American and Estonian oil shale semicokes and their sorptive potential. *Fuel*, 2010, **89**, 3300–3306.
21. Tamm, K., Kuusik, R., Uibu, M., Kallas, J. Transformations of sulfides during aqueous carbonation of oil shale ash. *Energy Procedia*, 2013, **37**, 5905–5912.
22. Velts, O., Uibu, M., Rudjak, I., Kallas, J., Kuusik, R. Utilization of oil shale ash to prepare PCC: Leachability dynamics and equilibrium in the ash-water system. *Energy Procedia*, 2009, **1**(1), 4843–4850.
23. ISO-6058:1984. *Water quality – Determination of calcium content – EDTA titrimetric method*.
24. EKUK Virumaa Affiliate Kohta-Järve Laboratory of Chemistry. *The quality procedure guide TJ 17 – Determination of sulfide in water*, 2002.
25. ISO-9963-1:1994. *Water quality – Determination of alkalinity – Part 1: Determination of total and composite alkalinity*.
26. Ritchie, I. M., Bing-An, X. The kinetics of lime slaking. *Hydrometallurgy*, 1990, **23**(2-3), 377–396.
27. Sun, W., Nešić, S., Young, D., Woollam, R. C. Equilibrium expressions related to the solubility of the sour corrosion product mackinawite. *Ind. Eng. Chem. Res.*, 2008, **47**(5), 1738–1742.
28. Almgren, T., Dyrssen, D., Elgquist, B., Johansson, O. Dissociation of hydrogen sulphide in seawater and comparison of pH scales. *Mar. Chem.*, 1976, **4**(3), 289–297.
29. Tamm, K., Uibu, M., Kallas, J., Kallaste, P., Velts-Jänes, O., Kuusik, R. Thermodynamic and kinetic study of CaS in aqueous systems. *Fuel Process. Technol.*, 2016, **142**, 242–249.
30. Irha, N., Uibu, M., Jefimova, J., Raado, L.-M., Hain T., Kuusik, R., Leaching behaviour of Estonian oil shale ash-based construction mortars. *Oil Shale*, 2014, **31**(4), 394–411.
31. Tamm, K., Kuusik, R., Uibu, M., Kallas, J. Transformations of sulfur compounds in oil shale ash suspension. In: *Waste Management and the Environment*

- VI: 6th International Conference on Waste Management and the Environment, New Forest, UK, 04.–06.07.2012 (Popov, V., Itoh, H., Brebbia, C. A., eds.). Wessex Institute of Technology Press, (WIT Transactions on Ecology and the Environment), 2012, 163.
32. Tamm, K., Kuusik, R., Uibu, M., Kallas, J. Behaviour of sulfur compounds during aqueous leaching of oil shale ash. In: *Proc. 4th Int. Conf. on Accelerated Carbonation for Environmental and Materials Engineering ACEME 2013*, Leuven, Belgium, 9–12 April 2013 (Nasser, R., Santos, R., Cizer, Ö., Van Gerven, T., eds.). Leuven, 2013, 541–544.
  33. Aavik, J. Characterization of oil shale ash leachate for optimizing the precipitation of calcium carbonate. Master's Degree, Tallinn University of Technology, 2011 (in Estonian).
  34. Johannsen, K., Rademacher, S. Modelling the kinetics of calcium hydroxide dissolution in water. *Acta Hydroch. Hydrob.*, 1999, **27**(2), 72–78.
  35. Giles, D. E., Ritchie, I. M., Xu, B.-A. The kinetics of dissolution of slaked lime. *Hydrometallurgy*, 1993, **32**(1), 119–128.
  36. Mölder, L., Elenurm, A., Tamvelius, H. Sulphur compounds in a hydraulic ash-disposal system. *Proc. Estonian Acad. Sci. Chem.*, 1995, **44**(2/3), 207–211.
  37. Velts, O., Hautaniemi, M., Kallas, J., Kuusik, R. Modeling calcium dissolution from oil shale ash: Part 1. Ca dissolution during ash washing in a batch reactor. *Fuel Process. Technol.*, 2010, **91**(5), 486–490.
  38. Velts, O., Hautaniemi, M., Kallas, J., Kuosa, M., Kuusik, R. Modeling calcium dissolution from oil shale ash: Part 2. Continuous washing of the ash layer. *Fuel Process. Technol.*, 2010, **91**(5), 491–495.
  39. Haario, H. *Modest User's Manual*. Profmath OY, Helsinki, Finland, 1994.
  40. Hindmarsh, A. C. ODEPACK, a systematized collection of ODE solvers. In: *Scientific Computing: IMACS Transactions on Scientific Computation* (Stepleman, R. S. et al., eds.), North-Holland, Amsterdam, 1983, **1**, 55–64.
  41. Uibu, M., Tamm, K., Velts-Jänes, O., Kallaste, P., Kuusik, R., Kallas, J. Utilization of oil shale combustion wastes for PCC production: Quantifying the kinetics of  $\text{Ca}(\text{OH})_2$  and  $\text{CaSO}_4 \cdot 2\text{H}_2\text{O}$  dissolution in aqueous systems. *Fuel Process. Technol.*, 2015, **140**, 156–164.

Presented by K. Kirsimäe

Received September 10, 2015

## **APPENDIX B. CURRICULUM VITAE**

## ELULOOKIRJELDUS

### 1. Isikuandmed

Ees- ja perekonnanimi: Kadriann Tamm  
Sünniaeg ja -koht: 02. september 1985. a., Tallinn  
Kodakondsus: eesti  
E-posti aadress: [kadriann.tamm@ttu.ee](mailto:kadriann.tamm@ttu.ee)

### 2. Hariduskäik

Õppeasutus (nimetus lõpetamise ajal)	Lõpetamise aeg	Haridus (eriala/kraad)
Tallinna Tehnikaülikool	2011	Tehnikateaduse magistrikraad
Tartu Ülikool	2007	Loodusteaduse bakalaureusekraad
Tallinna Mustamäe Gümnaasium	2004	Keskharidus

### 3. Keelteoskus (alg-, kesk- või kõrgtase)

Keel	Tase
Eesti keel	Emakeel
Inglise keel	Kõrgtase
Vene keel	Algtase

### 4. Täiendusõpe

Õppimise aeg	Täiendusõppe korraldaja nimetus
2011-2014	Tallinna Tehnikaülikool
2012, 2014	Outotec Research keskus
2012	IEAGHG
2008	Tallinna Ülikool
2001-2004	Tartu Ülikool

## 5. Teenistuskäik

Töötamise aeg	Tööandja nimetus	Ametikoht
2011- k.a.	Tallinna Tehnikaülikool	insener
2010-2011	Tallinna Tehnikaülikool	praktikant
2006-2008	Juuru E. Vilde nim. Gümnaasium	keemiaõpetaja

## 6. Kaitstud lõputööd

Tehnikateaduse magistrikraad: Väavliühendite käitumine põlevkivituha leostamisel ja märgkarboniseerimisel, Tallinna Tehnikaülikool, 2011. Juhendajad: juhtivteadur Rein Kuusik; vanemteadur Mai Uibu.

Loodusteaduse bakalaureusekraad: CaS-H<sub>2</sub>O süsteemi modelleerimine, Tartu Ülikool, 2007. Juhendaja: Prof. Toomas Tenno; Karin Hellat

## 7. Teadtöö põhisuunad

VALDKOND: 4. Loodusteadused ja tehnika; 4.11. Keemia ja keemiatehnika.

CERCS ERIALA: P360 Anorgaaniline keemia.

PÕHISUUND: Põlevkivi põletamisega kaasnevate tahkjäätmete uute kasutusvaldkondade alused, CO<sub>2</sub> mineraliseerimine tööstusheitmete baasil. Energeetikatööstuse heitmete koostise, omaduste ja töötlemismeetodite uurimine.

## 8. Teadustegevus

IUT33-19 Multikomponentsete mineraal-orgaaniliste süsteemide käitlemise alused: keemia, modelleerimine ja kestlik kasutus (1.01.2015–31.12.2020).

ETF9334 Happeliste gaaside emissioonide vähendamine ning PCC-tüüpi täitematerjali saamine põlevkivi põletusjäätmete baasil (1.01.2012–31.12.2015).

SF0140082s08 Karbonaat- ja fosfaatpõhiste anorgaaniliste süsteemide keemia ja rakendused (1.01.2008–31.12.2013).

## 9. Tunnustused

2011 Riiklike üliõpilaste teadustööde konkurss; II koht

2011 Eesti Teaduste Akadeemia üliõpilaste teadustööde konkursi, preemia

## 10. Juhendatud lõputööd

Priit Kallaste, magistrikraad, 2015, (juh) Kadriann Tamm, Mai Uibu, Põlevkivi mineraalsete jäätmete leostustasakaalud mudelsüsteemides, Tallinna Tehnikaülikool, Keemia ja materjalitehnoloogia teaduskond, Anorgaaniliste materjalide teaduslaboratoorium.

Priit Kallaste bakalaureusetöö, 2013 (juh) Kadriann Tamm, Tasakaalud süsteemis põlevkivituhk – vesi, Tallinna Tehnikaülikool, Keemia ja materjalitehnoloogia teaduskond, Anorgaaniliste materjalide teaduslaboratoorium.

Hans Priks bakalaureusetöö, 2013, (juh) Kadriann Tamm, Rein Kuusik, Tiosulfaat - ioon põlevkivituha leostamisel ja märgkarboniseerimisel, Tallinna Tehnikaülikool, Keemia ja materjalitehnoloogia teaduskond, Anorgaaniliste materjalide teaduslaboratoorium.

## ***CURRICULUM VITAE***

### 1. Personal data

Name: Kadriann Tamm

Date and place of birth: 02. september 1985.a., Tallinn

Citizenship: Estonian

E-mail address: [kadriann.tamm@ttu.ee](mailto:kadriann.tamm@ttu.ee)

### 2. Education

Educational institution	Graduation year	Education (field of study/degree)
Tallinn University of Technology	2011	Master of Science in Engineering
Tartu University	2007	Bachelor in Chemistry
Tallinna Mustamäe Gymnasium	2004	High school education

### 3. Language competence/skills (fluent, average, basic skills)

Language	Level
Estonia	Fluent
English	Fluent
Russian	Basic skills

### 4. Special courses

Period	Educational or other organization
2011-2014	Tallinn University of Technology
2012, 2014	Outotec Research Center
2012	IEAGHG
2008	Tallinn University
2001-2004	Tartu University

## 5. Professional employment

Period	Organization	Position
2011- to date	Tallinn University of Technology	engineer
2010-2011	Tallinn University of Technology	trainee
2006-2008	Juuru E. Vilde nom. Gymnasium	chemistry teacher

## 6. Defended theses

MSc thesis: The behavior of sulfur compounds in the process of oil shale ash aqueous suspension and aqueous carbonation, Tallinn University of Technology, 2011. Supervisors: Rein Kuusik; Mai Uibu.

BSc thesis: Modelling the system of CaS-H<sub>2</sub>O, Tartu University, 2007. Supervisors: Prof. Toomas Tenno; Karin Hellat

## 7. Main area of scientific work

FIELD OF RESEARCH: 4. Natural Sciences and Engineering; 4.11. Chemistry and Chemical Technology.

CERCS ERIALA: P360 Inorganic chemistry.

SPECIALITY: CO<sub>2</sub> aqueous mineralization processes. Characterization and processing of inorganic waste materials.

## 8. Scientific work

IUT33-19 Fundamentals of multicomponent mineral-organic systems: Chemistry, modeling and sustainable processing (1.01.2015–31.12.2020).

ETF9334 Abatement of emissions and production of PCC-type filler material on the basis of oil shale combustion wastes (1.01.2012–31.12.2015).

SF0140082s08 Chemistry and applications of carbonate-phosphate-based inorganic systems (1.01.2008–31.12.2013).

## 9. Awards

2011 National competition of student research papers II place

2011 Student research competition, Estonian Academic of Sciences

## 10. Dissertations supervised

Priit Kallaste, Master degree, 2015, (sup) Kadriann Tamm, Mai Uibu, Leaching equilibriums in oil shale mineral waste model systems, Tallinn University of Technology, Faculty of Chemical and Materials Technology, Laboratory of Inorganic Materials.

Priit Kallaste, Bachelor degree, 2013, (sup) Kadriann Tamm, Equilibriums in oil shale ash - water systems, Tallinn University of Technology, Faculty of Chemical and Materials Technology, Laboratory of Inorganic Materials.

Hans Priks, Bachelor degree, 2013, (sup) Kadriann Tamm, Rein Kuusik, Thiosulfate – ion leaching and aqueous carbonation of oil shale ash, Tallinn University of Technology, Faculty of Chemical and Materials Technology, Laboratory of Inorganic Materials.

**DISSERTATIONS DEFENDED AT  
TALLINN UNIVERSITY OF TECHNOLOGY ON  
CHEMISTRY AND CHEMICAL ENGINEERING**

1. **Endel Piiraja**. Oxidation and Destruction of Polyethylene. 1993.
2. **Meili Rei**. Lihatehnoloogia teaduslikud alused. Fundamentals of Food Technology. 1995.
3. **Meeme Põldme**. Phase Transformations in Hydrothermal Sintering Processing of Phosphate Rock. 1995.
4. **Kaia Tõnsuaadu**. Thermophosphates from Kovdor and Siilinjärvi Apatites. 1995.
5. **Anu Hamburg**. The Influence of Food Processing and Storage on the N-Nitrosamines Formation and Content in Some Estonian Foodstuffs. 1995.
6. **Ruth Kuldvee**. Computerized Sampling in Ion Chromatography and in Capillary Electrophoresis. 1999.
7. **Külliki Varvas**. Enzymatic Oxidation of Arachidonic Acid in the Coral *Gersemia fruticosa*. 1999.
8. **Marina Kudrjašova**. Application of Factor Analysis to Thermochromatography and Promotion Studies. 2000.
9. **Viia Lepane**. Characterization of Aquatic Humic Substances by Size Exclusion Chromatography and Capillary Electrophoresis. 2001.
10. **Andres Trikkel**. Estonian Calcareous Rocks and Oil Shale Ash as Sorbents for SO<sub>2</sub>. 2001.
11. **Marina Kritševskaja**. Photocatalytic Oxidation of Organic Pollutants in Aqueous and Gaseous Phases. 2003.
12. **Inna Kamenev**. Aerobic Bio-Oxidation with Ozonation in Recalcitrant Wastewater Treatment. 2003.
13. **Janek Reinik**. Methods for Purification of Xylidine-Polluted Water. 2003.
14. **Andres Krumme**. Crystallisation Behaviour of High Density Polyethylene Blends with Bimodal Molar Mass Distribution. 2003.
15. **Anna Goi**. Advanced Oxidation Processes for Water Purification and Soil Remediation. 2005.
16. **Pille Meier**. Influence of Aqueous Solutions of Organic Substances on Structure and Properties of Pinewood (*Pinus sylvestris*). 2007.
17. **Kristjan Kruusement**. Water Conversion of Oil Shales and Biomass. 2007.

18. **Niina Kulik**. The Application of Fenton-Based Processes for Wastewater and Soil Treatment. 2008.
19. **Raul Järviste**. The Study of the Changes of Diesel Fuel Properties a its Long Term Storage. 2008.
20. **Mai Uibu**. Abatement of CO<sub>2</sub> Emissions in Estonian Oil Shale-Based Power Production. 2008.
21. **Valeri Gorkunov**. Calcium-Aluminothermal Production of Niobium and Utilization of Wastes. 2008.
22. **Elina Portjanskaja**. Photocatalytic Oxidation of Natural Polymers in Aqueous Solutions. 2009.
23. **Karin Reinhold**. Workplace Assessment: Determination of Hazards Profile using a Flexible Risk Assessment Method. 2009.
24. **Natalja Savest**. Solvent Swelling of Estonian Oil Shales: Low Temperature Thermochemical Conversion Caused Changes in Swelling. 2010.
25. **Triin Märtson**. Methodology and Equipment for Optical Studies of Fast Crystallizing Polymers. 2010.
26. **Deniss Klauson**. Aqueous Photocatalytic Oxidation of Non-Biodegradable Pollutants. 2010.
27. **Oliver Järvik**. Intensification of Activated Sludge Process – the Impact of Ozone and Activated Carbon. 2011.
28. **Triinu Poltimäe**. Thermal Analysis of Crystallization Behaviour of Polyethylene Copolymers and Their Blends. 2011.
29. **Mariliis Sihtmäe**. (Eco)toxicological Information on REACH-Relevant Chemicals: Contribution of Alternative Methods to *in vivo* Approaches. 2011.
30. **Olga Velts**. Oil Shale Ash as a Source of Calcium for Calcium Carbonate: Process Feasibility, Mechanism and Modeling. 2011.
31. **Svetlana Jõks**. Gas-Phase Photocatalytic Oxidation of Organic Air Pollutants. 2012.
32. **Aleksandr Dulov**. Advanced Oxidation Processes for the Treatment of Water and Wastewater Contaminated with Refractory Organic Compounds. 2012.
33. **Aleksei Zaidentsal**. Investigation of Estonian Oil Shale Thermo-bituminization in Open and Closed System. 2012.
34. **Dmitri Šumigin**. Composites of Low-Density Polyethylene and Poly(Lactic Acid) With Cellulose and Its Derivatives. 2014.

35. **Aleksandr Käkinen**. The Role of Physico-chemical Properties and Test Environment on Biological Effects of Copper and Silver Nanoparticles. 2014.
36. **Ada Traumann**. Improvement of Work Environment through Modelling the Prevention of Health Risks Focusing on Indoor Pollutants. 2014.
37. **Marika Viisimaa**. Peroxygen Compounds and New Integrated Processes for Chlorinated Hydrocarbons Degradation in Contaminated Soil. 2014.
38. **Olga Budarnaja**. Visible-light-sensitive Photocatalysts for Oxidation of Organic Pollutants and Hydrogen Generation. 2014.
39. **Jelena Hruljova**. Role of Specifically Interacting Solvents in Solvent Swelling of Kukersite Oil Shale Kerogen. 2014.
40. **Irina Klimova**. Modification of Ammonium Nitrate Fertilizer. 2014.
41. **Julia Krasulina**. Upgrading of Liquid Products from Estonian Kukersite Oil Shale by Catalytic Hydrogenation. 2015.
42. **Irina Epold**. Degradation of Pharmaceuticals by Advanced Oxidation Technologies in Aqueous Matrices. 2015.